Elsevier Editorial System(tm) for Lithos
Manuscript Draft

Manuscript Number: LITHOS7621R1

Title: The petrology and geochemistry of Nyiragongo lavas of 2002, 2016, 1977 and 2017 AD, and the trace element partitioning between melilitite glass and melilite, nepheline, leucite, clinopyroxene, apatite, olivine and Fe-Ti oxides: a unique scenario

Article Type: Regular Article

Keywords: nepheline melilititites; trace elements; melilite; partition cofficients, Nyiragongo volcano; Africa

Corresponding Author: Dr. Leone Melluso,

Corresponding Author's Institution: Università di Napoli Federico II

First Author: Silvia Minissale, PhD

Order of Authors: Silvia Minissale, PhD; Alberto Zanetti, Dr.; Dario Tedesco, Prof.; Vincenzo Morra, Prof.; Leone Melluso

Abstract: The Nyiragongo lava of 2002, and the new one flowing from the spatter cone grown up in 2016 close to the lava lake, are melilite-nephelinites. They have low MgO (4 wt.%), are chemically almost indistinguishable from the lavas of 1977 and from that erupted in 2017, are multiply saturated in melilite, nepheline, leucite, clinopyroxene, olivine, apatite and magnetite, and are rich in fresh glass having significant concentration of SO3, F and Cl. Glasses and bulk-rocks plot close to one atmosphere cotectics in pertinent phase diagrams. The LA-ICP-MS analyses of the observed phases and mineral/glass partition coefficients indicate that REE and Y are moderately incompatible in melilite (e.g., DLa=0.46-0.48, DEu=0.56-0.57; DLu=0.18-0.25; DY=0.25-0.27), whereas Sr is compatible (DSr=1.6-1.8); clinopyroxene/melt partition coefficients are similar to melilite for LREE (e.g., DLa=0.36), and significantly higher for HREE (DLu=0.74), Y (DY=0.7), Zr (≈1) and Hf (DHf=1.6), while lower for Sr (DSr =0.38). Apatites have high concentration ratios for REE, particularly MREE (DLa=4.6-6.4, DNd= 5.8-7.7; DEu=4.9-6.9; DLu=1.3-1.6; DY=3.1-4.4), and high DSr (1.8-2.2). Nepheline and leucite are highly and differently selective for Rb, Cs, Ba and Sr; both phases show negligible concentration of REE (hence Eu, +Y), Th, U and first row transition elements. Olivine and magnetite have the expected high concentration of transition elements, with small preference of olivine for divalent cations and magnetite for trivalent cations. The distribution of trace elements in melilite compared with clinopyroxene, nepheline -or even feldspar- clearly indicate that melilite is not a silica-undersaturated equivalent of any of these phases, and that melilite removal cannot be considered the main cause of Eu troughs or of decreasing fractionation between light and heavy REE in more evolved melts, being these elements still significantly incompatible. At the same time, removal of the observed phenocrysts at this stage of crystallization cannot be the cause of anomalous fractionation of elements with similar geochemical behaviour found in the Nyiragongo lavas. These new data indicate that the magmatic system of the Nyiragongo is in a roughly steady state at least since the eruption of 1977 to the

activity of 2017, with periodic eruptions, withdrawal or feeding from the uppermost magma reservoir by broadly the same "cotectic" magma compositions, from which phases of the same composition nucleated in a very low-pressure regime.

Research Data Related to this Submission

There are no linked research data sets for this submission. The following reason is given:
The data used for this manuscript are fully reported within the text and in the supplementary tables attached

Revision Notes

Click here to download Revision Notes: Comments.doc

COMMENTS FROM EDITORS AND REVIEWERS

Our comments in red

Comment [z1]: …niente polemiche..ringraziamolo…e sottolinea che la discussione petrologica e' sintetica ma formidabile…i dati sono novelty

Dear Dr. Melluso, the reviews on your manuscript are complete. The comprehensive reviews are just below. Please carefully read and make changes following both reviews.

Dear Prof. Roden, thank you very much for your work as editorial responsible of the manuscript. Extensive comments are below

1.Both reviewers find that while the data are quite high quality, they are under-interpreted.

2.Reviewer 1 notes that coverage of relevant literature is weak - during revision please develop the discussion further and include relevant literature comparisons.

Upon returning the paper please indicate how you have responded to the reviewers. Michael Roden, co-editor

Reviewer #1: Review on the manuscript „The geochemistry of Nyiragongo lavas from 1977 to 2017 AD, and the trace element partitioning between melilite-nephelinite glass and melilite, nepheline, leucite, clinopyroxene, apatite, olivine and Fe-Ti oxides: a unique scenario" submitted by Silvia Minissale, Alberto Zanetti, Dario Tedesco, Vincenzo Morra, and Leone Melluso for publication in LITHOS. The manuscript presents major and trace element (TE) whole-rock, glass and mineral data from two melilititic samples from Nyirangongo and derives apparent mineral-glass partition coefficients for trace elements. Such data are potentially valuable as they can decipher the potential effects of mineral fractionation on TE systematics in such strongly undersaturated magmatic systems, for which almost no comparable data are existing.

Given the interesting data set, the discussion section is, however, weak. Not much more is done then calculating and presenting the glass-mineral trace element concentration ratios, and except for briefly explaining that based on this melilite is probably not able to produce Eu throughs in REE whole rock/glass patterns not much more is done. This is certainly not enough „brain-work" to justify publication in a high-level journal like LITHOS. The work is very much (too much?) focused on the locality itself. I would expect in a work like this to compare these results with published KD values for other magmatic systems. It has long been known that melt composition influences trace element partitioning beahaviour. There are many theoretical, experimental and field based studies on this topic. But this is barely touched in this manuscript.

Also, the introduction is much too short and much to focused on the locality itself (actually most of the Introduction should go in the Geological setting chapter). Here, the reader needs to understand the potential value of the presented data, that is how melt composition influences KD values for clinopyroxene, apatite, olivine, nepheline etc... The background on this topic is completely lacking, no comparable studies in other magmatic systems (e.g., basaltic, andesitic, dacitic, phonolitic, rhyolitic etc....) are mentioned - none at all (I am aware that there are only very few TE data for melilite are available, but for all ther other minerals there is a lot of studies arround!

Even for melilite there is the work of Mason & Martin, 1974, which shows that melilite may produce POSITIVE EU anomalies, but this study is on meteorites, which implies that REDOX conditions are an influencing factor here of EU anomalies form or not…. What about redox

conditions for the studied samples? Is it just because of their (presumably) oxidized nature that no EU anomalies develop - this might be another point for discussion - just mentioning. For plagioclase it was shown that redox is a factor controlling EU anomalies (Drake & Weill 1975). Also melilite TE data are available for Oldoinyo Lengai and by digging deeper in the melilite literature I am sure there are more data… I think that the melilite story is not thought through enough…..

In all, my major criticism I have is the lack of a comparison with literature data. If properly discussed and compared with literature data on other magmatic compositions, these data could be used to show how this extreme „endmember-type" melt composition influences trace element partitioning in magmatic systems. But by not doing so, the manuscript is not much more than a „data collection".

Other points:

1. Is it now LIHOS style to put the complete ANALYTICAL METHODS section in the Appendix?
2. The „naming" of the samples is inconsistent or confusing. In the petrography section samples NY02 and NY16 are mentioned, later they are called lava 2002 and lava 2016 in the Tables,
3. The classification of the samples is not very clear to me: In the petrography section the samples are classified as melilitites, later in the discussion, the authors speak about a melilite nephelinite melt - how does this come together?
4. What do the authors mean with is „highly alkaline" (Introduction section)
5. Figure 3 shows 4 bulk-rock data points - I though the study is based on two samples?
6. The legend in Figure 5 is not understandable - please label better - what is M2002-2??? shows some literature data on melilite
7. Figure 7 could be improved by plotting clinopyroxene, melilite and apatite in ONE subfigure.

Based on the above comments I cannot recommend publication of this manuscript in its present form.

Reviewer #2: This was a difficult paper to review in some respects as it consists mainly of the disposition and description of analytical data - without making any significant petrogenetic inferences from these data . The authors claim that their data can be used to model the petrogenesis of other east African rift lavas - but do not attempt to do this this - even for Nyiragongo . As the data presented seem to this reviewer to be accurate, and the interpretations regarding solid solutions etc are correct there is little to comment on; apart from that the text (which is quite well-written) requires some copy-editing with respect to the English syntax and removal of excess verbiage.

The authors must add some modal data for these lavas

Given the lack of discussion - is this paper suitable for Lithos ? - while the trace element data and D-vales are useful - I am not convinced this is a Lithos paper - perhaps the Journal of African Geology or Chemical Geology might be a better venue ? I have recommended minor revision but I leave it up to the Editor to recommend the final disposition on this paper as "minor revision" or "reject as not in scope of this journal"

Dear Prof. Roden,

Our manuscript is reporting brand new and as both referees find out, top-quality data on lava samples and their phases (glass, melilite, nepheline, clinopyroxene, leucite and so on), from the major and trace element points of view. These lavas are those currently erupted by the Nyiragongo, i.e. the only volcano with both a lava lake and a spatter cone inside the crater, and currently erupting melilite nephelinites on earth (which is quite a rarity, something roughly equivalent to the natrocarbonatites of the Oldoinyo Lengai). This manuscript first addresses the petrogenesis of these lavas by means of phase petrology (use of pertinent phase diagrams, use of similar compositions elsewhere, use of a few hundred brand new data of mineral chemistry reported in the appendix) and bulk-rock geochemistry. After having established that these phases are in equilibrium with the glass (and bulk-rocks) of such an extreme chemical composition at one atmosphere and roughly 1000°C, hence with elaboration of almost unexisting phase diagrams, there are attempts to calculate "partition coefficients" for the main phenocryst phases (melilite, nepheline, leucite, apatite, and a few data on minor phases such as clinopyroxene, olivine and magnetite). The trace element geochemistry of the observed phases, and the subsequent calculation of partition coefficients in natural magmas with LA-ICP-MS is a brand-new (novel) work, that has no equivalent in any other melilite-bearing volcanic rock worldwide (or also in the meteorites). No comparable data are currently known in literature, neither relevant literature comparisons are allowed, for the dearth of pertinent examples, and we hope that this manuscript will have a follow-up from other research groups. This manuscript deals also with the substantial lack of chemical modifications in the feeding system of this volcano at least in the last 40-42 years, hence there is also a volcanological feed-back.

We think the manuscript should be considered essential in shape and "with reasonable English", but has also notable "equivalents" in other major Lithos papers, e.g., Foley and Jenner, 2004, Wiedenmann et al. 2010 Lithos 118, 112-118. Essentiality should be considered as a value, not a drawback, particularly when all the reported data are of excellent quality and, it is our opinion; they have been extensively discussed and commented, in their novelty. It is certainly possible that something will be missing, not clear or wrong, in that case we are ready to work on it, to add or to respond to questions.

Changes were made according to comments of the reviewers (please see the new version with changes marked).

Kind regards

The authors

Abstract

The Nyiragongo lava of 2002, and the new one flowing from the spatter cone grown up in 2016 close to the lava lake, are melilite-nephelinites. They have low MgO (4 wt.%), are chemically almost indistinguishable from the lavas of 1977 and from that erupted in 2017, are multiply saturated in melilite, nepheline, leucite, clinopyroxene, olivine, apatite and magnetite, and are rich in fresh glass having significant concentration of SO_3, F and Cl. Glasses and bulk-rocks plot close to one atmosphere cotectics in pertinent phase diagrams. The LA-ICP-MS analyses of the observed phases and mineral/glass partition coefficients indicate that REE and Y are moderately incompatible in melilite (e.g., D_{La}=0.46-0.48, D_{Eu}=0.56-0.57; D_{Lu}=0.18-0.25; D_Y=0.25-0.27), whereas Sr is compatible (D_{Sr}=1.6-1.8); clinopyroxene/melt partition coefficients are similar to melilite for LREE (e.g., D_{La}=0.36), and significantly higher for HREE (D_{Lu}=0.74), Y (D_Y=0.7), Zr (≈1) and Hf (D_{Hf}=1.6), while lower for Sr (D_{Sr} =0.38). Apatites have high concentration ratios for REE, particularly MREE (D_{La}=4.6-6.4, D_{Nd}= 5.8-7.7; D_{Eu}=4.9-6.9; D_{Lu}=1.3-1.6; D_Y=3.1-4.4), and high D_{Sr} (1.8-2.2). Nepheline and leucite are highly and differently selective for Rb, Cs, Ba and Sr; both phases show negligible concentration of REE (hence Eu, +Y), Th, U and first row transition elements. Olivine and magnetite have the expected high concentration of transition elements, with small preference of olivine for divalent cations and magnetite for trivalent cations. The distribution of trace elements in melilite compared with clinopyroxene, nepheline -or even feldspar- clearly indicate that melilite is not a silica-undersaturated equivalent of any of these phases, and that melilite removal cannot be considered the main cause of Eu troughs or of decreasing fractionation between light and heavy REE in more evolved melts, being these elements still significantly incompatible. At the same time, removal of the observed phenocrysts at this stage of crystallization cannot be the cause of anomalous fractionation of elements with similar geochemical behaviour found in the Nyiragongo lavas. These new data indicate that the magmatic system of the Nyiragongo is in a roughly steady state at least since the eruption of 1977 to the activity of 2017,

with periodic eruptions, withdrawal or feeding from the uppermost magma reservoir by broadly the same “cotectic” magma compositions, from which phases of the same composition nucleated in a very low-pressure regime.

Highlights:

The Nyiragongo lavas of the period 1997-2017 are melilite-nephelinites

The glass compositions are identical to the bulk-rocks and are highly enriched in incompatible trace elements

The melilite, clinopyroxene, apatite, olivine, nepheline and leucite were studied from the major and trace element compositions

The petrology and geochemistry of Nyiragongo lavas of 2002, 2016, 1977 and 2017 AD, and the trace element partitioning between melilitite glass and melilite, nepheline, leucite, clinopyroxene, apatite, olivine and Fe-Ti oxides: a unique scenario

Silvia Minissale*, Alberto Zanetti**, Dario Tedesco***, Vincenzo Morra*, Leone Melluso*[1]

*DiSTAR, Università di Napoli Federico II, Via Cintia 26, 80126 Napoli, Italy

**CNR, IGG, Via Ferrata 1, 27100 Pavia, Italy

***DISTABIF, Campania University – Luigi Vanvitelli, 81100 Caserta, Italy and JOC, UN-MONUSCO, UN-Goma, DRC.

[1]corresponding author melluso@unina.it

Abstract

The Nyiragongo lava of 2002, and the new one flowing from the spatter cone grown up in 2016 close to the lava lake, are melilite-nephelinites. They have low MgO (4 wt.%), are chemically almost indistinguishable from the lavas of 1977 and from that erupted in 2017, are multiply saturated in melilite, nepheline, leucite, clinopyroxene, olivine, apatite and magnetite, and are rich in fresh glass having significant concentration of SO_3, F and Cl. Glasses and bulk-rocks plot close to one atmosphere cotectics in pertinent phase diagrams. The LA-ICP-MS analyses of the observed phases and mineral/glass partition coefficients indicate that REE and Y are moderately incompatible in melilite (e.g., D_{La}=0.46-0.48, D_{Eu}=0.56-0.57; D_{Lu}=0.18-0.25; D_{Y}=0.25-0.27), whereas Sr is compatible (D_{Sr}=1.6-1.8); clinopyroxene/melt partition coefficients are similar to

Formatted: Line spacing: Double

melilite for LREE (e.g., D_{La}=0.36), and significantly higher for HREE (D_{Lu}=0.74), Y (D_Y=0.7), Zr (≈1) and Hf (D_{Hf}=1.6), while lower for Sr (D_{Sr} =0.38). Apatites have high concentration ratios for REE, particularly MREE (D_{La}=4.6-6.4, D_{Nd}= 5.8-7.7; D_{Eu}=4.9-6.9; D_{Lu}=1.3-1.6; D_Y=3.1-4.4), and high D_{Sr} (1.8-2.2). Nepheline and leucite are highly and differently selective for Rb, Cs, Ba and Sr; both phases show negligible concentration of REE (hence Eu, +Y), Th, U and first row transition elements. Olivine and magnetite have the expected high concentration of transition elements, with small preference of olivine for divalent cations and magnetite for trivalent cations. The distribution of trace elements in melilite compared with clinopyroxene, nepheline -or even feldspar- clearly indicate that melilite is not a silica-undersaturated equivalent of any of these phases, and that melilite removal cannot be considered the main cause of Eu troughs or of decreasing fractionation between light and heavy REE in more evolved melts, being these elements still significantly incompatible. At the same time, removal of the observed phenocrysts at this stage of crystallization cannot be the cause of anomalous fractionation of elements with similar geochemical behaviour found in the Nyiragongo lavas. These new data indicate that the magmatic system of the Nyiragongo is in a roughly steady state at least since the eruption of 1977 to the activity of 2017, with periodic eruptions, withdrawal or feeding from the uppermost magma reservoir by broadly the same "cotectic" magma compositions, from which phases of the same composition nucleated in a very low-pressure regime.

1. Introduction

The Nyiragongo volcano belongs to the Virunga Volcanic Province, western branch of the East African Rift, which is composed by seven main volcanoes (from east to west: Muhavura, Gahinga, Sabinyo, Visoke, Karisimbi, Mikeno, Nyiragongo and Nyamulagira, the last two currently active) and hundreds minor centers to the north/northeast of lake Kivu, at the boundaries between the Democratic Republic of Congo, Rwanda and Uganda (Fig. 1a). The western branch of the East

African Rift is composed by three main volcanic areas: the Toro-Ankole, the Virunga and the south Kivu. The Nyiragongo is well known for the presence of the biggest lava lake on earth inside its crater, semi-permanently active since the discovery of the volcano in 1894. The volcanic rocks of Mt. Nyiragongo range in composition from (minor) alkali basalt to nephelinite, leucite nephelinite, melilite nephelinite and olivine melilitite (Sahama, 1962, 1978; Toscani et al., 1990; Demant et al., 1994; Platz et al., 2004; Chakrabarti et al., 2009; Andersen et al., 2012; Minissale, 2018), hence reaching a very high degree of silica undersaturation. The chemical composition of the recent Nyiragongo lavas, unique among the active lava lakes on earth, is of compelling interest given to their glassy, extremely fresh nature and their low amount of phenocryst charge.

In this study we present the petrology of the recent lavas of the volcano, and the distribution of trace elements in phenocrysts and microphenocrysts naturally equilibrated with melilite-nephelinitic glasses/magmas/melts. To date, there are no comparable datasets on the geochemical characteristics of melilite and other observed phases in *natural* magmas with similar chemistry elsewhere (cf. Onuma et al., 1981 and references therein; Arzamastsev et al., 2009). Therefore, these data and their inferences will be of the most importance for tracking the magmatic evolution and the petrogenesis of Nyiragongo and other melilite-bearing rocks in fossil or active volcanic areas (e.g., volcanic complexes in Kenya-Tanzania and Uganda; Mt. Vulture and Alban Hills, Italy; Eger Rift; Urach-Hegau-Kaiserstuhl, Germany; Kola Peninsula).

2. Geological setting and sampling sites

The Nyiragongo is a Quaternary stratovolcano characterized by a ~1000 m wide summit crater (with a crater rim at ~3500 m a.s.l.) which was generated by repeated magma emptying and refilling episodes throughout its volcanological history (e.g., Sahama, 1978; Demant et al., 1994). The summit crater of the Nyiragongo lies between the two extinct cones of Baruta (to the north) and Shaheru (to the south), built through the emplacement of pyroclastic rocks and lava flows (Fig. 1a).

79 The main cone of Nyiragongo has several degassing sites (Tedesco et al., 2010) and a semi-
80 permanent lava lake at least since 1928 (Tazieff, 1984, 1994), which has been involved in a few
81 eruptive events, the most recent of which took place in 1977 and 2002 (Tedesco et al., 2007;
82 Chakrabarti et al., 2009). Both eruptive events in 1977 and 2002 occurred outside the crater,
83 triggering drainage of magma stored in the crater lava lake and in its superficial reservoir. For the
84 first time in its recent history, the inner crater was also the site of intracalderic spatter activity,
85 which generated a small scoria cone and a lava flowing towards the lava lake in February 2016
86 (Burgi et al., 2018; Fig. 1b). This activity continued through 2017, and is still ongoing. Magmas
87 currently feeding the current activity are well known for their very low viscosity (the lowest
88 recorded viscosity among terrestrial magmas; Chakrabarti et al., 2009; Burgi et al., 2018) and for
89 their low phenocryst charge. Because of the extremely fluid lava and relatively steep slopes of the
90 volcano, the January 17, 2002 lava flow drained the inner lava lake reaching a speed >50 km/h
91 (Tedesco, 2003, Tedesco et al., 2007). The liquidus temperature of the magma in the lava lake is ca.
92 1100 °C, and the temperature measured at the lava lake surface and with geothermometric estimates
93 is ca. 980 °C (Sahama, 1978; Sawyer et al., 2008; Spampinato et al., 2013; Valade et al., 2018;
94 Burgi et al., 2018). The samples of this study were collected by D.T.; two of them were selected for
95 detailed trace element geochemistry of glasses and associated phases, due to their glassy and
96 extremely fresh appearance in the hand specimen and in thin section. Sample of the lava of 2002
97 belongs to the Muningi flow; it was collected along the 500-800 m long fracture on the Kivu lake
98 shore (Fig. 1d), at an individual flow entering Lake Kivu. The lava of the 2016 outpoured from the
99 intracrateric spatter cone; it was collected above the third platform inside the Nyiragongo main
100 crater, next to the spatter cone and the lava lake (Fig. 1b, 1c and Burgi et al., 2018).
101
102 **3. Analytical methods**
103

The bulk-rock major and trace elements of the samples used in this study were analysed by X-ray fluorescence (XRF) using a Panalytical Axios instrument at the University of Napoli (cf. Cucciniello et al., 2017, for further analytical details). Analytical uncertainties are in the order of 1-2% for major elements and 5-10% for trace elements (Table 1). The weight loss on ignition (L.O.I.) was determined with standard gravimetric techniques, after igniting one gram of rock powder at 1000 °C for 6 h. Lanthanides (REE) and other trace elements were determined by Inductively Coupled Plasma-Mass Spectrometry (ICP-MS) at Activation Laboratories (Ancaster, Ontario; see http://www.actlabs.com for a full description of the analytical techniques). The major element concentrations of mineral and glass phases were determined at DISTAR, University of Napoli Federico II, by Energy Dispersive Spectrometry (EDS) microanalyses using an Oxford Instruments Microanalysis Unit equipped with an INCA X-act detector and a JEOL JSM-5310 Scanning Electron Microscope (SEM) using a JEOL JSM5310. Measurements were done with an INCA X-stream pulse processor operating at 15 kV primary beam voltage, 50-100 mA filament current, variable spot size and 50 s net acquisition time. The following reference materials were used for calibration: diopside (Mg), wollastonite (Ca), albite (Al, Si, Na), rutile (Ti), almandine (Fe), Cr_2O_3 (Cr), rhodonite (Mn), orthoclase (K), apatite (P), fluorite (F), barite (Ba), strontianite (Sr), Smithsonian orthophosphates (La, Ce, Nd, Sm, Y), pure vanadium (V) and Corning glass (Th and U). LA-ICP-MS trace element analyses were performed in olivine, clinopyroxene, melilite, apatite, magnetite, nepheline, leucite and glass of selected areas (cf. Fig. 2). Analyses were carried out at IGG-CNR of Pavia by Laser Ablation-Inductively Coupled Plasma-High Resolution Mass Spectrometry (LA-ICP-HRMS). The microprobe consists of a double-focusing sector-field analyser (Finnigan Mat, Element I) coupled with a Q-switched Nd:YAG laser source (Quantel Brilliant). The fundamental emission of the laser source (1064 nm, in the near-IR region) was converted to 213 nm by three harmonic generators. Helium was used as carrier gas and mixed with Ar downstream of the ablation cell. Spot diameter was varied in the range of 40-60 μm. Quantification was carried out using the NIST SRM 610 glass as external standard (Pearce et al., 1996). Si was used as internal

130 standard for melilite, clinopyroxene, olivine, nepheline, leucite and glass, while Ca was used for
131 apatite and Ti for magnetite. Detection limits are in the range 100-500 ppb for Sc, Ti, and Cr; 10-
132 100 ppb for V, Rb, Sr, Zr, Cs, Ba, Gd, and Pb; 1-10 ppb for Y, Nb, La, Ce, Nd, Sm, Eu, Tb, Dy, Er,
133 Yb, Hf and Ta, and usually <1 ppb for Pr, Ho, Tm, Lu, Th, and U. Precision and accuracy (both
134 better than 10% for concentrations at parts per million level) were assessed by means of repeated
135 analyses of NIST SRM 612 and BCR-2g standards. The composition of the glass beneath the thin
136 section has been documented before the sample analysis to recognize piercing of the rock and to
137 eliminate any glass contribution. The gas background was measured for 60 s, as in any other routine
138 analysis, whereas signals during ablation were acquired for approximately 20-50 s. Analyses were
139 performed with 10 Hz repetition rate of laser and ~1-2.5 mJ/s laser power. Full details are reported
140 in Rocco et al. (2017). Precautions have been taken to avoid any bias on the analytical results.
141 Memory effects have been taken into account leaving more than 1 min between two consecutive
142 analyses and analysing glasses after the minerals. Spurious signals related to memory effects
143 usually affect more blanks (because less time is passed after the previous analysis), thus
144 determining worsening of the detection limits and hindering the quantification of elements at ultra-
145 trace concentration level. Surface contamination during sample polishing and/or handling before the
146 micro-analytical measurement and occurrence of micro-inclusions of glass/fluid have been
147 monitored by detailed inspection of the signal profiles acquired during ablation. Only intervals with
148 parallel signals have been integrated. Anomalous signal contributions at the beginning of the
149 ablation (due to surface contamination) and/or randomly occurring during ablation (possibly related
150 to inclusions and/or memory effect) has been accurately documented and excluded by integration.
151
152 **4. Petrography, classification, bulk-rock and glass geochemistry of the Nyiragongo lavas**
153
154 Samples of the lava of 2002 have a weakly porphyritic texture, consisting mainly of
155 microphenocrysts of melilite, nepheline, leucite, clinopyroxene and olivine (roughly in decreasing

order of abundance), plus diffuse magnetite and apatite microliths, set into a moderately vesicular brown, glassy groundmass (Fig. 2.1, 2.2). Sporadic aggregates of nepheline are also observed. The lava of 2016 is characterized by a moderately porphyritic texture, dominated by euhedral melilite microphenocrysts, euhedral to subhedral olivine, nepheline (occasionally forming almost monomineralic -micro*urtitic*- aggregates; Fig. 2.2), leucite and clinopyroxene microphenocrysts, generally smaller than those observed in the lava of 2002 (Fig. 2.1). The groundmass consists of a poorly vesicular brown glass with sparse magnetite and apatite microlites (Fig. 2.2). Worth noting that we did not find perovskite or schorlomitic garnet in the lava samples. A few Fe-sulfides were found in the lava of 2002. Modal analyses are reported in the Table 1. The lava of 1977 has the same mineral assemblage, with a very finely crystalline groundmass. For this reason it was not selected for subsequent LA-ICP-MS work.

Bulk-rocks

Significant issues are pointed out: the lavas of 1977, 2002, 2016 and 2017 are poor in SiO_2 (39.1-40.8 wt.%), and rich in Fe_2O_{3t} (12.9-13.4 wt.%), alkalies (11.2-12 wt.%) and P_2O_5 (1.3-1.6 wt.%) (Table 1). They plot in the foidite field of the T.A.S. classification diagram (Fig. 3). The samples are classified as melilitites (melilite nephelinites; normative larnite 10-12%), following Woolley et al. (1996). The bulk-rock compositions are evolved, given that MgO is <4.2 wt.%, the Mg# is far lower than that expected in primitive melts [Mg#, $100Mg/(Mg+Fe_t)$=34-37], and the concentration of Cr and Ni is close to the detection limits, as is in the glass compositions (see below). The chemical composition of the two lavas is barely distinguishable from that of the products erupted in 1977 and 2017 (Table 1). The overall chemical affinity is potassic, as is commonplace in other mafic/ultramafic alkaline rocks of the western branch of the West African Rift (e.g., Foley et al., 2012; Pouclet et al., 2017). The P.I. [molar (Na+K)/Al] is 1.04-1.06, hence the bulk-rocks are weakly peralkaline (cf. Marks and Markl, 2017). The concentration of REE of the lavas is high ($\sum$REE=779-800 ppm), and REE are highly fractionated: La/Yb_n is 42-46, whereas Eu/Eu*

(normalized Eu divided by interpolated Eu) is 1-1.1. The Zr/Hf is very high (73) and higher than in other melilitites of the area (the Zr/Hf=57 in the 1957 lava of Mugogo: cf. Chakrabarti et al., 2009; Condomines et al., 2015; Zr/Hf=35 in a reference mantle composition; Lyubetskaya and Korenaga, 2008). The concentration of Nb and Ta is very high (>220 ppm and 12.8 ppm, respectively), and the Nb/Ta ratio is 17, very close to a typical mantle value (15.3; Lyubetskaya and Korenaga, 2008). The Nb/U (25-28), Zr/Nb (1.2-1.3), La/Nb (0.8-0.9) are low, and so is the Th/U of bulk-rocks (and glass) =2.3-2.5, matching the data of Platz et al. (2004), This ratio is significantly lower than the chondritic ratio (≈4), and lower than the U/Th of other melilitites of the Virunga area (the Th/U is 4.3-4.5 in the 1957 lava of Mugogo: cf. Condomines et al., 2015). The lava sample of 2016 has moderate S (0.2 wt.%), Cl (0.13 wt.%) and F (0.17 wt.%) (Table 1).

Glass

The major and trace element concentration of the glass is indistinguishable from that of the bulk-rock compositions (Fig. 3; Table 2, Table 3, Supplementary Table 1). The glassy groundmass of the 2002 lava has a homogeneous composition; it is characterized by low SiO_2 (39.8-40.6 wt.%), Al_2O_3 (13.4-14.6 wt.%), high Na_2O (5.5-7.9 wt.%) and K_2O (3.6-5.8 wt.%), low MgO (2.1-3.9 wt.%), high FeO_t (12-13 wt.%), TiO_2 (2.2-3.2 wt.%) and CaO (10.8-12.6 wt.%; Table 5). The concentration of P_2O_5 is high (1.17±0.17 wt.%). The Mg# is in the range of 23-35, and the glass is slightly peralkaline (P.I., molar (Na+K)/Al=1.12±0.07). Also the glass composition of the 2016 lava is homogeneous for SiO_2 (39.7-41.0 wt.%), Al_2O_3 (14.2-15.3 wt.%), Na_2O (4.5-5.6 wt.%) K_2O (5.2-6.1 wt.%), MgO (3.8-4.4 wt.%), FeO_t (11.4-12.4 wt.%), TiO_2 (2.0-3.3 wt.%) and CaO (11.1-12.5 wt.%; Table 1). The concentration of P_2O_5 is high (1.24±0.25 wt.%). The Mg# ranges from 37 to 40 and the glass is slightly less peralkaline (P.I.=0.99±0.04). The chemical differences between the two lavas are minor. The volatile concentrations in glass of the 2002 lava are rich in SO_3 (0.62±0.1 wt.%), and less so in Cl (0.11±0.06 wt.%), whereas F is close to the detection limits of the employed analytical technique. Similar concentrations are obtained also in the 2016 lava

208 (SO_3=0.41±0.3 wt.%; Cl=0.51±0.13 wt.%; F=0.11±0.05 wt.%; Supplementary Table 1). Worth
209 noting that SO_3- or Cl- saturation in the magmatic system was not achieved at this degree of
210 crystallization, given the lack of sulphur- or chlorine-bearing feldspathoids (haüyne, nosean,
211 sodalite). Nevertheless, sodalite is described in Shaheru lavas (Andersen et al., 2012). This is a
212 significant difference with strictly comparable rocks of magmatic systems such as Mt. Vulture
213 (Italy) and Kaiserstuhl (Germany), having (rare) melilite-rich rocks along with haüyne, nepheline
214 and leucite, and high and comparable bulk-rock sulphur (and chlorine) concentrations (cf. Sahama,
215 1962; Melluso et al., 2011b and references therein; Braunger et al., 2018).
216
217 **5. Major and trace element composition of the mineral phases**
218
219 *Melilite.* The melilite of Nyiragongo lava of 2002 is a solid solution of åkermanite ($Ca_2MgSi_2O_7$,
220 43-55 mol.%), soda-melilite ($CaNaAlSi_2O_7$, 27-35 mol.%), Fe-åkermanite ($Ca_2FeSi_2O_7$,14-18
221 mol.%) and gehlenite ($Ca_2Al_2SiO_7$, 2-6 mol.%), in order of decreasing abundance. The Mg# varies
222 little (65-81), with a significant variation in Al_2O_3 (=5.5-10.8 wt.%) and Na_2O (2.3-6.2 wt.%),
223 indicating that the main atomic substitutions are CaMg->NaAl and, subordinately, Mg->Fe^{2+},
224 already observed in the composition of magmatic melilites worldwide (references in Fig. 4a;
225 Supplementary Table 2). Melilite of the lava of 2016 has just slightly different composition with
226 respect to that of 2002 lava (53-66 mol.% åkermanite, 23-26 mol.% soda-melilite, 14-22 mol.% Fe-
227 åkermanite and 2-6 mol.% gehlenite). The Mg# varies from 77 to 79 (Supplementary Table 2). The
228 Sr concentration is relatively low (0.4-0.7 wt.% SrO), similarly to melilite of other Nyiragongo
229 rocks (e.g., Platz et al., 2004). Melilite has low Sc, Ni and Cr, widely variable V (8-153 ppm), and
230 high Zn (>210 ppm) and Co (>39 ppm). The Sr concentration obtained with LA-ICP-MS is high
231 and varies little (4700-5200 ppm), consistently with the relatively uniform major element
232 composition of this phase, and with microprobe analyses. The concentration of LREE is quite
233 remarkable (e.g., La=67-170 ppm; Ce=124-200 ppm), The REE patterns are steep and highly

LREE-enriched (La/Yb_n=55-118), may have peaks at Eu in the chondrite-normalized diagrams (Eu/Eu*=0.8-1.5 in the 2016 lava, Eu/Eu*=0.9-2.1 in the 2002 lava; Table 2). The high concentration of LREE is to be related to the presence of the important eightfold coordination site hosting the large ions Ca and Na (cf. Bindi and Bonazzi, 2003; Merlini et al., 2008). The HREE concentrations are a few times the chondritic values, due to the low concentration of ferromagnesian elements and the small -tetrahedral- site hosting Mg and Fe that should be the site for hosting also HREE. The concentration of Rb, Ba, Y, Zr, Hf, Nb, Ta, U, Th and Pb is low to negligible (Table 2), as is that of titanium.

Nepheline and leucite. Nepheline in sample NY02 has composition $Ne_{56-75}Ks_{23-41}Sil_{2-6}$ (components in wt.%), whereas in the lava of 2016 is slightly more potassic ($Ne_{54-64}Ks_{35-45}Sil_{1-3}$), having K_2O up to 12.3 wt.%, matching the most potassium-rich nephelines found in Africa (Boctor and Yoder, 1986; Melluso et al., 2011a; Antao and Nicholls, 2018). Similar range of compositions has been found in the 1977 lava (Fig. 4b). The Na/(Na+K) ratio of nepheline varies significantly (0.58-0.76; Supplementary Table 3); this large variation is to be expected for both temperature decrease and cocrystallization with leucite. The low excess silica in magmatic nepheline is expected when this phase crystallizes in highly silica-undersaturated magmas (e.g., Boctor and Yoder, 1986; Melluso et al., 2010, 2011a, 2011b and references therein; Fig. 4b). The concentration of CaO in nepheline, though significant, does not reach 1.7 wt.% (Supplementary Table 3). The composition of leucite is stoichiometric and quite homogeneous for both samples; it is relatively poor in Ba (0-1 wt.% BaO). Concerning trace elements, the concentration of Sr is one order of magnitude higher in nepheline (600-829 ppm) than in leucite (36-83 ppm). Conversely, Rb, Cs and Ba are one to three orders of magnitude higher in leucite (up to 1596 ppm, 39 ppm and 3536 ppm, respectively) than in nepheline (up to 149 ppm, 0.4 ppm and 305 ppm, respectively; Table 2). Rare earths and most other analyzed elements show negligible concentrations in both phases (Table 2).

Clinopyroxene. Clinopyroxene is rare. The Ca-Mg-Fe diagram indicates that the compositions of the 2016 lava are mostly diopsides (Fig. 4c) and have Mg# from 68 to 78. The Al_2O_3 concentration (1.2–8.8 wt.%) considerably increases with decreasing Mg#, as well as that of TiO_2 (1.1-5.4 wt.%). The Al^{VI} [Al_t-(2-Si) apfu for six oxygens] is totally negligible nothwistanding high and increasing Al_t and not-very-oxidized conditions (hence low calculated Fe^{3+} in Ca-rich pyroxene, relatively low magnetite component of spinel), pointing out that these clinopyroxenes are solid solutions of diopside, hedenbergite and the low-pressure molecule $CaTiAl_2O_6$ (up to 16 mol.%), like other clinopyroxenes of Nyiragongo, or in other melilitites worldwide (Boctor and Yoder, 1986; Dunworth and Wilson, 1998; Platz et al., 2004; Melluso et al., 2011a). The Na_2O concentration is low (<0.4 wt.% Na_2O), as expected in clinopyroxene crystallized in not-yet peralkaline magmas. The clinopyroxene of the 2002 lava reaches even higher concentration of Al_2O_3 and TiO_2 (up to 11.5 and 8.3 wt.%, respectively; up to 24 mol. % $CaTiAl_2O_6$; Supplementary Table 4). Similar ranges are found in the lava of 1977, with also more Fe-rich compositions (Fig. 4c). Due to the presence of important octahedral site(s) in clinopyroxene, the first row transition elements have relatively high concentration (e.g., V=200-220 ppm, Sc=23-24 ppm, Table 2), and so is for other trace elements with marked affinity for octahedral sites (e.g., Zr=336-348 ppm). Clinopyroxene has far higher concentrations of HREE than melilite (see above), but lower LREE and therefore LREE/HREE ratios (La/Yb_n=20-23; Fig. 5 Table 2). Eu/Eu* varies from 1 to 1.2.

Olivine. Olivine is quite a rare phase. The composition of the olivine microlites in the lava of 2002 is rather homogeneous, ranging from $Ca_2Mg_{71}Fe_{27}$ to $Ca_2Mg_{75}Fe_{23}$, hence the forsterite content [fo=Mg*100/(Mg+Fe)] ranges from 71 to 74 (Supplementary Table 5; Fig. 4c). The olivine composition of the lava of 2016 is nearly identical in composition ($Ca_2Mg_{75}Fe_{23}$; $fo_{73\text{-}76}$; Supplementary Table 6). The lava of 1977 has a far larger range of compositions, towards Ca-rich fayalite ($fo_{85\text{-}13}$; CaO up to 4.2 wt.%). Relatively highly forsterite-rich olivines with high CaO (up to 1.7 wt.%), as those of the Nyiragongo samples of this study, are common feature in Ca-rich

286 melilite-bearing mafic/ultramafic volcanics worldwide (e.g., Melluso et al., 2010, 2011a and
287 references therein; Braunger et al., 2018), and may have their extreme in the kirschsteinite
288 ($CaFeSiO_4$) found in evolved lavas of the Shaheru cone (Sahama and Hytönen, 1957; Fig. 4c) and
289 in the groundmass of some Alban Hills lavas in Italy (the "*cecilite*"; Melluso et al., 2010 and
290 references therein). The Nyiragongo olivines have high Co (193-221 ppm), Ni (287-413 ppm) and
291 Zn (161-272 ppm), low Sc (2.5-4.6 ppm), V (9-34 ppm) and Cr (<114 ppm). Other elements vary
292 irregularly, including Y, Sr, Zr and REE (Table 2).
293
294 *Apatite.* Apatite compositions are hydroxylapatite and fluorapatite: F ranges from 0.5 to 2 wt.%
295 (Supplementary Table 6). Apatite is rich in REE (∑REE=4300-5300 ppm), has strong LREE/HREE
296 fractionation (La/Yb_n=127-139) and no Eu troughs (Eu/Eu*=0.9-1). Apatite has also high Y (132-
297 164 ppm) and Sr (5000-6000 ppm), and significant Th (29-41 ppm) and U (7-8 ppm). Other
298 elements are in low concentration (Table 2; Fig. 5).
299
300 *Magnetite.* The spinel phase in the Nyiragongo lavas is a quite homogeneous magnetite-ulvöspinel
301 solid solution: Usp_{48-61} in the lava of 2002 and Usp_{51-55} in the lava of 2016 (Supplementary Table 7).
302 The concentration of Al_2O_3 varies from 4.4 to 6.8 wt.%, and MgO varies even less (5.9-7 wt.%).
303 Magnetite has the expected notable concentrations of transition elements (V>3000 ppm, Cr=250-
304 400 ppm, Co=330-350 ppm, Ni=630-720 ppm, Zn=650-860 ppm), with low Sc (7-9 ppm), and
305 negligible concentrations of REE and other elements, excluding Zr (70-90 ppm) Nb (48-52 ppm),
306 Hf (1-2 ppm) and Ta (4.6-4.8 ppm) (Table 2).
307
308 **6. Discussion**
309
310 **6.1. Petrology and assessment of mineral/melt equilibria**
311

The evolved nature of the present-day Nyiragongo magmas and their derivation from more primitive olivine melilitite compositions is indicated by the geochemistry (e.g., relatively low MgO and Sc, negligible Cr and Ni), mineral chemistry (see above) and the position in pertinent synthetic systems, such as the larnite-enstatite-nepheline pseudoternary phase diagram (Pan and Longhi, 1990) (Fig. 6a). This diagram also indicates that Nyiragongo magmas are close to, or plot on, low-pressure cotectics involving mafic phases and two feldspathoids, in an area far from the thermal/compositional barrier separating feldspar-bearing melts from melilite-bearing melts. The limited major and trace element compositional variations, together with the petrographic evidence, suggest that all mineral phases (melilite+ two feldspathoids +olivine +clinopyroxene +apatite +magnetite) in the studied samples crystallized almost contemporaneously at atmospheric pressure in equilibrium with the host melilite nephelinite melt, which is characterized by an evolved composition, a very fresh glass-rich matrix, a highly depolymerized nature (low SiO_2 and Al_2O_3, high alkalis and iron, slight peralkalinity, NBO/T=0.46-0.47, compared to ≈0 for a rhyolite melt and ≈1 for an olivine melilitite melt), low silica activity (a_{SiO2}≤0.4 at 1000°C, according to Barker, 2001, compared to a_{SiO2}=1 in quartz-bearing systems), and a temperature close to 1000°C (cf. Burgi et al., 2018 and references therein). The assemblage of the Nyiragongo lavas of 2002 and 2016 matches that of a pseudo-invariant point ol+cpx+mel+lc+ne+liq postulated at ca. 1100°C by Gupta et al. (1973) and Gupta (2015) (Fig. 6b), which indicates: a) the derivation of Nyiragongo magmas of 2002 and 2016 from more olivine-rich precursors, yet present in the area (cf. Platz et al., 2004; Minissale, 2018), and, more importantly, b) the mineral assemblage of Nyiragongo magmas of 2002 and 2017 can be considered broadly in equilibrium from a thermodynamic point of view (cf. also Fig. 2.1 and 2.2). To this latter respect, we note that the highest Mg# of melilite we analyzed (80.6) is slightly higher than the highest Mg# of clinopyroxene (78.4) and forsterite content of olivine (76.3). Given the different Fe/Mg partitioning of between these phases and silicate melts (e.g., different $Kd_{Fe/Mg}$; cf. Roeder and Emslie, 1970; Bédard, 2010), of which that of melilite is largely unknown, though supposedly more similar to that of clinopyroxene (Supplementary Fig. 1), we

tentatively suggest that the Mg# of the phases indicate the onset of cotectic crystallization in broadly the same melt composition having Mg#=35-40.

6.2. Mineral/glass partition coefficients

The Nyiragongo is a unique case where mineral and glass compositional data can be fruitfully used in order to calculate partition coefficients for highly silica undersaturated magmas, taking also into account the high concentration of elements in lavas and coexisting equilibrium phases, which is generally sufficient to achieve high analytical reproducibility and limited non-equilibrium partitioning. We remark the role of liquidus crystallization of melilite in magmas where any feldspar could not crystallize, due to the very high degree of silica undersaturation (equivalent to the so-called melilite-plagioclase incompatibility in alkali-rich, *orthomagmatic* rocks; Yoder, 1973), and the uniform composition of glasses, phases and bulk-rocks. Very intriguingly, there are no comparable datasets about trace element partitioning in melilite and in the other liquidus phases of the Nyiragongo magmas in the recent literature (cf. Arzamastsev et al., 2009 for other cases). Mineral/glass partition coefficients are reported in Table 3 and Fig. 7.

Melilite. Rare earth elements, and particularly HREE, are incompatible in melilite (e.g., D_{La}=0.46-0.48; D_{Lu}=0.18-0.25; Table 3), as already pointed out by the work of Onuma et al. (1981) on similar samples and Beckett et al. (1990) on meteorites, and also has a small peak at Eu (D_{Eu}=0.56-0.57) compared to Sm and Gd (Table 3). Melilite has an expected quite large partition coefficient for Sr (D_{Sr}=1.8-2.2). Actually, this phase can have Sr as a major cation (Fitton and Hughes, 1981; Velde and Rachdi, 1988; Melluso et al., 2010), but this feature is rare, usually related to a late stage of crystallization, depending upon presence -or absence- of significant amounts of earlier Sr-scavenging phases (e.g., perovskite, apatite, titanite), and ultimately refers to more evolved magmatic systems than those of this study, or to the late groundmass phases of holocrystalline rocks. The partitioning of Sr in melilite may be the same as in a calcic plagioclase of “basaltic”

364 systems (cf. Sun et al., 2018, and references therein). Therefore, melilite removal in significant
365 amounts should create a trough at Sr in the mantle normalized diagrams of more evolved rocks,
366 with respect to neighbouring elements such as La, Ce and Nd. The concentration of Eu and the Eu
367 peaks in the REE patterns of melilite are minor or absent, when compared to the worldwide
368 composition of liquidus *feldspars* (plagioclase, anorthoclase and potassic sanidine, having Eu/Eu*>
369 or >> 20-30, at Eu concentration=0.5-2 ppm; Supplementary Fig. 2) in less silica-undersaturated
370 rocks.
371 Nepheline and leucite have distinctly different trace element distribution, particularly for LFSE,
372 which are justified by the dominant cations and the size of the sites. The largest low-charged cations
373 (Cs, Ba, Rb) are significantly hosted in leucite, whereas Sr (and far less so, Eu) markedly prefers
374 nepheline, though still being a highly incompatible element (Table 3). The concentration ratios of
375 Rb and Cs for leucite are of the same magnitude of those obtained by Foley and Jenner (2004) in
376 the olivine lamproite of Gaussberg, whereas Ba (thus D_{Ba}) is far higher in the Nyiragongo leucite
377 (Table 3).
378 Clinopyroxene. The few mineral/glass partition coefficients of REE in clinopyroxene are very
379 similar to values obtained by Onuma et al. (1981), with the exception of lower La and Ce. Again,
380 these numbers indicate that LREE are highly incompatible in diopsidic clinopyroxene of highly
381 alkaline magmas at atmospheric -and higher- pressure (cf. Hart and Dunn, 1993; Fedele et al., 2009
382 and references therein; Ambrosio and Azzone, 2018 and references therein; Supplementary Fig. 3),
383 with HREE being less incompatible, due to their stronger octahedral site preference. Transition
384 elements Sc, Ni and Cr are more compatible than in melilite, whereas V, Zn, Y and Zr are still
385 moderately incompatible (Table 3).
386 The low-forsterite olivine of Nyiragongo has significant partition coefficients for Ni, Co and Zn
387 (Table 3).
388 The REE patterns of apatite have a relative concentration peak in the middle REE relative to the
389 glass compositions, and high apatite/glass partition coefficients (>1 for all the elements). Y is also a

390 highly compatible element (Table 3). The values reported in Table 3 are roughly 5-6 times lower
391 than those calculated in apatites of trachytic or more silicic magmas (cf. Fedele et al., 2015 and
392 references therein). Rather, they are more similar to some calculated for different (*basaltic* to
393 *andesitic*), subalkaline, melt compositions by Prowatke and Klemme (2006), indicating a major
394 compositional control in the partitioning of REE in apatite (likely the degree of polymerization in
395 the melts, cf. Watson and Green, 1981). Apatite has negligible effects on the concentration of
396 HFSE, Rb, Pb, Ba and their ratios. On the other hand, the concentration of Sr is expectedly high
397 (Table 2). As noted elsewhere (Melluso et al., 2017, 2018 and references therein), removal of
398 apatite (though being a significant host for REE, Y and Sr) is unlikely to be the main cause of
399 "complementary", strongly concave REE patterns in evolved highly alkaline rocks, when found.
400 Magnetite scavenges the first row of transition elements (Sc, Ti, V, Cr, Ni, Zn), as expected.
401 Significant partition coefficients are also observed for Zr, Nb, Hf and Ta, though being these
402 elements still highly incompatible (Table 2 and 3).
403 The trace element distribution found in the Nyiragongo phases cannot justify the development of
404 significant Eu troughs in highly alkaline liquids derived from any amount of melilite removal (cf.
405 also Marks and Markl, 2017). Indeed, more evolved rocks from the nearby Shaheru cone (MgO<3
406 wt.%) still do not have Eu troughs in the REE patterns (cf. Platz et al., 2004; Minissale, 2018;
407 Supplementary Figure 4), and melilite-rich cumulate intrusive rocks do not show Eu peaks in the
408 chondrite normalized REE diagrams (e.g., Verhulst et al., 2000; Srivastava and Sinha, 2004).
409
410 **7. Conclusions**
411
412 Natural partitioning of elements between phenocrysts and their incompatible element-rich melilite-
413 nephelinite glasses (and bulk-rock compositions) of recent Nyiragongo activity, the most silica
414 undersaturated magmas currently erupted on earth, and forming lava lakes, provides a fresh look to
415 the distribution of REE and other trace elements in melilite (when this phase can be considered the

main “mafic” phenocryst on the liquidus, i.e., when clinopyroxene and olivine are minor), and in the companion felsic and mafic mineral phases. We think that removal of significant amounts of melilite is very difficult to be convincingly demonstrated in any volcanic or plutonic complex bearing this phase worldwide (cf. Braunger et al., 2018 for examples). In addition, melilite cannot be considered as the analogue of any feldspar and feldspathoid -or clinopyroxene- in feldspar-free magmas, also from the perspective of trace element partitioning. Melilite, nepheline, leucite, olivine, diopsidic clinopyroxene, magnetite and apatite are unable to significantly fractionate ratios between highly charged cations with similar geochemical behaviour (Zr/Hf, Nb/Ta, Th/U). Hence, the causes of some anomalous trace element ratios found in the Nyiragongo lavas (cf. Platz et al., 2004; Chakrabarti et al., 2009; Condomines et al., 2015) must be sought in processes different from fractional crystallization involving any amount of these phases. Even though mineral chemistry and mineral assemblages are not indicative of a peralkaline rock/magma, the tendency of the Nyiragongo magmatic system to evolve to peralkaline compositions is well evidenced in some of the rocks of the Shaheru cone, having late-stage (or post-magmatic) phases more typical of peralkaline compositions (e.g., combeite, götzenite, Andersen et al., 2012), as well as phases of highly evolved, highly silica undersaturated rocks (e.g., fayalite and kirschsteinite; Fig. 4). The presence of growing crystals of relatively low-density phases such as nepheline and leucite also indicate the possibility of accumulation (floating) processes in shallow magmatic reservoirs (e.g., Demant et al., 1994; Platz et al., 2004). The substantially identical composition of the 2002 and 2016 lavas, as well as that of the lavas erupted in 1977 and 2017, implies a steady-state magma supply system in this interval of the Nyiragongo recent activity, where only mildly evolved magmas reach the summit area from different pathways starting from the subvolcanic reservoir (cf. Burgi et al., 2018), and where more complex petrogenetic processes (e.g., magma mixing between highly evolved magmas, refilling the shallow reservoirs from hotter, more primitive melts) are not active, judging from the substantially uniform mineral assemblage, mineral chemistry and bulk-rock geochemistry.

Acknowledgements

We gratefully thank Roberto de' Gennaro (particularly), Ciro Cucciniello, Lorenzo Fedele, John Longhi, Michael Marks, Michel Condomines, Sergio Bravi, Pierre-Yves Burgi, Roger Mitchell, and the late Fabio Mazzeo for their help with the analytical work, for their continued interest to the topic, and for interesting discussions. This research was granted by PRIN 2015 (20158A9CBM) to Leone Melluso. Two anonymous reviewers offered useful comments to help improve an initial draft.

References

Ambrosio, M.R., Azzone, R.G., 2018. The influence of crystal and melt compositions on the REE+Y partitioning between clinopyroxene and basanitic/tephritic melts of Cretaceous alkaline magmatism on the southeastern part of the South American Platform, southeast Brazil. The Canadian Mineralogist 56, 303-329.

Andersen, T., Elburg, M., Erambert, M., 2012. Petrology of combeite- and götzenite-bearing nephelinite at Nyiragongo, Virunga Volcanic Province in the East African Rift. Lithos 152, 105-121.

Antao, S.M., Nicholls, J.W., 2018. Crystal chemistry of three volcanic K-rich nepheline samples from Oldoinyo Lengai, Tanzania and Mount Nyiragongo, Eastern Congo, Africa. Frontiers in Earth Science 6, 155. https://dx.doi.org/10.3389/feart.2018.00155

Arzamastsev, A.A., Arzamastseva, L.V., Bea, F., Montero, P., 2009. Trace elements in minerals as indicators of the evolution of alkaline ultrabasic dike series: LA-ICP-MS data for the magmatic provinces of northeastern Fennoscandia and Germany. Petrology 17, 46-72.

Barker, D.S., 2001. Calculated silica activities in carbonatite liquids. Contributions to Mineralogy and Petrology 141, 704-709.

468 Beckett, J.R., Spivack, A.J., Hutcheon, I.D., Wasserburg, G.J., Stolper, E.M., 1990. Crystal
469 chemical effects on the partitioning of trace elements between mineral and melt –an
470 experimental study of melilite with applications to refractory inclusions from carbonaceous
471 chondrites. Geochimica et Cosmochimica Acta 54, 755-774.
472 Bédard, J.H., 2010. Parameterization of the Fe=Mg exchange coefficient (Kd) between
473 clinopyroxene and silicate melts. Chemical Geology 274, 169-176.
474 Bindi, L., Bonazzi, P., 2003. Low-temperature study of natural melilite ($Ca_{1.89}Sr_{0.01}Na_{0.08}K_{0.02}$)
475 ($Mg_{0.92}Al_{0.08}$) ($Si_{1.97}Al_{0.03}$)O_7: towards a commensurate value of the q vector. Physics and
476 Chemistry of Minerals 30, 523-526.
477 Boctor N.Z., Yoder, H.S. jr., 1986. Petrology of some melilite-bearing rocks from Cape Province,
478 Republic of South Africa: relationships to kimberlites. American Journal of Science 286, 513-
479 539.
480 Braunger, S., Marks, M.A.W., Walter, B.F., Neubauer, R., Reich, R., Wenzel, T., Parsapoor, A.,
481 Markl, G., 2018. The petrology of the Kaiserstuhl volcanic complex, SW Germany: the
482 importance of metasomatized and oxidized lithospheric mantle for carbonatite generation.
483 Journal of Petrology 59, 1731-1762, https://dx.doi.org/10.1093/petrology/egy078
484 Burgi, P.-Y., Minissale, S., Melluso, L., Mahinda, C.K., Cuoco, E., Tedesco, D., 2018. Models of
485 the formation of the February 29, 2016 new spatter cone inside Mount Nyiragongo. Journal of
486 Geophysical Research 123, https://dx.doi.org/10.1029/2018JB015927
487 Chakrabarti, R., Basu, A.R., Santo, A.P., Tedesco, D., Vaselli, O., 2009. Isotopic and geochemical
488 evidence for a heterogeneous mantle plume origin of the Virunga volcanics, Western rift, East
489 African Rift system. Chemical Geology 259, 273-289.
490 Condomines, M., Carpentier, M., Ongendangenda, T., 2015. Extreme radium deficit in the 1957 AD
491 Mugogo lava (Virunga volcanic field, Africa): its bearing on olivine-melilitite genesis.
492 Contributions to Mineralogy and Petrology 169, 29.

493 Cucciniello, C., Choudary, A.K., Zanetti, A., Sheth, H.C., Vichare, S., Pereira, R., 2014.
494 Mineralogy, geochemistry and petrogenesis of the Khopoli mafic intrusion, Deccan Traps,
495 India. Mineralogy and Petrology 108, 333-351.
496 Cucciniello, C., Melluso, L., le Roex, A.P., Jourdan, F., Morra, V., de' Gennaro, R., Grifa, C., 2017.
497 From nephelinite, basanite and basalt to peralkaline trachyphonolite and comendite in the
498 Ankaratra volcanic complex, Madagascar: $^{40}Ar/^{39}Ar$ ages, phase compositions and bulk-rock
499 geochemical and isotopic evolution. Lithos 274-275, 363-382.
500 https://dx.doi.org/10.1016/j.lithos.2016.12.026
501 Dawson, J.B., Hinton, R.W., Steele, I.M., 2008. The composition of anorthoclase and nepheline in
502 Mount Kenya phonolite and Kilimanjaro trachyte, and crystal-glass partitioning of elements.
503 The Canadian Mineralogist 46, 1455-1464
504 Demant, A., Lestrade, P., Ruanza, T.L, Kampunzu, A.B., Durieux, J., 1994. Volcanological and
505 petrological evolution of Nyiragongo volcano, Virunga volcanic field, Zaire. Bulletin of
506 Volcanology 56, 47-61.
507 Dunworth, E.A., Wilson, M., 1998. Olivine melilitites from the SW German Tertiary volcanic
508 province: mineralogy and petrogenesis. Journal of Petrology 39, 1805-1836.
509 Fedele, L., Lustrino, M., Melluso, L., Morra, V., Zanetti, A., Vannucci, R., 2015. Trace element
510 distribution in plagioclase, alkali feldspar, Ti-magnetite, biotite and apatite in evolved potassic
511 liquids from Campi Flegrei (Southern Italy). American Mineralogist 100, 233-249.
512 https://dx.doi.org/10.2138/am-2015-4995
513 Fedele, L., Zanetti, A., Lustrino, M., Melluso, L., Morra, V., Vannucci, R., 2009. Insights on
514 clinopyroxene/liquid trace element partitioning in natural trachyte-phonolite systems: a EMP/LA-
515 ICP-MS case study from Campi Flegrei (Italy). Contributions to Mineralogy and Petrology 158,
516 337-356. https://dx.doi.org/10.1007/s00410-009-0386-5
517 Fitton, J.G., Hughes, D.J., 1981. Strontian melilite in a nephelinite lava from Etinde, Cameroon.
518 Mineralogical Magazine 44, 261-264.

519 Foley, S.F., Jenner, G.A., 2004. Trace element partitioning in lamproitic magmas – the Gaussberg
520 olivine leucitite. Lithos 75, 19-38.
521 Foley, S.F., Link, K., Tiberindwa, J.V., Barifaijo, E., 2012. Patterns and origin of igneous activity
522 around the Tanzanian craton. Journal of African Earth Sciences 62, 1-18.
523 Gupta, A.K. (2015) Origin of potassium-rich silica-deficient igneous rocks. Springer, 536 pp. ISBN:
524 978-81-322-2082-1
525 Gupta, A.K., Venkateswaran, G.P., Lidiak, E.G., Edgar, A.D., 1973. The system diopside-nepheline-
526 akermanite-leucite and its bearing on the genesis of alkali-rich mafic and ultramafic volcanic
527 rocks. The Journal of Geology 81, 209-218.
528 Guzmics, T., Mitchell, R.H., Szabò, C., Berkesi, M., Milke, R., Ratter, K., 2012. Liquid
529 immiscibility between silicate, carbonate and sulfide melts in melt inclusions hosted in co-
530 precipitated minerals from Kerimasi volcano (Tanzania): evolution of carbonated nephelinitic
531 magma. Contributions to Mineralogy and Petrology 164, 101-122.
532 Hart, S.R., Dunn, T., 1993. Experimental cpx/melt partitioning of 24 elements. Contributions to
533 Mineralogy and Petrology 113, 1-8.
534 Lyubetskaya, T., Korenaga, J., 2007. Chemical composition of Earth's primitive mantle and its
535 variance: 1. methods and results. Journal of Geophysical Research 112, B03211,
536 https://dx.doi.org/10.1019/2005JB004223
537 Marks, M.A.W., Markl, G., 2017. A global review of agpaitic rocks. Earth-Science Reviews 173,
538 229-258.
539 Melluso L., Conticelli S., de' Gennaro R., 2010. Kirchsteinite in the Capo di Bove melilite leucitite
540 lava (cecilite), Alban Hills, Italy. Mineralogical Magazine 74, 887-902.
541 Melluso L., Guarino V., Lustrino M., Morra V., de' Gennaro R., 2017. The REE- and HFSE-
542 bearing phases in the Itatiaia alkaline complex (Brazil), and geochemical evolution of feldspar-
543 rich felsic melts. Mineralogical Magazine 81, 217-250.

544 Melluso, L., Hergt, J.M., Zanetti, A., 2014. The late crystallization stages of low-Ti, low-Fe
545 tholeiitic magmas: insights from evolved Antarctic and Tasmanian rocks. Lithos 188, 72-83.
546 https://dx.doi.org/10.1016/j.lithos.2013.10.032
547 Melluso, L., le Roex, A.P., Morra, V., 2011a. Petrogenesis and Nd-Pb-Sr- isotope geochemistry of
548 the olivine melilitites and olivine nephelinites ("*ankaratrites*") in Madagascar. Lithos 127, 505-
549 521. https://dx.doi.org/10.1016/j.lithos.2011.08.003
550 Melluso L., Lustrino M., Ruberti E., Brotzu P., Gomes C.B., Morbidelli L., Morra V., Svisero D.P.,
551 d'Amelio F., 2008. Major and trace element composition of olivine, perovskite, clinopyroxene,
552 Cr-Fe-Ti oxides, phlogopite and host kamafugites and kimberlites, Alto Paranaíba, Brazil. The
553 Canadian Mineralogist 46, 19-40. https://dx.doi.org/10.3749/canmin.46.1.19
554 Melluso, L., Morra, V., de' Gennaro, R., 2011b. Coexisting Ba-feldspar and melilite in a
555 melafoidite lava of Mt. Vulture, Italy: role of volatiles and alkaline earths in bridging a
556 petrological incompatibility. The Canadian Mineralogist 49, 983-1000.
557 https://dx.doi.org/10.3749/canmin.49.4.983
558 Melluso L., Srivastava R.K., Guarino V., Zanetti A., Sinha A.K., 2010. Mineral compositions and
559 magmatic evolution of the Sung Valley ultramafic-alkaline-carbonatitic complex (NE India).
560 The Canadian Mineralogist 48, 205-229. https://dx.doi.org/10.3749/canmin.48.1.205
561 Melluso, L., Tucker, R.D., Cucciniello, C., le Roex, A.P., Morra, V., Zanetti, A., Rakotoson, R.L.,
562 2018. The magmatic evolution and genesis of the Quaternary basanite-trachyphonolite suite of
563 Itasy (Madagascar) as inferred by geochemistry, Sr-Nd-Pb isotopes and trace element distribution
564 in coexisting phases. Lithos 310-311, 50-64. https://dx.doi.org/10.1016/j.lithos.2018.04.003
565 Merlini, M., Gemmi, M., Cruciani, G., Artioli, G., 2008. High-temperature behaviour of melilite: in
566 situ X-ray diffraction study of gehlenite-åkermanite-Na melilite solid solution. Physics and
567 Chemistry of Minerals 35, 147-155.
568 Minissale, S., 2018. Petrogenesis of alkaline and strongly alkaline volcanism: examples from
569 African Rift. PhD dissertation, Università di Napoli Federico II, 143 pp.

570 Onuma, N., Ninomiya, S., Nagasawa, H., 1981. Mineral/groundmass partition coefficients for
571 nepheline, melilite, clinopyroxene and perovskite in melilite-nepheline basalt, Nyiragongo,
572 Zaire. Geochemical Journal 15, 221-228.
573 Pan, V., Longhi, J., 1990. The system Mg_2SiO_4- Ca_2SiO_4- $CaAl_2O_4$- $NaAlSiO_4$- SiO_2: one
574 atmosphere liquidus equilibria of analogs of alkaline mafic lavas. Contributions to Mineralogy
575 and Petrology 105, 569-584.
576 Platz, T., Foley, S.F., André, L., 2004. Low-pressure fractionation of the Nyiragongo volcanic
577 rocks, Virunga province, D.R. Congo. Journal of Volcanology and Geothermal Research 136,
578 269-295.
579 Pouclet, A., Bellon, H., Bram, K., 2017. The Cenozoic volcanism in the Kivu rift: assessment of the
580 tectonic setting, geochemistry, and geochronology of the volcanic activity in the south-Kivu and
581 Virunga regions. Journal of African Earth Sciences 121, 219-246.
582 Prowatke, S., Klemme, S., 2006. Trace element partitioning between apatite and silicate melts.
583 Geochimica et Cosmochimica Acta 70, 4513-4527.
584 Rocco, I., Zanetti, A., Melluso, L., Morra, V., 2017. Ancient depleted and enriched mantle
585 lithosphere domains in northern Madagascar: geochemical and isotopic evidence from spinel-to-
586 plagioclase-bearing ultramafic xenoliths. Chemical Geology, 466, 70-85.
587 https://dx.doi.org/10.1016/j.chemgeo.2017.05.016
588 Roeder, P.L., Emslie, R.F., 1970. Olivine-liquid equilibrium. Contributions to Mineralogy and
589 Petrology 29, 275-289.
590 Sahama, Th.G., 1962. Petrology of Mt. Nyiragongo: a review. Transactions of the Edinburgh
591 Geological Society 19, 1-28.
592 Sahama, Th.G., 1978. The Nyiragongo main cone. Musee Royal de l'Afrique Centrale, Tervuren
593 (Belgique). Annales Sciences Geologiques 81, 88.
594 Sahama, Th.G., Hytönen, K., 1957. Kirschsteinite, a natural analogue to synthetic iron monticellite,
595 from the Belgian Congo. Mineralogical Magazine 31, 698-699.

596 Sawyer, G.M., Carn, S.A., Tsanev, V.I., Oppenheimer, C., Burton, M., 2008. Investigation into
597 magma degassing at Nyiragongo volcano, Democratic Republic of Congo. Geochemistry
598 Geophysics Geosystems 9, Q02017
599 Spampinato, L., Ganci, G., Hernandez, P.A., Calvo, D., Tedesco, D., Perez, N.M., Calvari, S., Del
600 Negro, C., Yalire, M.M., 2013, Thermal insights into the dynamics of Nyiragongo lava lake
601 from ground and satellite measurements. Journal of Geophysical Research 118, 5771-5784.
602 https://dx.doi.org./10.1002/2013JB010520
603 Sun, C., Graff, M., Liang, Y., 2018. Trace element partitioning between plagioclase and silicate
604 melt: the importance of temperature and plagioclase composition, with implications for
605 terrestrial and lunar magmatism. Geochimica et Cosmochimica Acta 206, 273-295.
606 Tazieff, H., 1984. Mt. Nyiragongo: Renewed activity of the lava lake. Journal of Volcanology and
607 Geothermal Research 20, 267–280.
608 Tazieff, H., 1994. Permanent lava lakes: Observed facts and induced mechanisms. Journal of
609 Volcanology and Geothermal Research 63, 3-11.
610 Tedesco, D., 2003. The pre-2002 activity - 1995 Nyiragongo and Nyamulagira activity in the
611 Virunga National Park: a volcanic crisis. Acta Vulcanologica 14-15, 149-155.
612 Tedesco, D., Tassi, F., Vaselli, O., Poreda, R.J., Darrah, T., Cuoco, E., Yalire, M., 2010. Gas
613 isotopic signatures (He, C, and Ar) in the Lake Kivu region (western branch of the East African
614 rift system): Geodynamic and volcanological implications. Journal of Geophysical Research,
615 115, B01205; https://dx.doi.org/10.1029/2008JB006227
616 Tedesco, D., Vaselli, O., Papale, P., Carn, S.A., Voltaggio, M., Sawyer, G.M., Durieux, J.,
617 Kasereka, M., Tassi, F., 2007. January 2002 volcano-tectonic eruption of Nyiragongo volcano,
618 Democratic Republic of Congo. Journal of Geophysical Research B112, B09202.
619 Toscani, L., Capedri, S., Oddone M., 1990. New chemical and petrographic data of some
620 undersaturated lavas from Nyiragongo and Mikeno (Virunga-Western African rift – Zaire).
621 Neues Jahrbuch für Mineralogie Abhandlungen 161, 287-302.

Velde, D., Rachdi, H.En-N., 1988. Influence of Sr on an established petrological incompatibility: the association melilite+K-feldspar in a nephelinite from Djebel Targou, central Morocco. Journal of Petrology 29, 585-597.

Valade, S., Ripepe, M., Giuffrida, G., Karume, K., Tedesco, D., 2018. Dynamics of Mount Nyiragongo lava lake inferred from thermal imaging and infrasound array. Earth and Planetary Science Letters 500, 192-204.

Verhulst, A., Balaganskaya, E., Kirnarsky, Y., Demaiffe, D., 2000. Petrological and geochemical (trace elements and Sr-Nd isotopes) characteristics of the Paleozoic Kovdor ultramafic, alkaline and carbonatite intrusion (Kola Peninsula, NW Russia). Lithos 51, 1-25.

Watson, E.B., Green, T.H., 1981. Apatite/liquid partition coefficients for the rare earth elements and strontium. Earth and Planetary Science Letters 56, 405-421.

Wiedenmann, D., Keller, J., Zaitsev, A.N., 2010. Melilite-group minerals at the Oldoinyo Lengai, Tanzania. Lithos 118, 112-118.

Wiedenmann, D., Zaitsev, A.N., Britvin, S.N., Krivovichev, S.V., Keller, J., 2009. Alumoåkermanite, $(Ca,Na)_2(Al,Mg,Fe^{2+})(Si_2O_7)$, a new mineral from the active carbonatite-nephelinite-phonolite volcano Oldoinyo Lengai, northern Tanzania. Mineralogical Magazine 73, 373-384.

Woolley, A.R., Bergman, S.C., Edgar, A.D., Le Bas, M.J., Mitchell, R.H., Scott Smith , B.H., 1996. Classification of lamprophyres, lamproites, kimberlites, and the kalsilitic, melilitic, and leucitic rocks. The Canadian Mineralogist 34, 175-186.

Yoder, H.S. jr., 1973. Melilite stability and paragenesis. Fortschritte der Mineralogie (International Journal of Earth Sciences) 50, 140-173.

Figure captions

Fig. 1. Geomorphological sketch map of the Nyiragongo volcano (a) with the sampling sites of the investigated samples of 2016 (b, c) and 2002 (d). Note that the structural position of the other volcanic complexes of the Virunga is not consistent with the elongation of the Albertine Rift (cf. also Pouclet et al., 2017).

Fig. 2.1. a) b) c) d). Petrographic appearance of the Nyiragongo lavas of 2002 and 2016. Note the abundant melilite laths, the nepheline cluster and the apatite microphenocryst with a laser pit.

Fig. 2.2. a) b) c) d). Backscattered electron (BSE) images of sites in the Nyiragongo lavas of 2002 and 2016: microlites of melilite, olivine, feldspathoids and microphenocrysts of magnetite and apatite are visible in a generally clean glassy matrix. The iron- and calcium-rich nature of the glass is also evident from the more whitish grey tones with respect to most mafic phases. Also note a cotectic intergrowth of nepheline and melilite (±leucite) in b), resembling a granophyre.

Fig. 3. Total alkali vs. silica (T.A.S.) classification diagram (Le Maitre, 2002) with bulk-rock (red circles) and glass analyses (orange rhombs) from the investigated Nyiragongo samples. Other rocks of Nyiragongo (grey) are taken from Platz et al. (2004) and Minissale (2018).

Fig. 4. Composition of the main mineral phases of the 2002 and 2016 lavas. a) Composition of the Nyiragongo melilites in the Åkermanite-Fe-Åkermanite-soda-melilite diagram (mol.%). Melilites of Kaiserstuhl (black lines) are from Braunger et al. (2018); melilites of Italy (grey squares) from Melluso et al. (2011b, 2012 and references therein); melilitites of Madagascar (dark grey triangles) from Melluso et al., 2011a; melilites of Tanzania (grey crosses) from a compilation in Melluso et al. (2010), Wiedenmann et al. (2009, 2010) and Guzmics et al. (2012); b) nepheline compositions of 1977, 2002 and 2016 lavas as plotted in the nepheline-kalsilite-silica diagram (in wt.%); other Nyiragongo nephelines are grey rhombs; the green circle is the Nyiragongo nepheline studied by Antao and Nicholls (2018); nepheline of the Madagascar olivine melilitites from Melluso et al. 2011a (dark grey triangles); c) clinopyroxene and olivine compositions of the 1977, 2002 and 2016 lavas as plotted in the Ca-Mg-Fe diagram (mol.%); clinopyroxenes of other Nyiragongo rocks are from Minissale (2018); clinopyroxenes

of the Madagascan melilitites from Melluso et al. (2011a); olivines from other Nyiragongo rocks (grey circles) from Minissale (2018) and Sahama and Hytönen (1957; the black square).

Fig. 5. a) b) mantle-normalized patterns of bulk-rocks, glass, clinopyroxene, melilite and apatite, relative to mantle composition of Lyubetskaya and Korenaga (2007). Note that K and P were not plotted. The trace element analyses of melilites of Kaiserstuhl and Turyi (taken from Arzamastsev et al., 2009) are also plotted for comparison.

Fig. 6. Phase diagrams with the composition of glasses and bulk-rocks of Nyiragongo (Pan and Longhi, 1990; Gupta, 2015). The continuous lines in (a) are mostly thermal barriers connecting the composition of various phases. They should be seen as projections of planes connecting also olivine (forsterite).

Fig. 7. Diagrams with mineral-glass partition coefficients for REE, compared with known partition coefficients from the literature (data from Table 3).

Table captions

Table 1. bulk-rock compositions of the 2002 and 2016 lavas, together with that of the 1977 eruption and that of the lava outpouring from the spatter cone in 2017. Modal analyses of microphenocrysts and glass are also reported.

Table 2. LA-ICP-MS composition of the phases of 2002 and 2016 lavas (in ppm).

Table 3. The average composition of glasses (in ppm), and partition coefficients, obtained by dividing the average concentration of the elements in the various phases and the average composition of the relative glass. Reference partition coefficients from the literature are also reported (Onuma et al., 1981; Foley and Jenner, 2004, Prowatke and Klemme, 2006; Dawson et al., 2008; Fedele et al., 2015; Ambrosio and Azzone, 2018).

Supplementary Tables

Supplementary Table 1. Glass compositions of the 2002 and 2016 lavas

Supplementary Table 2. Melilite compositions of the 2002, 2016 and 1977 lavas.

Supplementary Table 3. Nepheline and leucite compositions of the 2002, 2016 and 1977 lavas.

Supplementary Table 4. Clinopyroxene compositions of the 2002, 2016 and 1977 lavas.

Supplementary Table 5. Olivine compositions of the 2002, 2016 and 1977 lavas.

Supplementary Table 6. Apatite compositions of the 2002 and 2016 lavas.

Supplementary Table 7. Magnetite compositions of the 2002 and 2016 lavas.

Supplementary figures

Supplementary Fig. 1. Rhodes diagram for olivine, clinopyroxene and melilite compositions of the lavas of 2002 and 2016. The curves are traced at K_dFe-Mg=0.23, 0.27, 0.30 and 0.33 (Bédard, 2010; Roeder and Emslie, 1970). Note that the Mg# of bulk-rocks and mineral phases is calculated with all Fe as divalent.

Supplementary Fig. 2. The chondrite normalized patterns of the Nyiragongo melilites, and comparison with various types of feldspar taken from various places and magmatic series (data are taken from Dawson et al., 2009; Arzamastsev et al., 2009; Cucciniello et al. 2014; Fedele et al., 2015; Melluso et al., 2014, 2018).

Supplementary Fig. 3. Extended bulk-rock concentration ratios for clinopyroxene and melilite. Reference patterns for clinopyroxene of kamafugites, lamproites and silica-undersaturated trachytes are also shown (data from Foley and Jenner, 2004; Melluso et al., 2008; Fedele et al., 2009). Note that the clinopyroxene of the kamafugite (Melluso et al., 2008) coexists with perovskite which heavily scavenges LREE, hence the partition coefficients for a number of elements are much lower than in the Nyiragongo clinopyroxene.

Supplementary Fig. 4. Chondrite-normalized REE diagram of the Nyiragongo-Shaheru bulk rocks with those of this study. The data are taken from this study, Platz et al. (2004); Chakrabarti et al., 2009 and Minissale (2018).

The petrology and geochemistry of Nyiragongo lavas ~~from~~ of 2002, 2016, 1977 ~~to~~ and 2017 AD, and the trace element partitioning between ~~melilite-nephelinite~~melilitite glass and melilite, nepheline, leucite, clinopyroxene, apatite, olivine and Fe-Ti oxides: a unique scenario

Silvia Minissale*, Alberto Zanetti**, Dario Tedesco***, Vincenzo Morra*, Leone Melluso*[1]

*DiSTAR, Università di Napoli Federico II, Via Cintia 26, 80126 Napoli, Italy

~~**~~***CNR, IGG, Via Ferrata 1, 27100 Pavia, Italy

~~******~~DISTABIF, Campania University – Luigi Vanvitelli, 81100 Caserta, Italy and JOC, UN-MONUSCO, UN-Goma, DRC.

[1]corresponding author melluso@unina.it

Formatted: Italian (Italy)

Formatted: Italian (Italy)

Formatted: Italian (Italy)

Abstract

The Nyiragongo lava of 2002, and the new one flowing from the spatter cone grown up in 2016 close to the lava lake, are melilite-nephelinites. They have low MgO (4 wt.%), are chemically almost indistinguishable from the lavas of 1977 and from that erupted in 2017, are multiply saturated in melilite, nepheline, leucite, clinopyroxene, olivine, apatite and magnetite, and are rich in fresh glass having significant concentration of SO_3, F and Cl. Glasses and bulk-rocks plot close to one atmosphere cotectics in pertinent phase diagrams. The LA~~M~~-ICP-MS analyses of the observed phases and mineral/glass ~~concentration ratios~~partition coefficients indicate that REE and Y are moderately incompatible ~~elements~~ in melilite (e.g., D_{La}=0.46-0.48, D_{Eu}=0.56-0.57; D_{Lu}=0.18-0.25; D_Y=0.25-0.27), whereas Sr is compatible (D_{Sr}=1.6-1.8); clinopyroxene/melt partition coefficients ~~concentration ratios~~ are similar to melilite for LREE (e.g., D_{La}=0.36), and significantly higher for HREE (D_{Lu}=0.74), Y (D_Y=0.7), Zr (≈1) and Hf (D_{Hf}=1.6), while lower for Sr (D_{Sr} =0.38). Apatites have high concentration ratios for REE, particularly MREE (D_{La}=4.6-6.4, D_{Nd}= 5.8-7.7; D_{Eu}=4.9-6.9; D_{Lu}=1.3-1.6; D_Y=3.1-4.4), and high D_{Sr} (1.8-2.2). Nepheline and leucite are highly and differently selective for Rb, Cs, Ba and Sr; both phases show negligible concentration of REE (hence Eu, +Y), Th, U and first row transition elements. Olivine and magnetite have the expected high concentration of transition elements, with small preference of olivine for divalent cations and magnetite for trivalent cations. The distribution of trace elements in melilite compared with

clinopyroxene, nepheline -or even feldspar- clearly indicate that melilite is not a silica-undersaturated equivalent of any of these phases, and that melilite removal cannot be considered the main cause of Eu troughs or of decreasing fractionation between light and heavy REE in more evolved melts, being these elements still significantly incompatible. At the same time, removal of the observed phenocrysts at this stage of crystallization cannot be the cause of anomalous fractionation of elements with similar geochemical behaviour found in the Nyiragongo lavas. These new data indicate that the magmatic system of the Nyiragongo is in a roughly ~~in a~~ steady state at least since the eruption of 1977 to the activity of 2017, with ~~the~~ periodic eruptions, withdrawal or feeding from the uppermost magma reservoir by broadly the same "cotectic" magma compositions, from which phases of the same composition nucleated in a very ~~low~~ low-pressure regime.

1. Introduction

The Nyiragongo volcano belongs to the Virunga Volcanic Province, ~~in the~~ western branch of the East African Rift, ~~and~~which is composed by seven main volcanoes (from east to west: Muhavura, Gahinga, Sabinyo, Visoke, Karisimbi, Mikeno, Nyiragongo and Nyamulagira, the last two currently active) and ~~several~~hundreds minor centers to the north/northeast of lake Kivu, at the boundaries between the Democratic Republic of Congo, Rwanda and Uganda (Fig. 1a). The western branch of the East African Rift is composed by three main volcanic areas: the Toro-Ankole, the Virunga and the south Kivu. The Nyiragongo ~~The summit crater of the Nyiragongo lies between the two extinct cones of Baruta (to the north) and Shaheru (to the south), built through the emplacement of pyroclastic rocks and lava flows (Fig. 1a).~~

~~The Nyiragongo volcanic complex in Africa and~~ is well known for the presence of the biggest lava lake on earth inside its crater, semi-permanently active since the discovery of the volcano in 1894. The

~~V~~volcanic rocks of Mt. Nyiragongo range in composition from (minor) alkali basalt to ~~dominant~~ nephelinite, leucite nephelinite, melilite nephelinite and olivine melilitite (Sahama, 1962, 1978; Toscani et al., 1990; Demant et al., 1994; Platz et al., 2004; Chakrabarti et al., 2009; Andersen et al., 2012; Minissale, 2018), hence reaching a very high degree of silica undersaturation.~~-~~

The chemical composition of the recent Nyiragongo lavas, unique among the active lava lakes on earth ~~(e.g., Chakrabarti et al., 2009)~~, is of compelling interest given to their glassy, extremely fresh nature and their low amount of phenocryst charge. ~~The recent lavas of Nyiragongo volcano represent a unique opportunity to obtain updated information on the petrology and on mineral trace~~

~~element concentrations and mineral/melt trace element partitioning that can be used to model the behaviour of trace elements in silica poor, plagioclase free magmas *worldwide*.~~

-In this study we present the petrology of the recent lavas of the volcano, and the distribution of trace elements in phenocrysts and microphenocrysts naturally equilibrated with melilite-nephelinitic glasses/magmas/melts ~~of two of the most recent eruptive events of the Nyiragongo volcano~~.

~~The distribution of trace elements between melts and their equilibrium mineral phases provides an important petrogenetic tool to understand high temperature geochemistry and magmatic processes. Nevertheless,~~Indeed, ~~reliable data sets describing mineral/melt trace element behaviour in strongly silica undersaturated, highly alkaline *natural* liquids are still scarce or lacking (cf. Onuma et al., 1981 and references therein). In this study we present the distribution of trace elements in phenocrysts and microphenocrysts naturally equilibrated with melilite nephelinitic glasses/magmas/melts of two of the most recent eruptive events of the Nyiragongo volcano in Africa.~~ . To date, there are no comparable datasets on the geochemical characteristics of melilite and ~~the~~ other ~~major~~observed phases ~~on other rocks~~in *natural* magmas -with similar chemistry elsewhere (cf. Onuma et al., 1981 and references therein; Arzamastsev et al., 2009). ~~,~~ ~~hence~~Therefore, these data and their inferences will be ~~useful~~of the most importance for tracking the ~~petrogenesis~~magmatic evolution and the petrogenesis of Nyiragongo and other ~~similar~~melilite-bearing rocks in ~~other volcanic~~fossil or active volcanic areas (~~for examples,~~e.g., volcanic complexes in Kenya-Tanzania and Uganda; Mt. Vulture and Alban Hills, Italy; Eger Rift; Urach-Hegau-Kaiserstuhl, Germany; ~~melilite bearing rocks of the~~ Kola Peninsula). ~~Owing to their glassy, extremely fresh nature and their low amount of phenocryst charge (which helps to maintain very low viscosity), the recent lavas of Nyiragongo volcano represent a unique opportunity to obtain updated information on mineral trace element concentrations and mineral/melt trace element partitioning that can be used to model the behaviour of trace elements in silica poor, plagioclase free magmas *worldwide*, particularly in active volcanic areas as are Virunga and the eastern branch of the African Rift (Kenya Tanzania).~~

~~This volcanic complex is well known for the presence of the biggest lava lake on earth inside its crater, semi permanently active since the discovery of the volcano in 1894. Owing to their glassy, extremely fresh nature and their low amount of phenocryst charge (which helps to maintain very low viscosity), the recent lavas of Nyiragongo volcano represent a unique opportunity to obtain updated information on mineral trace element concentrations and mineral/melt trace element partitioning that can be used to model the behaviour of trace elements in silica poor, plagioclase-~~

Formatted: Font: Italic

~~free magmas *worldwide*, particularly in active volcanic areas as are Virunga and the eastern branch of the African Rift (Kenya-Tanzania).~~

2. Geological setting and sampling sites

~~Nyiragongo volcano belongs to the Virunga Volcanic Province, in the western branch of the East African Rift, and composed by seven main volcanoes (from east to west: Muhavura, Gahinga, Sabinyo, Visoke, Karisimbi, Mikeno, Nyiragongo and Nyamulagira) and several minor centers to the north/northeast of lake Kivu, at the boundaries between the Democratic Republic of Congo, Rwanda and Uganda (Fig. 1a). The western branch of the East African Rift is composed by three main volcanic areas: the Toro-Ankole, the Virunga and the south Kivu. The summit crater of the Nyiragongo lies between the two extinct cones of Baruta (to the north) and Shaheru (to the south), built through the emplacement of pyroclastic rocks and lava flows (Fig. 1a).~~ The Nyiragongo is a Quaternary stratovolcano characterized by a ~1000 m wide summit crater (with a crater rim at~~hose walls reach~~ ~3500 m a.s.l.) which was generated by repeated magma emptying and refilling episodes throughout its volcanological history (e.g., Sahama, 1978; Demant et al., 1994). The summit crater of the Nyiragongo lies between the two extinct cones of Baruta (to the north) and Shaheru (to the south), built through the emplacement of pyroclastic rocks and lava flows (Fig. 1a). The main cone of Nyiragongo ~~is the site of~~ has several degassing sites (Tedesco et al., 2010) and a semi-permanent lava lake at least since 1928 (Tazieff, 1984, 1994), which has been ~~repeatedly (questo possiamo dirlo con certezza solo x gli ultimi due eventi, che sono anche gli unici due "witnessed" dall'uomo) drained during~~involved in a few eruptive events, the most recent of which took place in 1977 and 2002 (Tedesco et al., 2007; Chakrabarti et al., 2009). Both eruptive events in 1977 and 2002 occurred outside the crater, triggering drainage of magma stored in the crater lava lake and ~~possibly~~ in its superficial reservoir. For the first time in its recent history, the inner crater was also the site of intracalderic spatter activity, which generated a small scoria cone and a lava flowing towards the lava lake in February 2016 (Burgi et al., 2018; Fig. 1b). This activity continued through~~o~~ 2017, and is still ongoing. ~~Volcanic rocks of Mt. Nyiragongo range in composition from minor alkali basalt to dominant nephelinite, leucite-nephelinite, melilite-nephelinite and olivine melilitite (Sahama, 1962, 1978; Toscani et al., 1990; Demant et al., 1994; Platz et al., 2004; Chakrabarti et al., 2009; Andersen et al., 2012; Minissale, 2018), and the~~The M~~m~~agmas currently ~~forming~~ feeding the current activity are well known for their very low viscosity (the lowest recorded viscosity among terrestrial magmas; Chakrabarti et al., 2009; Burgi et al., 2018) and for their low phenocryst charge. Because of the extremely fluid lava and relatively steep slopes of the

volcano, the January 17, 2002 lava flow drained the inner lava lake reaching a speed >50 km/h (Tedesco, 2003, Tedesco et al., 2007~~3~~). The liquidus temperature of the magma in the lava lake is ca. 1100 °C, and the temperature measured at the lava lake surface and with geothermometric estimates is ca. 980 °C (Sahama, 1978; Sawyer et al., 2008; Spampinato et al., 2013; Valade et al., 2018; Burgi et al., 2018). The s~~S~~amples of this study were collected by D.T.; two of them were selected for detailed trace element geochemistry of glasses and associated phases, due to their glassy and extremely fresh appearance in the hand specimen and in thin section. Sample of the lava of 2002 ~~lava~~ belongs to the Munin~~n~~gi flow; it was collected along the 500-800 m long fracture on the Kivu lake shore (Fig. 1d), at an individual flow entering Lake Kivu. The lava of the 2016 outpoured from the intracrateric spatter cone; it was collected above the third platform inside the Nyiragongo main crater, next to the spatter cone and the lava lake (Fig. 1b, 1c and Burgi et al., 2018).

3. Analytical methods

Formatted: Font: Bold

Formatted: Font: Bold

~~Whole~~The bulk-rock major and trace elements of the samples used in this study were analysed by X-ray fluorescence (XRF) using a Panalytical Axios instrument at the University of Napoli (cf. Cucciniello et al., 2017, for further analytical details). Analytical uncertainties are in the order of 1-2% for major elements and 5-10% for trace elements (Table 1). The weight loss on ignition (L.O.I.) was determined with standard gravimetric techniques, after igniting one gram of rock powder at 1000 °C for 6 h. Lanthanides (REE) and other trace elements were determined by Inductively Coupled Plasma-Mass Spectrometry (ICP-MS) at Activation Laboratories (Ancaster, Ontario; see http://www.actlabs.com for a full description of the analytical techniques). The major element concentrations of mineral and glass phases were determined at DISTAR, University of Napoli Federico II, by Energy Dispersive Spectrometry (EDS) microanalyses using an Oxford Instruments Microanalysis Unit equipped with an INCA X-act detector and a JEOL JSM-5310 Scanning Electron Microscope (SEM) using a JEOL JSM5310. Measurements were done with an INCA X-stream pulse processor operating at 15 kV primary beam voltage, 50-100 mA filament current, variable spot size and 50 s net acquisition time. The following reference materials were used for calibration: diopside (Mg), wollastonite (Ca), albite (Al, Si, Na), rutile (Ti), almandine (Fe), Cr_2O_3 (Cr), rhodonite (Mn), orthoclase (K), apatite (P), fluorite (F), barite (Ba), strontianite (Sr), Smithsonian orthophosphates (La, Ce, Nd, Sm, Y), pure vanadium (V) and Corning glass (Th and U). LA-ICP-MS trace element analyses were performed in olivine, clinopyroxene, melilite, apatite, magnetite, nepheline, leucite and glass of selected areas (cf. Fig. 2). Analyses were carried out at

IGG-CNR of Pavia by Laser Ablation-Inductively Coupled Plasma-High Resolution Mass Spectrometry (LA-ICP-HRMS). The microprobe consists of a double-focusing sector-field analyser (Finnigan Mat, Element I) coupled with a Q-switched Nd:YAG laser source (Quantel Brilliant). The fundamental emission of the laser source (1064 nm, in the near-IR region) was converted to 213 nm by three harmonic generators. Helium was used as carrier gas and mixed with Ar downstream of the ablation cell. Spot diameter was varied in the range of 40-60 µm. Quantification was carried out using the NIST SRM 610 glass as external standard (Pearce et al., 1996). Si was used as internal standard for melilite, clinopyroxene, olivine, nepheline, leucite and glass, while Ca was used for apatite and Ti for magnetite. Detection limits are in the range 100-500 ppb for Sc, Ti, and Cr; 10-100 ppb for V, Rb, Sr, Zr, Cs, Ba, Gd, and Pb; 1-10 ppb for Y, Nb, La, Ce, Nd, Sm, Eu, Tb, Dy, Er, Yb, Hf and Ta, and usually <1 ppb for Pr, Ho, Tm, Lu, Th, and U. Precision and accuracy (both better than 10% for concentrations at parts per million level) were assessed by means of repeated analyses of NIST SRM 612 and BCR-2g standards. The composition of the glass beneath the thin section has been documented before the sample analysis to recognize piercing of the rock and to eliminate any glass contribution. The gas background was measured for 60 s, as in any other routine analysis, whereas signals during ablation were acquired for approximately 20-50 s. Analyses were performed with 10 Hz repetition rate of laser and ~1-2.5 mJ/s laser power. Full details are reported in Rocco et al. (2017). Precautions have been taken to avoid any bias on the analytical results. Memory effects have been taken into account leaving more than 1 min between two consecutive analyses and analysing glasses after the minerals. Spurious signals related to memory effects usually affect more blanks (because less time is passed after the previous analysis), thus determining worsening of the detection limits and hindering the quantification of elements at ultra-trace concentration level. Surface contamination during sample polishing and/or handling before the micro-analytical measurement and occurrence of micro-inclusions of glass/fluid have been monitored by detailed inspection of the signal profiles acquired during ablation. Only intervals with parallel signals have been integrated. Anomalous signal contributions at the beginning of the ablation (due to surface contamination) and/or randomly occurring during ablation (possibly related to inclusions and/or memory effect) has been accurately documented and excluded by integration.

~~3~~4. Petrography, classification, bulk-rock and glass geochemistry of the Nyiragongo lavas

~~The analytical techniques are fully described in the Appendix.~~

~~Samples were collected by D.T.; two of them were selected for the present study due to their glassy appearance in the hand specimen and in thin section. Sample of the 2002 lava belongs to the Muningi flow; it was collected along the 500-800 m long fracture on the Kivu lake shore (Fig. 1d), at an individual flow entering Lake Kivu. The lava of the 2016 outpoured from the intracrateric spatter cone; it was collected above the third platform inside the Nyiragongo main crater, next to the lava lake (Fig. 1b, 1c).~~ Samples ~~NY02~~ of the lava of 2002 ~~lava displays~~ have a weakly porphyritic texture, consisting mainly of microphenocrysts of melilite, nepheline, leucite, clinopyroxene and olivine (roughly in decreasing order of abundance), plus diffuse magnetite and apatite microliths, set into a moderately vesicular brown, glassy groundmass (Fig. 2.1, 2.2). Sporadic aggregates of nepheline are also observed. ~~Sample~~ The ~~NY16~~ lava of 2016 is characterized by a moderately porphyritic texture, dominated by euhedral melilite microphenocrysts, euhedral to subhedral olivine, nepheline (occasionally forming almost monomineralic -micro*urtitic*- aggregates; Fig. 2.2), leucite and clinopyroxene microphenocrysts, generally smaller than those observed in ~~sample NY02~~the lava of 2002 (Fig. 2.1). The groundmass consists of a poorly vesicular brown glass with sparse magnetite ~~(locally occurring also as microphenocrysts)~~ and apatite microlites (Fig. 2.2). Worth noting that we did not find perovskite or schorlomitic garnet in the lava samples. A few Fe-sulfides were found in the lava of 2002. Modal analyses are reported in the Table 1. The lava of 1977 has the same mineral assemblage, with a very finely crystalline groundmass. For this reason it was not selected for subsequent LA-ICP-MS work.

Bulk-rocks

Significant issues are pointed out: the lavas of 1977, 2002, 2016 and 2017~~6~~ are poor in SiO_2 (39.1-40.8 wt.%), and rich in Fe_2O_{3t} (12.9-13.4 wt.%), alkalies (11.2-12 wt.%) and P_2O_5 (1.3-1.6 wt.%) (Table 1). They plot in the foidite field of the T.A.S. classification diagram (Fig. 3). The ~~two~~ samples are classified as melilitites (melilite nephelinites; normative larnite 10-12%), following ~~LeMaitre (2002).~~Woolley et al. (1996). The bulk-rock compositions are evolved, given that MgO is <4.2 wt.%, the Mg# is far lower than that expected in primitive melts [Mg#, $100Mg/(Mg+Fe_t)$=34-37~~]~~), and the concentration of Cr and Ni is close to the detection limits, as is in the glass compositions (see below). The chemical composition of the two lavas is barely distinguishable from that of the products erupted in 1977 and 2017 (Table 1). The overall chemical affinity is potassic, as is commonplace in other mafic/ultramafic alkaline rocks of the western branch of the West African Rift (e.g., Foley et al., 2012; Pouclet et al., 2017). The P.I. [molar (Na+K)/Al] is 1.04-1.06, hence the bulk-rocks are weakly peralkaline (cf. Marks and Markl, 2017). The concentration of REE of the ~~two~~ lavas is high (∑REE=779-800 ppm), and REE are highly fractionated: La/Yb_n is 42-46,

whereas Eu/Eu* (normalized Eu divided by interpolated Eu) is 1-1.1. The Zr/Hf is very high (73) and higher than in other melilitites of the area (the Zr/Hf=57 in the 1957 lava of Mugogo: cf. Chakrabarti et al., 2009; Condomines et al., 2015; Zr/Hf=35 in a reference mantle composition; Lyubetskaya and Korenaga, 2008). The concentration of Nb and Ta is very high (>220 ppm and 12.8 ppm, respectively), and the Nb/Ta ratio is 17, very close to a typical mantle value (15.3; Lyubetskaya and Korenaga, 2008). The whereas Nb/U (25-28), Zr/Nb (1.2-1.3), La/Nb (0.8-0.9) are low Nb/U (25-28), Zr/Nb (1.2-1.3), La/Nb (0.8-0.9) are low, and so is the . On the other hand, the Nb/Ta ratio is 17, very close to a typical mantle value (15.3; Lyubetskaya and Korenaga, 2008). The Th/U of bulk-rocks (and glass) is =2.3-2.5, matching the data of Platz et al. (2004). This ratio is, significantly lower than the chondritic ratio (≈4), and lower than the U/Th of other melilitites of the Virunga area (the Th/U is 4.3-4.5 in the 1957 lava of Mugogo: cf. Condomines et al., 2015). The lava sample of 2016 has moderate S (0.2 wt.%), Cl (0.13 wt.%) and F (0.17 wt.%) (Table 1).

Glass

The major and trace element concentration of the glass is indistinguishable from that of the bulk-rock compositions (Fig. 3; Table 2, Table 3, Supplementary Table 1). The glassy groundmass of the 2002 lava sample NY02 has a homogeneous composition; it is characterized by low SiO_2 (39.8-40.6 wt.%), Al_2O_3 (13.4-14.6 wt.%), high Na_2O (5.5-7.9 wt.%) and K_2O (3.6-5.8 wt.%), low MgO (2.1-3.9 wt.%), high FeO_t (12-13 wt.%), TiO_2 (2.2-3.2 wt.%) and CaO (10.8-12.6 wt.%; Table 5). The concentration of P_2O_5 is high (1.17±0.17 wt.%). The Mg# is in the range of 23-35, and the glass is slightly peralkaline (P.I., molar (Na+K)/Al=1.12±0.07). Also the Glass glass composition of the 2016 lava sample NY16 also has a is homogeneous composition for SiO_2 (39.7-41.0 wt.%), Al_2O_3 (14.2-15.3 wt.%), Na_2O (4.5-5.6 wt.%) K_2O (5.2-6.1 wt.%), MgO (3.8-4.4 wt.%), FeO_t (11.4-12.4 wt.%), TiO_2 (2.0-3.3 wt.%) and CaO (11.1-12.5 wt.%; Table 1). The concentration of P_2O_5 is high (1.24±0.25 wt.%). The Mg# ranges from 37 to 40 and the glass is slightly less peralkaline (P.I.=0.99±0.04). The chemical differences between the two lavas are minor. The volatile concentrations in glass of the 2002 lava are rich in SO_3 (0.62±0.1 wt.%), and less so in Cl (0.11±0.06 wt.%), whereas F is close to the detection limits of the employed analytical technique. Similar concentrations are obtained also in the 2016 lava (SO_3=0.41±0.3 wt.%; Cl=0.51±0.13 wt.%; F=0.11±0.05 wt.%; Supplementary Table 1). Worth noting that SO_3- or Cl- saturation in the magmatic system was not achieved at this degree of crystallization, given the lack of sulphur- or chlorine-bearing feldspathoids (haüyne, nosean, sodalite). Nevertheless, sodalite is described in Shaheru lavas (Andersen et al., 2012). This is a significant difference with strictly comparable rocks of magmatic systems such as Mt. Vulture (Italy) and Kaiserstuhl (Germany), having (rare) melilite-

rich rocks along with haüyne, nepheline and leucite, and high and comparable bulk-rock sulphur (and chlorine) concentrations (cf. Sahama, 1962; Melluso et al., 2011b and references therein; Braunger et al., 2018).

45. Major and trace element composition of the mineral phases

Melilite. The melilite of Nyiragongo lava of 2002 ~~lava~~ is a solid solution of åkermanite ($Ca_2MgSi_2O_7$, 43-55 mol.%), soda-melilite ($CaNaAlSi_2O_7$, 27-35 mol.%), Fe-åkermanite ($Ca_2FeSi_2O_7$,14-18 mol.%) and gehlenite ($Ca_2Al_2SiO_7$, 2-6 mol.%), in order of decreasing abundance. The Mg# varies little (65-81), with a significant variation in Al_2O_3 (=5.5-10.8 wt.%) and Na_2O (2.3-6.2 wt.%), indicating that the main atomic substitutions are CaMg->NaAl and, subordinately, Mg->Fe^{2+}, already observed in the composition of magmatic melilites worldwide (references in Fig. 4a; Supplementary Table 2). Melilite of the lava of 2016 ~~lava~~ has just slightly different composition with respect to that of 2002 lava (53-66 mol.% åkermanite, 23-26 mol.% soda-melilite, 14-22 mol.% Fe-åkermanite and 2-6 mol.% gehlenite). The Mg# varies from 77 to 79 (Supplementary Table 2). The Sr concentration is relatively low (0.4-0.7 wt.% SrO), similarly to melilite of other Nyiragongo rocks (e.g., Platz et al., 2004). Melilite has low Sc, Ni and Cr, widely variable V (8-153 ppm), and high Zn (>210 ppm) and Co (>39 ppm). The Sr concentration obtained with LA~~M~~-ICP-MS is high and varies little (4700-5200 ppm), consistently with the relatively uniform major element composition of this phase, and with microprobe analyses. The concentration of LREE is quite remarkable (e.g., La=67-170 ppm; Ce=124-200 ppm), The REE patterns are steep and highly LREE-enriched (La/Yb_n=55-118), may have peaks at Eu in the chondrite-normalized diagrams (Eu/Eu*=0.8-1.5 in the 2016 lava, Eu/Eu*=0.9-2.1 in the 2002 lava; Table 2). The high concentration of LREE is to be related to the presence of the important eightfold coordination site hosting the large ions Ca and Na (cf. Bindi and Bonazzi, 2003; Merlini et al., 2008). The HREE concentrations are a few times the chondritic values, due to the low concentration of ferromagnesian elements and the small -tetrahedral- site hosting Mg and Fe that should be the site for hosting also HREE. The concentration of Rb, Ba, Y, Zr, Hf, Nb, Ta, U, Th and Pb is low to negligible (Table 2), as is that of titanium.

Nepheline and leucite. Nepheline in sample NY02 has composition $Ne_{56-75}Ks_{23-41}Sil_{2-6}$ (components in wt.%), whereas in the lava of 2016 is slightly more potassic ($Ne_{54-64}Ks_{35-45}Sil_{1-3}$), having K_2O up to 12.3 wt.%, matching the most potassium-rich nephelines found in Africa (Boctor and Yoder, 1986; Melluso et al., 2011a; Antao and Nicholls, 2018). Similar range of compositions has been

Formatted: English (United Kingdom)
Formatted: English (United Kingdom)

found in the 1977 lava (Fig. 4b). The Na/(Na+K) ratio of nepheline varies significantly (0.58-0.76; Supplementary Table 3); this large variation is to be expected for both temperature decrease and cocrystallization with leucite. The low excess silica in magmatic nepheline is expected when this phase crystallizes in highly silica-undersaturated magmas (e.g., Boctor and Yoder, 1986; Melluso et al., 2010, 2011a, 2011b and references therein; Fig. 4b). The concentration of CaO in nepheline, though significant, does not reach 1.7 wt.% (Supplementary Table 3). The composition of leucite is stoichiometric and quite homogeneous for both samples; it is relatively poor in Ba (0-1 wt.% BaO). Concerning trace elements, the concentration of Sr is one order of magnitude higher in nepheline (600-829 ppm) than in leucite (36-83 ppm). Conversely, Rb, Cs and Ba are one to three orders of magnitude higher in leucite (up to 1596 ppm, 39 ppm and 3536 ppm, respectively) than in nepheline (up to 149 ppm, 0.4 ppm and 305 ppm, respectively; Table 2). Rare earths and most other analyzed elements show negligible concentrations in both phases (Table 2).

Clinopyroxene. Clinopyroxene is rare. The Ca-Mg-Fe diagram indicates that the compositions of the 2016 lava are mostly diopsides (Fig. 4c) and have Mg# from 68 to 78. The Al_2O_3 concentration (1.2–8.8 wt.%) considerably increases with decreasing Mg#, as well as that of TiO_2 (1.1-5.4 wt.%). The Al^{VI} [Al_t-(2-Si) apfu for six oxygens] is totally negligible nothwistanding high and increasing Al_t and not-very-oxidized conditions (hence low calculated Fe^{3+} in Ca-rich pyroxene, relatively low magnetite component of spinel), pointing out that these clinopyroxenes are solid solutions of diopside, hedenbergite and the low-pressure molecule $CaTiAl_2O_6$ (up to 16 mol.%), like other clinopyroxenes of Nyiragongo, or in other melilitites worldwide (Boctor and Yoder, 1986; Dunworth and Wilson, 1998; Platz et al., 2004; Melluso et al., 2011a). The Na_2O concentration is low (<0.4 wt.% Na_2O), as expected in clinopyroxene crystallized in not-yet peralkaline magmas. The clinopyroxene of the 2002 lava reaches even higher concentration of Al_2O_3 and TiO_2 (up to 11.5 and 8.3 wt.%, respectively; up to 24 mol. % $CaTiAl_2O_6$; Supplementary Table 4). Similar ranges are found in the lava of 1977, with also more Fe-rich compositions (Fig. 4c). Due to the presence of important octahedral site(s) in clinopyroxene, the first row transition elements have relatively high concentration (e.g., V=200-220 ppm, Sc=23-24 ppm, Table 2), and so is for other trace elements with marked affinity for octahedral sites (e.g., Zr=336-348 ppm). Clinopyroxene has far higher concentrations of HREE than melilite (see above), but lower LREE and therefore LREE/HREE ratios (La/Yb_n=20-23; Fig. 5 Table 2). Eu/Eu* varies from 1 to 1.2.

~~*Apatite.* Apatite compositions are hydroxylapatite and fluorapatite: F ranges from 0.5 to 2 wt.% (Supplementary Table 5). Apatite is rich in REE (∑REE=4300-5300 ppm), has strong LREE/HREE~~

~~fractionation (La/Yb_n=127-139) and no Eu troughs (Eu/Eu*=0.9-1). Apatite has also high Y (132-164 ppm) and Sr (5000-6000 ppm), and significant Th (29-41 ppm) and U (7-8 ppm). Other elements are in low concentration (Table 2; Fig. 5).~~

Olivine. Olivine is ~~as~~ quite a rare phase ~~as clinopyroxene~~. The composition of the ~~rare~~ olivine microlites in the lava of 2002 is rather homogeneous, ranging from $Ca_2Mg_{71}Fe_{27}$ to $Ca_2Mg_{75}Fe_{23}$, hence the forsterite content [fo=Mg*100/(Mg+Fe)] ranges from 71 to 74 (Supplementary Table ~~6~~5; Fig. 4c). The olivine composition of the lava of 2016 is nearly identical in composition ($Ca_2Mg_{75}Fe_{23}$; fo_{73-76}; Supplementary Table 6). The lava of 1977 has a far larger range of compositions, towards Ca-rich fayalite (~~F~~fo_{85-13}; CaO up to 4.2 wt.%). Relatively highly forsterite-rich olivines with high CaO (up to 1.7 wt.%), as those of the Nyiragongo samples of this study, are common feature in Ca-rich melilite-bearing mafic/ultramafic volcanics worldwide (e.g., Melluso et al., 2010, 2011a and references therein; Braunger et al., 2018), and may have their extreme in the kirschsteinite ($CaFeSiO_4$) found in evolved lavas of the Shaheru cone (Sahama and Hytönen, 1957; Fig. 4c) and in the groundmass of some Alban Hills lavas in Italy (the "*cecilite*"; Melluso et al., 2010 and references therein). The Nyiragongo olivines have high Co (193-221 ppm), Ni (287-413 ppm) and Zn (161-272 ppm), low Sc (2.5-4.6 ppm), V (9-34 ppm) and Cr (<114 ppm). Other elements vary irregularly, including Y, Sr, Zr and REE (Table 2).

Apatite. Apatite compositions are hydroxylapatite and fluorapatite: F ranges from 0.5 to 2 wt.% (Supplementary Table ~~5~~6). Apatite is rich in REE (∑REE=4300-5300 ppm), has strong LREE/HREE fractionation (La/Yb_n=127-139) and no Eu troughs (Eu/Eu*=0.9-1). Apatite has also high Y (132-164 ppm) and Sr (5000-6000 ppm), and significant Th (29-41 ppm) and U (7-8 ppm). Other elements are in low concentration (Table 2; Fig. 5).

Magnetite. The spinel phase in the ~~melilitites~~ Nyiragongo lavas is a quite homogeneous magnetite-ulvöspinel solid solution: Usp_{48-61} in the lava of 2002 and Usp_{51-55} in the lava of 2016 (Supplementary Table 7). The concentration of Al_2O_3 varies from 4.4 to 6.8 wt.%, and MgO varies even less (5.9-7 wt.%). Magnetite has the expected notable concentrations of transition elements (V>3000 ppm, Cr=250-400 ppm, Co=330-350 ppm, Ni=630-720 ppm, Zn=650-860 ppm), with low Sc (7-9 ppm), and negligible concentrations of REE and other elements, excluding Zr (70-90 ppm) Nb (48-52 ppm), Hf (1-2 ppm) and Ta (4.6-4.8 ppm) (Table 2).

~~5~~6. Discussion

Formatted: Subscript

56.1. Petrology and a& Assessment of mineral/melt equilibria

The evolved nature of the present-day Nyiragongo magmas and their derivation from more primitive olivine melilitite compositions is indicated by the geochemistry (e.g., relatively low MgO and Sc, negligible Cr and Ni), mineral chemistry (see above) and the position in pertinent synthetic systems, such as the larnite-enstatite-nepheline pseudoternary phase diagram (Pan and Longhi, 1990) (Fig. 6a). This diagram also indicates that the Nyiragongo magmas are close to, or plot on, low-pressure cotectics involving mafic phases and two feldspathoids, in an area far from the thermal/compositional barrier separating feldspar-bearing melts from melilite-bearing melts. The limited major and trace element compositional variations, together with the petrographic evidence, suggest that all mineral phases (melilite+ two feldspathoids +clinopyroxene +olivine +clinopyroxene +apatite +magnetite), in the studied samples crystallized almost contemporaneously at atmospheric pressure in equilibrium with the host melilite nephelinite melt, which is characterized by an evolved composition, (e.g., relatively low MgO and Sc, negligible Cr and Ni), a very fresh glass-rich matrix, a highly depolymerized nature (low SiO_2 and Al_2O_3, high alkalis and iron, slight peralkalinity, NBO/T=0.46-0.47, compared to ≈0 for a rhyolite melt and ≈1 for an olivine melilitite melt), low silica activity (a_{SiO2}≤0.4 at 1000°C, according to Barker, 2001, compared to a_{SiO2}=1 in quartz-bearing systems), and a temperature of the lava lake close to 1000°C (cf. Burgi et al., 2018 and references therein). The assemblage of the Nyiragongo lavas of 2002 and 2016 matches that of a pseudo-invariant point ol+cpx+mel+lc+ne+liq postulated at ca. 1100°C by Gupta et al. (1973) and Gupta (2015) (Fig. 6b), which indicates: a) the derivation of Nyiragongo magmas of 2002 and 2016 from more olivine-rich precursors, yet present in the area (cf. Platz et al., 2004; Minissale, 2018), and, more importantly, b) the mineral assemblage of Nyiragongo magmas of 2002 and 2017 can be considered broadly in equilibrium from a thermodynamic point of view (cf. also Fig. 2.1 and 2.2). To this latter respect, we note that the highest Mg# of melilite we analyzed (80.6) is slightly higher than the highest Mg# of clinopyroxene (78.4) and forsterite content of olivine (76.3). Given the different Fe/Mg partitioning of between these phases and silicate melts (e.g., different $Kd_{Fe/Mg}$; cf. Roeder and Emslie, 1970; Bédard, 2010), of which that of melilite is largely unknown, though supposedly more similar to that of clinopyroxene (Supplementary Fig. 1), we tentatively suggest that the Mg# of the phases indicate the onset of cotectic crystallization in broadly the same melt composition having Mg#=35-40.

We argue that the mineral and glass data can be fruitfully used in order to calculate mineral/liquid element ratios, actually close analogues of partition coefficients, taking also into account the high

~~concentration of elements in lavas and minerals, which is generally sufficient to achieve high analytical reproducibility and limited non-equilibrium partitioning. We remark the role of liquidus crystallization of melilite in magmas where any feldspar could not crystallize, due to the very high degree of silica undersaturation (which is equivalent to the so-called melilite-plagioclase incompatibility in alkali-rich, *orthomagmatic* rocks).~~

~~5~~6.~~1~~2. Mineral/glass partition coefficients ~~concentration ratios~~

~~Very intriguingly, there are no comparable datasets about trace element partitioning in melilite and in the other liquidus phases of the Nyiragongo magmas in the recent literature (cf. Arzamastsev et al., 2009 for other cases).~~ The Nyiragongo is a unique case where mineral and glass compositional data can be fruitfully used in order to calculate partition coefficients for highly silica undersaturated magmas, taking also into account the high concentration of elements in lavas and ~~minerals~~coexisting equilibrium phases, which is generally sufficient to achieve high analytical reproducibility and limited non-equilibrium partitioning. We remark the role of liquidus crystallization of melilite in magmas where any feldspar could not crystallize, due to the very high degree of silica undersaturation (equivalent to the so-called melilite-plagioclase incompatibility in alkali-rich, *orthomagmatic* rocks; Yoder, 1973), and the uniform composition of glasses, phases and bulk-rocks. Very intriguingly, there are no comparable datasets about trace element partitioning in melilite and in the other liquidus phases of the Nyiragongo magmas in the recent literature (cf. Arzamastsev et al., 2009 for other cases).

Mineral/glass ~~elemental ratios~~partition coefficients are reported in Table 3 and Fig. 7.

Melilite. Rare earth elements, and particularly HREE, are incompatible in melilite (e.g., D_{La}=0.46-0.48; D_{Lu}=0.18-0.25; Table 3), as already pointed out by the work of Onuma et al. (1981) on similar samples and Beckett et al. (1990) on meteorites, and also has a small peak at Eu (D_{Eu}=0.56-0.57) compared to Sm and Gd (Table 3). Melilite has an expected quite large ~~concentration ratio~~partition coefficient for Sr (D_{Sr}=1.8-2.2). Actually, this phase can have Sr as a major cation (Fitton and Hughes, 1981; Velde and Rachdi, 1988; Melluso et al., 2010), but this feature is rare, usually related to a late stage of crystallization, depending upon presence -or absence- of significant amounts of earlier Sr-scavenging phases (e.g., perovskite, apatite, titanite), and ultimately refers to more evolved magmatic systems than those of this study, or to the late groundmass phases of holocrystalline rocks. The ~~Sr~~ partitioning of Sr in melilite may be the same as in ~~in~~ a calcic plagioclase ~~in~~ of "basaltic" systems (cf. Sun et al., 2018, and references therein). Therefore, melilite

removal in significant amounts should create a trough at Sr in the mantle normalized diagrams of more evolved rocks, with respect to neighbouring elements such as La, Ce and Nd. The concentration of Eu and the Eu peaks in the REE patterns of melilite are ~~small~~ minor or absent, when compared to the worldwide composition of liquidus *feldspars* (plagioclase, anorthoclase and potassic sanidine, having Eu/Eu*> or >> 20-30, at Eu concentration=0.5-2 ppm; Supplementary Fig. 2) in less silica-undersaturated rocks.

Nepheline and leucite have distinctly different trace element distribution, particularly for LFSE, which are justified by the dominant cations and the size of the sites. The largest low-charged cations (Cs, Ba, Rb) are significantly hosted in leucite, whereas Sr (and far less so, Eu) markedly prefers nepheline, though still being a highly incompatible element (Table 3). The concentration ratios of Rb and Cs for leucite are of the same magnitude of those obtained by Foley and Jenner (2004) in the olivine lamproite of Gaussberg, whereas Ba (thus D_{Ba}) is far higher in the Nyiragongo leucite (Table 3).

Clinopyroxene. The few mineral/glass ~~concentration ratios~~partition coefficients of REE in clinopyroxene are very similar to values obtained by Onuma et al. (1981), with the exception of lower La and Ce. Again, these numbers indicate that LREE are highly incompatible in diopsidic clinopyroxene of ~~mafic~~ highly alkaline magmas at atmospheric -and higher- pressure (cf. Hart and Dunn, 1993; Fedele et al., 2009 and references therein; Ambrosio and Azzone, 2018 and references therein; Supplementary Fig. 3), with HREE being less incompatible, due to their stronger octahedral site preference. Transition elements Sc, Ni and Cr are more compatible than in melilite, whereas V, Zn, Y and Zr are still moderately incompatible (Table 3).

The low-forsterite olivine of Nyiragongo has significant partition coefficients for Ni, Co and Zn (Table 3).

~~Magnetite scavenges the first row of transition elements (Sc, Ti, V, Cr, Ni, Zn), as expected. Significant concentration ratios are also observed for Zr, Nb, Hf and Ta (Table 2 and 3).~~

~~The Our few~~The REE patterns of apatite have a relative concentration peak in the middle REE relative to the glass compositions, and high apatite/glass ~~concentration ratios~~partition coefficients (>1 for all the elements). ~~Notably, the values reported in Table 3 are roughly 5-6 times lower than those calculated in apatites of trachytic or more silicic magmas (cf. Fedele et al., 2015 and references therein). Rather, they are more similar to some calculated for different (*basaltic* to *andesitic*), subalkaline, melt compositions by Prowatke and Klemme (2006), indicating a major compositional control in the partitioning of REE in apatite (likely the degree of polymerization in the melts, cf. Watson and Green, 1981).~~ Y is also a highly compatible element (Table 3). The values reported in Table 3 are roughly 5-6 times lower than those calculated in apatites of trachytic or

more silicic magmas (cf. Fedele et al., 2015 and references therein). Rather, they are more similar to some calculated for different (*basaltic* to *andesitic*), subalkaline, melt compositions by Prowatke and Klemme (2006), indicating a major compositional control in the partitioning of REE in apatite (likely the degree of polymerization in the melts, cf. Watson and Green, 1981). Apatite has negligible effects on the concentration of HFSE, Rb, Pb, Ba and their ratios. On the other hand, the concentration of Sr is expectedly high (Table 2). As noted elsewhere (Melluso et al., 2017, 2018 and references therein), removal of apatite (though being a significant host for REE, Y and Sr) is unlikely to be the main cause of "complementary", strongly concave REE patterns in evolved highly alkaline rocks, when found.

Magnetite scavenges the first row of transition elements (Sc, Ti, V, Cr, Ni, Zn), as expected. Significant partition coefficients are also observed for Zr, Nb, Hf and Ta, though being these elements still highly incompatible (Table 2 and 3).

~~Nepheline and leucite have distinctly different trace element distribution, particularly for LFSE, which are justified by the markedly different cationic sites and their size. The largest low-charged cations (Cs, Ba, Rb) are significantly hosted in leucite, whereas Sr (and far less so, Eu) markedly prefers nepheline, though still being a highly incompatible element (Table 3). The concentration ratios of Rb and Cs for leucite are of the same magnitude of those obtained by Foley and Jenner (2004) in the olivine lamproite of Gaussberg, whereas Ba (thus D_{Ba}) is far higher in the Nyiragongo leucite (Table 3).~~

The trace element distribution found in the Nyiragongo phases cannot justify the development of significant Eu troughs in highly alkaline liquids derived from any amount of melilite removal (cf. also Marks and Markl, 2017). Indeed, more evolved rocks from the nearby Shaheru cone (MgO<3 wt.%) still do not have Eu troughs in the REE patterns (cf. Platz et al., 2004; Minissale, 2018; Supplementary Figure 4), and melilite-rich cumulate intrusive rocks do not show Eu peaks in the chondrite normalized REE diagrams (e.g., Verhulst et al., 2000; Srivastava and Sinha, 2004).

~~The trace element distribution found in the Nyiragongo phases cannot justify the development of significant Eu troughs in highly alkaline liquids derived from any amount of melilite removal (cf. also Marks and Markl, 2017). Indeed, more evolved rocks from the nearby Shaheru cone (MgO<3 wt.%) still do not have negative Eu troughs troughs in the REE patterns (cf. Platz et al., 2004; Minissale, 2018; Supplementary Figure 4), and melilite-rich cumulate intrusive rocks significantly made up of melilite do not show Eu peaks in the chondrite normalized REE diagrams (e.g., Verhulst et al., 2000; Srivastava and Sinha, 2004; Melluso et al., 2010).~~

~~6~~7. Conclusions

Natural partitioning of elements between phenocrysts and their incompatible element-rich melilite-nephelinite glasses (and bulk-rock compositions) of recent Nyiragongo activity, the most silica undersaturated magmas currently erupted on earth~~-~~, and forming lava lakes~~, on earth~~, provides a fresh look to the distribution of REE and other trace elements in melilite (when this phase can be considered the main "mafic" phenocryst on the liquidus, i.e., when clinopyroxene and olivine are minor), and in the companion felsic and mafic mineral phases. We think that removal of significant amounts of melilite is very difficult to be convincingly demonstrated in any volcanic or plutonic complex bearing this phase worldwide (cf. Braunger et al., 2018 for examples). In addition, melilite cannot be considered as the analogue of any feldspar and~~,~~ feldspathoid -or clinopyroxene- in feldspar-free magmas, also from the perspective of trace element partitioning. Melilite, nepheline, leucite, olivine, diopsidic clinopyroxene, magnetite and apatite are unable to significantly fractionate ratios between highly charged cations with similar geochemical behaviour (Zr/Hf, Nb/Ta, Th/U). Hence, the causes of some anomalous trace element ratios found in the Nyiragongo lavas (cf. Platz et al., 2004; Chakrabarti et al., 2009; Condomines et al., 2015) must be sought in processes different from fractional crystallization involving any amount of these phases. Even though mineral chemistry and mineral assemblages are not indicative of a peralkaline rock/magma, the tendency of the Nyiragongo magmatic system to evolve to peralkaline compositions is well evidenced in some of the rocks of the Shaheru cone, having late-stage (or ~~even~~ post-magmatic) phases more typical of peralkaline compositions (e.g., combeite, götzenite, Andersen et al., 2012), as well as phases of highly evolved, highly silica undersaturated rocks (e.g., fayalite and kirschsteinite; Fig. 4). The presence of growing crystals of relatively low-density phases such as nepheline and leucite also indicate the possibility of accumulation (floating) processes in shallow magmatic reservoirs (e.g., Demant et al., 1994; Platz et al., 2004). ~~Last but not least, the~~ The substantially identical composition of the 2002 and 2016 lavas, as well as that of the lavas erupted in 1977 and 2017, implies a steady-state magma supply system in this interval of the Nyiragongo recent activity, where only mildly evolved magmas reach the summit area from different pathways starting from the subvolcanic reservoir (cf. Burgi et al., 2018), and where more complex petrogenetic processes (e.g., magma mixing between highly evolved magmas, refilling the shallow reservoirs from hotter, more primitive melts) are not active, judging from the substantially ~~observed~~ uniform mineral assemblage~~s~~, mineral chemistry and bulk-rock geochemistry.

Acknowledgements

Formatted: Tab stops: 3 cm, Left

Formatted: English (United States)

We gratefully thank Roberto de' Gennaro (particularly), Ciro Cucciniello, Lorenzo Fedele, John Longhi, Michael Marks, Michel Condomines, Sergio Bravi, Pierre-Yves Burgi, Roger Mitchell, and the late Fabio Mazzeo for their help with the analytical work, for their continued interest to the topic, and for interesting discussions. This research was granted by PRIN 2015 (20158A9CBM) to Leone Melluso. Two anonymous reviewers offered ~~interesting~~useful comments to help improve an initial draft.

References

Ambrosio, M.R., Azzone, R.G., 2018. The influence of crystal and melt compositions on the REE+Y partitioning between clinopyroxene and basanitic/tephritic melts of Cretaceous alkaline magmatism on the southeastern part of the South American Platform, southeast Brazil. The Canadian Mineralogist 56, 303-329.

Andersen, T., Elburg, M., Erambert, M., 2012. Petrology of combeite- and götzenite-bearing nephelinite at Nyiragongo, Virunga Volcanic Province in the East African Rift. Lithos 152, 105-121.

Antao, S.M., Nicholls, J.W., 2018. Crystal chemistry of three volcanic K-rich nepheline samples from Oldoinyo Lengai, Tanzania and Mount Nyiragongo, Eastern Congo, Africa. Frontiers in Earth Science 6, 155. https://dx.doi.org/10.3389/feart.2018.00155

Arzamastsev, A.A., Arzamastseva, L.V., Bea, F., Montero, P., 2009. Trace elements in minerals as indicators of the evolution of alkaline ultrabasic dike series: LA-ICP-MS data for the magmatic provinces of northeastern Fennoscandia and Germany. Petrology 17, 46-72.

Barker, D.S., 2001. Calculated silica activities in carbonatite liquids. Contributions to Mineralogy and Petrology 141, 704-709.

Beckett, J.R., Spivack, A.J., Hutcheon, I.D., Wasserburg, G.J., Stolper, E.M., 1990. Crystal chemical effects on the partitioning of trace elements between mineral and melt –an experimental study of melilite with applications to refractory inclusions from carbonaceous chondrites. Geochimica et Cosmochimica Acta 54, 755-774.

Bédard, J.H., 2010. Parameterization of the Fe=Mg exchange coefficient (Kd) between clinopyroxene and silicate melts. Chemical Geology 274, 169-176.

Bindi, L., Bonazzi, P., 2003. Low-temperature study of natural melilite ($Ca_{1.89}Sr_{0.01}Na_{0.08}K_{0.02}$) ($Mg_{0.92}Al_{0.08}$) ($Si_{1.97}Al_{0.03}$)$O_7$: towards a commensurate value of the q vector. Physics and Chemistry of Minerals 30, 523-526.

Formatted: English (United States)

Formatted: English (United States)

Formatted: Italian (Italy)

Formatted: English (United States)

Formatted: English (United States)

Formatted: Default Paragraph Font, Font: Times New Roman

Formatted: Font: Times New Roman

Formatted: English (United States)

574 Boctor N.Z., Yoder, H.S. jr., 1986. Petrology of some melilite-bearing rocks from Cape Province,
575 Republic of South Africa: relationships to kimberlites. American Journal of Science 286, 513-
576 539.
577 Braunger, S., Marks, M.A.W., Walter, B.F., Neubauer, R., Reich, R., Wenzel, T., Parsapoor, A.,
578 Markl, G., 2018. The petrology of the Kaiserstuhl volcanic complex, SW Germany: the
579 importance of metasomatized and oxidized lithospheric mantle for carbonatite generation.
580 Journal of Petrology 59, 1731-1762, https://dx.doi.org/10.1093/petrology/egy078
581 Burgi, P.-Y., Minissale, S., Melluso, L., Mahinda, C.K., Cuoco, E., Tedesco, D., 2018. Models of
582 the formation of the February 29, 2016 new spatter cone inside Mount Nyiragongo. Journal of
583 Geophysical Research 123, https://dx.doi.org/10.1029/2018JB015927
584 Chakrabarti, R., Basu, A.R., Santo, A.P., Tedesco, D., Vaselli, O., 2009. Isotopic and geochemical
585 evidence for a heterogeneous mantle plume origin of the Virunga volcanics, Western rift, East
586 African Rift system. Chemical Geology 259, 273-289.
587 Condomines, M., Carpentier, M., Ongendangenda, T., 2015. Extreme radium deficit in the 1957 AD
588 Mugogo lava (Virunga volcanic field, Africa): its bearing on olivine-melilitite genesis.
589 Contributions to Mineralogy and Petrology 169, 29.
590
591 Cucciniello, C., Choudary, A.K., Zanetti, A., Sheth, H.C., Vichare, S., Pereira, R., 2014.
592 Mineralogy, geochemistry and petrogenesis of the Khopoli mafic intrusion, Deccan Traps,
593 India. Mineralogy and Petrology 108, 333-351.
594 Cucciniello, C., Melluso, L., le Roex, A.P., Jourdan, F., Morra, V., de' Gennaro, R., Grifa, C., 2017.
595 From nephelinite, basanite and basalt to peralkaline trachyphonolite and comendite in the
596 Ankaratra volcanic complex, Madagascar: $^{40}Ar/^{39}Ar$ ages, phase compositions and bulk-rock
597 geochemical and isotopic evolution. Lithos 274-275, 363-382.
598 https://dx.doi.org/10.1016/j.lithos.2016.12.026
599 Dawson, J.B., Hinton, R.W., Steele, I.M., 2008. The composition of anorthoclase and nepheline in
600 Mount Kenya phonolite and Kilimanjaro trachyte, and crystal-glass partitioning of elements.
601 The Canadian Mineralogist 46, 1455-1464
602 Demant, A., Lestrade, P., Ruanza, T.L, Kampunzu, A.B., Durieux, J., 1994. Volcanological and
603 petrological evolution of Nyiragongo volcano, Virunga volcanic field, Zaire. Bulletin of
604 Volcanology 56, 47-61.
605 Dunworth, E.A., Wilson, M., 1998. Olivine melilitites from the SW German Tertiary volcanic
606 province: mineralogy and petrogenesis. Journal of Petrology 39, 1805-1836.

Formatted: Font: Times New Roman

Formatted: English (United States)

Formatted: Italian (Italy)

Formatted: Italian (Italy)

Fedele, L., Lustrino, M., Melluso, L., Morra, V., Zanetti, A., Vannucci, R., 2015. Trace element distribution in plagioclase, alkali feldspar, Ti-magnetite, biotite and apatite in evolved potassic liquids from Campi Flegrei (Southern Italy). American Mineralogist 100, 233-249. https://dx.doi.org/10.2138/am-2015-4995

Fedele, L., Zanetti, A., Lustrino, M., Melluso, L., Morra, V., Vannucci, R., 2009. Insights on clinopyroxene/liquid trace element partitioning in natural trachyte-phonolite systems: a EMP/LA-ICP-MS case study from Campi Flegrei (Italy). Contributions to Mineralogy and Petrology 158, 337-356. https://dx.doi.org/10.1007/s00410-009-0386-5

Fitton, J.G., Hughes, D.J., 1981. Strontian melilite in a nephelinite lava from Etinde, Cameroon. Mineralogical Magazine 44, 261-264.

Foley, S.F., Jenner, G.A., 2004. Trace element partitioning in lamproitic magmas – the Gaussberg olivine leucitite. Lithos 75, 19-38.

Foley, S.F., Link, K., Tiberindwa, J.V., Barifaijo, E., 2012. Patterns and origin of igneous activity around the Tanzanian craton. Journal of African Earth Sciences 62, 1-18.

Gupta, A.K. (2015) Origin of potassium-rich silica-deficient igneous rocks. Springer, 536 pp. ISBN: 978-81-322-2082-1

Gupta, A.K., Venkateswaran, G.P., Lidiak, E.G., Edgar, A.D., 1973. The system diopside-nepheline-akermanite-leucite and its bearing on the genesis of alkali-rich mafic and ultramafic volcanic rocks. The Journal of Geology 81, 209-218.

Guzmics, T., Mitchell, R.H., Szabò, C., Berkesi, M., Milke, R., Ratter, K., 2012. Liquid immiscibility between silicate, carbonate and sulfide melts in melt inclusions hosted in co-precipitated minerals from Kerimasi volcano (Tanzania): evolution of carbonated nephelinitic magma. Contributions to Mineralogy and P~~p~~etrology 164, 101-122.

Hart, S.R., Dunn, T., 1993. Experimental cpx/melt partitioning of 24 elements. Contributions to Mineralogy and Petrology 113, 1-8.

~~Le Maitre, R.W., 2002. Igneous Rocks: A Classification and Glossary of Terms (2nd ed.), Cambridge Univ. Press, Cambridge, UK, 236 pp.~~

Lyubetskaya, T., Korenaga, J., 2007. Chemical composition of Earth's primitive mantle and its variance: 1. methods and results. Journal of Geophysical Research 112, B03211, https://dx.doi.org/10.1019/2005JB004223

Marks, M.A.W., Markl, G., 2017. A global review of agpaitic rocks. Earth-Science Reviews 173, 229-258.

Melluso L., Conticelli S., de' Gennaro R., 2010. Kirchsteinite in the Capo di Bove melilite leucitite lava (cecilite), Alban Hills, Italy. Mineralogical Magazine 74, 887-902.

Melluso L., Guarino V., Lustrino M., Morra V., de' Gennaro R., 2017. The REE- and HFSE-bearing phases in the Itatiaia alkaline complex (Brazil), and geochemical evolution of feldspar-rich felsic melts. Mineralogical Magazine 81, 217-250.

Melluso, L., Hergt, J.M., Zanetti, A., 2014. The late crystallization stages of low-Ti, low-Fe tholeiitic magmas: insights from evolved Antarctic and Tasmanian rocks. Lithos 188, 72-83. https://dx.doi.org/10.1016/j.lithos.2013.10.032

Melluso, L., le Roex, A.P., Morra, V., 2011a. Petrogenesis and Nd-Pb-Sr- isotope geochemistry of the olivine melilitites and olivine nephelinites ("*ankaratrites*") in Madagascar. Lithos 127, 505-521. https://dx.doi.org/10.1016/j.lithos.2011.08.003

Melluso L., Lustrino M., Ruberti E., Brotzu P., Gomes C.B., Morbidelli L., Morra V., Svisero D.P., d'Amelio F., 2008. Major and trace element composition of olivine, perovskite, clinopyroxene, Cr-Fe-Ti oxides, phlogopite and host kamafugites and kimberlites, Alto Paranaíba, Brazil. The Canadian Mineralogist 46, 19-40. https://dx.doi.org/10.3749/canmin.46.1.19

Melluso, L., Morra, V., de' Gennaro, R., 2011b. Coexisting Ba-feldspar and melilite in a melafoidite lava of Mt. Vulture, Italy: role of volatiles and alkaline earths in bridging a petrological incompatibility. The Canadian Mineralogist 49, 983-1000. https://dx.doi.org/10.3749/canmin.49.4.983

Melluso L., Srivastava R.K., Guarino V., Zanetti A., Sinha A.K., 2010. Mineral compositions and magmatic evolution of the Sung Valley ultramafic-alkaline-carbonatitic complex (NE India). The Canadian Mineralogist 48, 205-229. https://dx.doi.org/10.3749/canmin.48.1.205

Melluso, L., Tucker, R.D., Cucciniello, C., le Roex, A.P., Morra, V., Zanetti, A., Rakotoson, R.L., 2018. The magmatic evolution and genesis of the Quaternary basanite-trachyphonolite suite of Itasy (Madagascar) as inferred by geochemistry, Sr-Nd-Pb isotopes and trace element distribution in coexisting phases. Lithos 310-311, 50-64. https://dx.doi.org/10.1016/j.lithos.2018.04.003

Merlini, M., Gemmi, M., Cruciani, G., Artioli, G., 2008. High-temperature behaviour of melilite: in situ X-ray diffraction study of gehlenite-åkermanite-Na melilite solid solution. Physics and Chemistry of Minerals 35, 147-155.

Minissale, S., 2018. Petrogenesis of alkaline and strongly alkaline volcanism: examples from African Rift. PhD dissertation, Università di Napoli Federico II, 143 pp.

Onuma, N., Ninomiya, S., Nagasawa, H., 1981. Mineral/groundmass partition coefficients for nepheline, melilite, clinopyroxene and perovskite in melilite-nepheline basalt, Nyiragongo, Zaire. Geochemical Journal 15, 221-228.

Formatted: Font: Italic
Formatted: Italian (Italy)
Formatted: Italian (Italy)
Formatted: Italian (Italy)
Field Code Changed
Formatted: Font: Times New Roman
Formatted: Italian (Italy)
Field Code Changed
Formatted: Italian (Italy)
Formatted: Italian (Italy)
Formatted: Italian (Italy)
Formatted: Italian (Italy)
Field Code Changed
Formatted: Italian (Italy)
Formatted: Italian (Italy)
Formatted: Italian (Italy)

Pan, V., Longhi, J., 1990. The system Mg_2SiO_4- Ca_2SiO_4- $CaAl_2O_4$- $NaAlSiO_4$- SiO_2: one atmosphere liquidus equilibria of analogs of alkaline mafic lavas. Contributions to Mineralogy and Petrology 105, 569-584.

Platz, T., Foley, S.F., André, L., 2004. Low-pressure fractionation of the Nyiragongo volcanic rocks, Virunga province, D.R. Congo. Journal of Volcanology and Geothermal Research 136, 269-295.

Pouclet, A., Bellon, H., Bram, K., 2017. The Cenozoic volcanism in the Kivu rift: assessment of the tectonic setting, geochemistry, and geochronology of the volcanic activity in the south-Kivu and Virunga regions. Journal of African Earth Sciences 121, 219-246.

Prowatke, S., Klemme, S., 2006. Trace element partitioning between apatite and silicate melts. Geochimica et Cosmochimica Acta 70, 4513-4527.

Rocco, I., Zanetti, A., Melluso, L., Morra, V., 2017. Ancient depleted and enriched mantle lithosphere domains in northern Madagascar: geochemical and isotopic evidence from spinel-to-plagioclase-bearing ultramafic xenoliths. Chemical Geology, 466, 70-85. https://dx.doi.org/10.1016/j.chemgeo.2017.05.016

Roeder, P.L., Emslie, R.F., 1970. Olivine-liquid equilibrium. Contributions to Mineralogy and Petrology 29, 275-289.

Sahama, Th.G., 1962. Petrology of Mt. Nyiragongo: a review. Transactions of the Edinburgh Geological Society 19, 1-28.

Sahama, Th.G., 1978. The Nyiragongo main cone. Musee Royal de l'Afrique Centrale, Tervuren (Belgique). Annales Sciences Geologiques 81, 88.

Sahama, Th.G., Hytönen, K., 1957. Kirschsteinite, a natural analogue to synthetic iron monticellite, from the Belgian Congo. Mineralogical Magazine 31, 698-699.

Sawyer, G.M., Carn, S.A., Tsanev, V.I., Oppenheimer, C., Burton, M., 2008. Investigation into magma degassing at Nyiragongo volcano, Democratic Republic of Congo. Geochemistry Geophysics Geosystems 9, Q02017

~~Spampinato, L., Ganci, G., Hernandez, P.A., Calvo, D., Tedesco, D., Perez, E.Z., N.M., Calvari, S., Del Negro, C, Yalire, NM.M., (2013.). Thermal insights into the dynamics of Nyiragongo lava lake from ground and satellite measurements. Journal of. Geophysical. Research. doi:SOLID EARTH, ISSN: 0148-0227~~ Spampinato, L., Ganci, G., Hernandez, P.A., Calvo, D., Tedesco, D., Perez, N.M., Calvari, S., Del Negro, C., Yalire, M.M., 2013, Thermal insights into the dynamics of Nyiragongo lava lake from ground and satellite measurements. Journal of Geophysical Research 118, 5771-5784. https://dx.doi.org/~~, doi: DOI:~~ 10.1002/2013JB010520

Sun, C., Graff, M., Liang, Y., 2018. Trace element partitioning between plagioclase and silicate melt: the importance of temperature and plagioc~~eo~~lase composition, with implications for terrestrial and lunar magmatism. Geochimica et Cosmochimica Acta 206, 273-295.

Tazieff, H., 1984. Mt. Nyiragongo: Renewed activity of the lava lake. Journal of Volcanology and Geothermal Research 20, 267–280.

Tazieff, H., 1994. Permanent lava lakes: Observed facts and induced mechanisms. Journal of Volcanology and Geothermal Research 63, 3~~–~~-11.

Tedesco, D., 2003. The pre-2002 activity - 1995 Nyiragongo and Nyamulagira activity in the Virunga National Park: a volcanic crisis. Acta Vulcanologica 14-15, 149-155.

Tedesco, D., Tassi, F., Vaselli, O., Poreda, R.J., Darrah, T., Cuoco, E., ~~and~~ Yalire, M., 2010. Gas isotopic signatures (He, C, and Ar) in the Lake Kivu region (western branch of the East African rift system): Geodynamic and volcanological implications~~"~~. Journal of~~,~~ Geophysical~~,~~ Research~~,~~, 115, B01205; https://dx.doi.~~doi:~~org/10.1029/2008JB006227~~.~~

Tedesco, D., Vaselli, O., Papale, P., Carn, S.A., Voltaggio, M., Sawyer, G.M., Durieux, J., Kasereka, M., Tassi, F., 2007. January 2002 volcano-tectonic eruption of Nyiragongo volcano, Democratic Republic of Congo. Journal of Geophysical Research B112, B09202.

Toscani, L., Capedri, S., Oddone M., 1990. New chemical and petrographic data of some undersaturated lavas from Nyiragongo and Mikeno (Virunga-Western African rift – Zaire). Neues Jahrbuch für Mineralogie Abhandlungen 161, 287-302.

Velde, D., Rachdi, H.En-N., 1988. Influence of Sr on an established petrological incompatibility: the association melilite+K-feldspar in a nephelinite from Djebel Targou, central Morocco. Journal of Petrology 29, 585-597.

Valade, S., Ripepe, M., Giuffrida, G., Karume, K., Tedesco, D., 2018. Dynamics of Mount Nyiragongo lava lake inferred from thermal imaging and infrasound array. Earth and Planetary~~,~~ Science~~,~~ Letters~~,~~ ~~Vol.~~ 500, ~~Pages~~ 192-204.

Verhulst, A., Balaganskaya, E., Kirnarsky, Y., Demaiffe, D., 2000. Petrological and geochemical (trace elements and Sr-Nd isotopes) characteristics of the Paleozoic Kovdor ultramafic, alkaline and carbonatite intrusion (Kola Peninsula, NW Russia). Lithos 51, 1-25.

Watson, E.B., Green, T.H., 1981. Apatite/liquid partition coefficients for the rare earth elements and strontium. Earth and Planetary Science Letters 56, 405-421.

Wiedenmann, D., Keller, J., Zaitsev, A.N., 2010. Melilite-group minerals at the Oldoinyo Lengai, Tanzania. Lithos 118, 112-118.

Wiedenmann, D., Zaitsev, A.N., Britvin, S.N., Krivovichev, S.V., Keller, J., 2009. Alumoåkermanite, $(Ca,Na)_2(Al,Mg,Fe^{2+})(Si_2O_7)$, a new mineral from the active carbonatite-nephelinite-phonolite volcano Oldoinyo Lengai, northern Tanzania. Mineralogical Magazine 73, 373-384.

Woolley, A.R., Bergman, S.C., Edgar, A.D., Le Bas, M.J., Mitchell, R.H., Scott Smith , B.H., 1996. Classification of lamprophyres, lamproites, kimberlites, and the kalsilitic, melilitic, and leucitic rocks. The Canadian Mineralogist 34, 175-186.

Yoder, H.S., jr., 1973. -Melilite stability and paragenesis. Fortschritte der Mineralogie (International Journal of Earth Sciences) 50, 140-173.

~~Appendix. Analytical techniques~~

~~Whole-rock major and trace elements were analysed by X-ray fluorescence (XRF) using a Panalytical Axios instrument at the University of Napoli (cf. Cucciniello et al., 2017, for further analytical details). Analytical uncertainties are in the order of 1-2% for major elements and 5-10% for trace elements (Table 1). The weight loss on ignition (L.O.I.) was determined with standard gravimetric techniques, after igniting one gram of rock powder at 1000 °C for 6 h. Lanthanides (REE) and other trace elements were determined by Inductively Coupled Plasma-Mass Spectrometry (ICP-MS) at Activation Laboratories (Ancaster, Ontario; see http://www.actlabs.com for a full description of the analytical techniques). The major element concentrations of mineral and glass phases were determined at DISTAR, University of Napoli Federico II, by Energy Dispersive Spectrometry (EDS) microanalyses using an Oxford Instruments Microanalysis Unit equipped with an INCA X-act detector and a JEOL JSM-5310 Scanning Electron Microscope (SEM) using a JEOL JSM5310. Measurements were done with an INCA X-stream pulse processor operating at 15 kV primary beam voltage, 50-100 mA filament current, variable spot size and 50 s net acquisition time. The following reference materials were used for calibration: diopside (Mg), wollastonite (Ca), albite (Al, Si, Na), rutile (Ti), almandine (Fe), Cr_2O_3 (Cr), rhodonite (Mn), orthoclase (K), apatite (P), fluorite (F), barite (Ba), strontianite (Sr), Smithsonian orthophosphates (La, Ce, Nd, Sm, Y), pure vanadium (V) and Corning glass (Th and U). LA-ICP-MS trace element analyses were performed in olivine, clinopyroxene, melilite, apatite, magnetite, nepheline, leucite and glass of selected areas (cf. Fig. 2). Analyses were carried out at IGG-CNR of Pavia by Laser Ablation-Inductively Coupled Plasma-High Resolution Mass Spectrometry (LA-ICP-HRMS). The microprobe consists of a double-focusing sector-field analyser (Finnigan Mat, Element I) coupled~~

Formatted: English (United Kingdom)

Formatted: Font: Not Italic

Formatted: Font: Not Italic

Formatted: Font: Not Italic

Formatted: Font: Not Italic

Formatted: Right: -0.01 cm, Line spacing: 1.5 lines

Formatted: English (United Kingdom)

~~with a Q-switched Nd:YAG laser source (Quantel Brilliant). The fundamental emission of the laser source (1064 nm, in the near-IR region) was converted to 213 nm by three harmonic generators. Helium was used as carrier gas and mixed with Ar downstream of the ablation cell. Spot diameter was varied in the range of 40-60 μm. Quantification was carried out using the NIST SRM 610 glass as external standard (Pearce et al., 1996). Si was used as internal standard for melilite, clinopyroxene, olivine, nepheline, leucite and glass, while Ca was used for apatite and Ti for magnetite. Detection limits are in the range 100-500 ppb for Sc, Ti, and Cr; 10-100 ppb for V, Rb, Sr, Zr, Cs, Ba, Gd, and Pb; 1-10 ppb for Y, Nb, La, Ce, Nd, Sm, Eu, Tb, Dy, Er, Yb, Hf and Ta, and usually <1 ppb for Pr, Ho, Tm, Lu, Th, and U. Precision and accuracy (both better than 10% for concentrations at parts per million level) were assessed by means of repeated analyses of NIST SRM 612 and BCR-2g standards. The composition of the glass beneath the thin section has been documented before the sample analysis to recognize piercing of the rock and to eliminate any glass contribution. The gas background was measured for 60 s, as in any other routine analysis, whereas signals during ablation were acquired for approximately 20-50 s. Analyses were performed with 10 Hz repetition rate of laser and ~1-2.5 mJ/s laser power. Full details are reported in Rocco et al. (2017). Precautions have been taken to avoid any bias on the analytical results. Memory effects have been taken into account leaving more than 1 min between two consecutive analyses and analysing glasses after the minerals. Spurious signals related to memory effects usually affect more blanks (because less time is passed after the previous analysis), thus determining worsening of the detection limits and hindering the quantification of elements at ultra-trace concentration level. Surface contamination during sample polishing and/or handling before the micro-analytical measurement and occurrence of micro-inclusions of glass/fluid have been monitored by detailed inspection of the signal profiles acquired during ablation. Only intervals with parallel signals have been integrated. Anomalous signal contributions at the beginning of the ablation (due to surface contamination) and/or randomly occurring during ablation (possibly related to inclusions and/or memory effect) has been accurately documented and excluded by integration.~~

Formatted: English (United Kingdom)

Figure captions

Fig. 1. Geomorphological sketch map of the Nyiragongo volcano (a) with the ~~field~~ sampling ~~areas~~ sites of the investigated samples of 2016 (b, c) and 2002 (d). Note that the structural position of the other volcanic complexes of the Virunga is not consistent with the elongation of the Albertine Rift (cf. also Pouclet et al., 2017).

Formatted: English (United Kingdom)

Fig. 2.1. a) b) c) d). Petrographic appearance of the Nyiragongo lavas of 2002 and 2016. Note the abundant melilite laths, the nepheline cluster and the apatite microphenocryst with a laser pit.

Fig. 2.2. a) b) c) d). Backscattered electron (BSE) images of sites in the Nyiragongo lavas of 2002 and 2016: microlites of melilite, olivine, feldspathoids and microphenocrysts of magnetite and apatite are visible in a generally clean glassy matrix. The iron- and calcium-rich nature of the glass is also evident from the more whitish grey tones with respect to most mafic phases. Also note a cotectic intergrowth of nepheline and melilite (±leucite) in b), resembling a granophyre.

Fig. 3. Total alkali vs. silica (T.A.S.) classification diagram (Le Maitre, 2002) with bulk-rock (red circles) and glass analyses (orange rhombs) from the investigated Nyiragongo samples. Other rocks of Nyiragongo (grey) are taken from Platz et al. (2004) and Minissale (2018).

Fig. 4. Composition of the main mineral phases of the 2002 and 2016 lavas. a) Composition of the Nyiragongo melilites in the Åkermanite-Fe-Åkermanite-soda-melilite diagram (mol.%). Melilites of Kaiserstuhl (black lines) are from Braunger et al. (2018); melilites of Italy (grey squares) from Melluso et al. (2011b, 2012 and references therein); melilititesof Madagascar (dark grey triangles) from Melluso et al., 2011a; melilites of Tanzania (grey ~~triangles~~crosses) from a compilation in Melluso et al. (2010), ~~and~~ Wiedenmann et al. (2009, 2010) and Guzmics et al. (2012); b) nepheline compositions of 1977, 2002 and 2016 lavas as plotted in the nepheline-kalsilite-silica diagram (in wt.%)~~as (red circles)~~; other Nyiragongo nephelines are grey rhombs; the green circle is the Nyiragongo nepheline studied by Antao and Nicholls (2018); nepheline of the Madagascar olivine melilititesfrom Melluso et al. 2011a (dark grey triangles); c) clinopyroxene and olivine compositions of the 1977, 2002 and 2016 lavas as plotted in the Ca-Mg-Fe diagram (mol.%); clinopyroxenes of other Nyiragongo rocks are from Minissale (2018); clinopyroxenes of the Madagascan melilititesfrom Melluso et al. (2011a); olivines from other Nyiragongo rocks (grey circles) from Minissale (2018) and Sahama and Hytönen (1957; the blackquare~~ue circle~~).

Fig. 5. a) b) mantle-normalized patterns of bulk-rocks, glass, clinopyroxene, melilite and apatite, relative to mantle composition of Lyubetskaya and Korenaga (2007). Note that K and P were not plotted. The trace element analyses of melilites of Kaiserstuhl and Tur~~yiiy~~yi (taken from Arzamastsev et al., 2009) are also plotted for comparison.

Fig. 6. Phase diagrams with the composition of glasses and bulk-rocks of Nyiragongo (Pan and Longhi, 1990; Gupta, 2015). The continuous lines in (a) are mostly thermal barriers connecting the composition of various phases. They should be seen as projections of planes connecting also olivine (forsterite).

Fig. 7. Diagrams with mineral-glass ~~elemental ratios~~partition coefficients for REE, compared with known partition coefficients from the literature (data from Table 3).

Table captions

Table 1. bulk-rock compositions of the 2002 and 2016 lavas, together with that of the 1977 eruption and that of the lava outpouring from the spatter cone in 2017 ~~spatter cone~~. Modal analyses of microphenocrysts and glass are also reported.

Table 2. LA-ICP-MS composition of the phases of 2002 and 2016 lavas (in ppm).

Table 3. The average composition of glasses (in ppm), and ~~elemental ratios~~partition coefficients, obtained by dividing the average concentration of the elements in the various phases and the average composition of the relative glass. Reference partition coefficients from the literature are also reported (Onuma et al., 1981; Foley and Jenner, 2004, Prowatke and Klemme, 2006~~;~~; Dawson et al., 2008; Fedele et al., 2015; Ambrosio and Azzone, 2018~~; Dawson et al., 2008~~).

Supplementary Tables

Supplementary Table 1. Glass compositions of the 2002 and 2016 lavas

Supplementary Table 2. Melilite compositions of the 2002 ~~and~~ , 2016 and 1977 lavas.

Supplementary Table 3. Nepheline and leucite compositions of the 2002, 2016 and 1977 ~~2002 and 2016~~ lavas.

Supplementary Table 4. Clinopyroxene compositions of the 2002, 2016 and 1977 ~~2002 and 2016~~ lavas.

Supplementary Table 5. Olivine compositions of the 2002, 2016 and 1977 lavas.

Supplementary Table ~~5~~6. Apatite compositions of the 2002 and 2016 lavas.

~~Supplementary Table 6. Olivine compositions of the 2002 and 2016 lavas.~~

Supplementary Table 7. Magnetite compositions of the 2002 and 2016 lavas.

Supplementary figures

Supplementary Fig. 1. Rhodes diagram for olivine, clinopyroxene and melilite compositions of the lavas of 2002 and 2016. The curves are traced at K_dFe-Mg=0.23, 0.27, 0.30 and 0.33 (Bédard, 2010; Roeder and Emslie, 1970). Note that the Mg# of bulk-rocks and mineral phases is calculated with all Fe as divalent.

Supplementary Fig. 2 ~~(Fig. 8?)~~. The chondrite normalized patterns of the Nyiragongo melilites, and comparison with various types of feldspar taken from various places and magmatic series (data are taken from Dawson et al., 2009; Arzamastsev et al., 2009; Cucciniello et al. 2014; Fedele et al., 2015; Melluso et al., 2014, 2018).

Supplementary Fig. 3 ~~(2?)~~. Extended bulk-rock concentration ratios for clinopyroxene and melilite. Reference patterns for clinopyroxene of kamafugites, lamproites and silica-undersaturated trachytes are also shown (data from Foley and Jenner, 2004; Melluso et al., 2008; Fedele et al., 2009). Note that the clinopyroxene of the kamafugite (Melluso et al., 2008) coexists with perovskite which heavily scavenges LREE, hence the ~~concentration ratios~~partition coefficients for a number of elements are much lower than in the Nyiragongo clinopyroxene.

Supplementary Fig. 4. Chondrite-normalized REE diagram of the Nyiragongo-Shaheru bulk rocks with those of this study. The data are taken from this study, Platz et al. (2004); Chakrabarti et al., 2009 and Minissale~~,~~ (2018).

Formatted: Font: Times New Roman

Formatted: Font: Times New Roman

Formatted: Font: Times New Roman

Formatted: Font: Times New Roman

Figure 1

Click here to download high resolution image

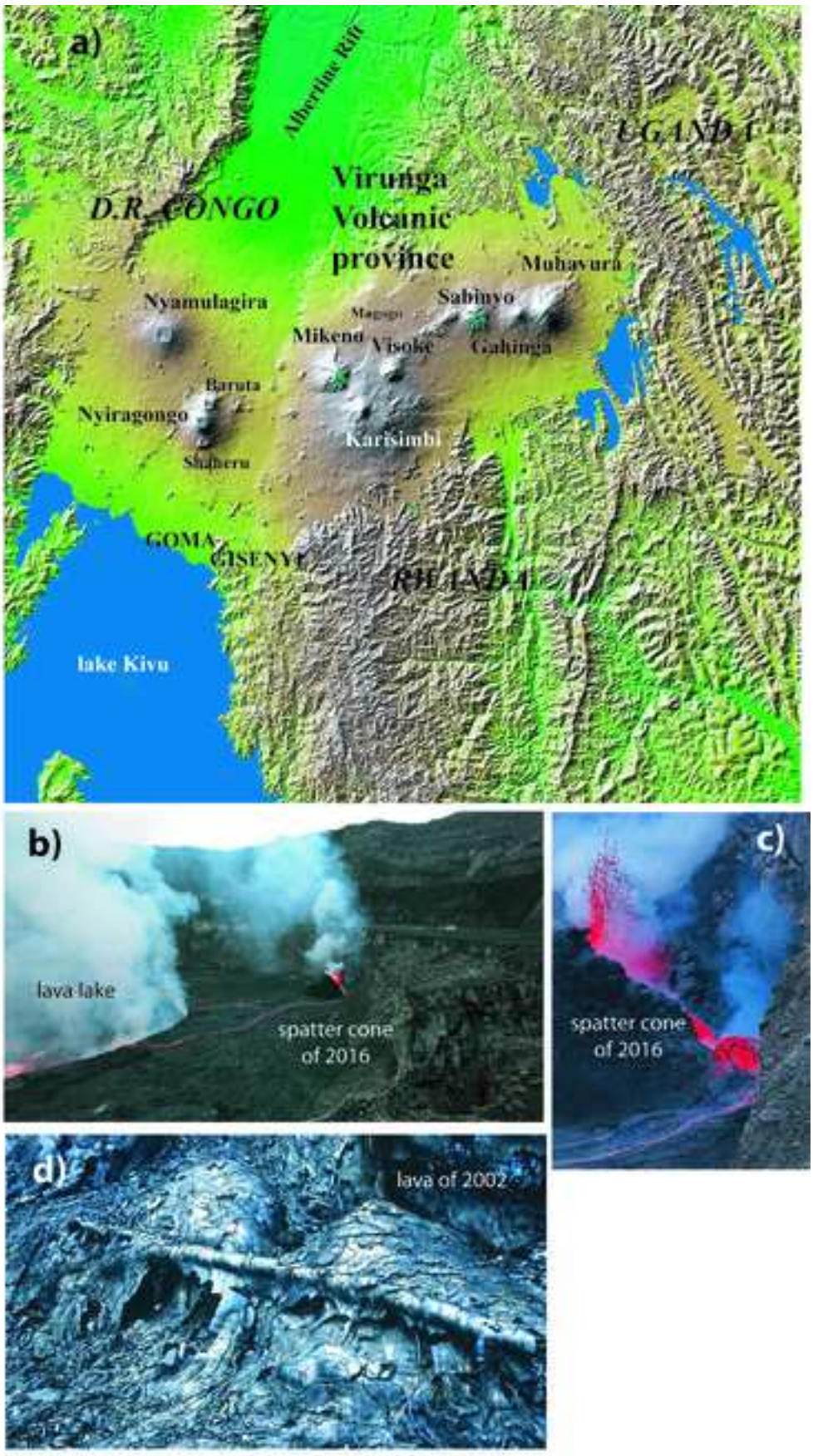

Figure 2.1
Click here to download high resolution image

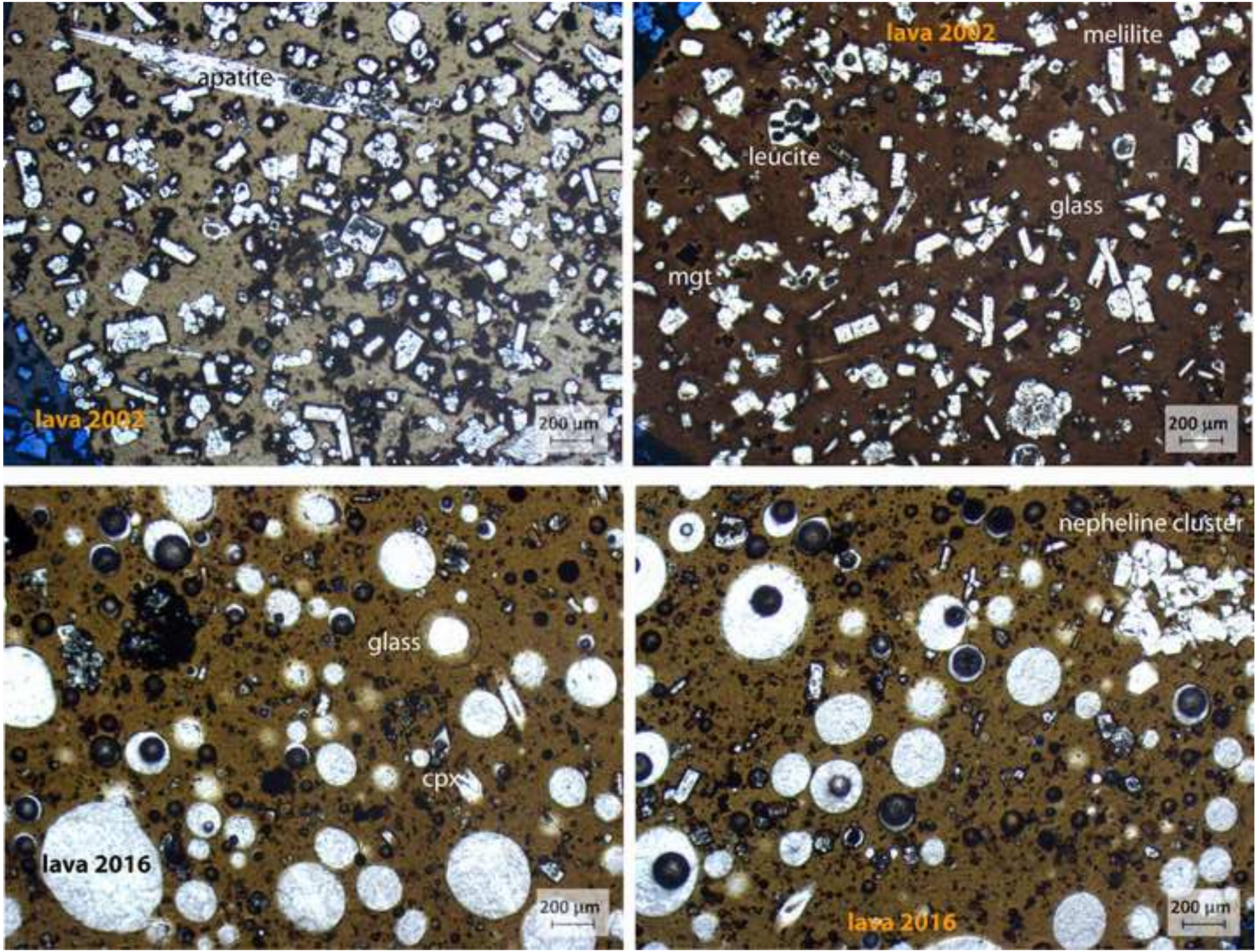

Figure 2.2

Click here to download high resolution image

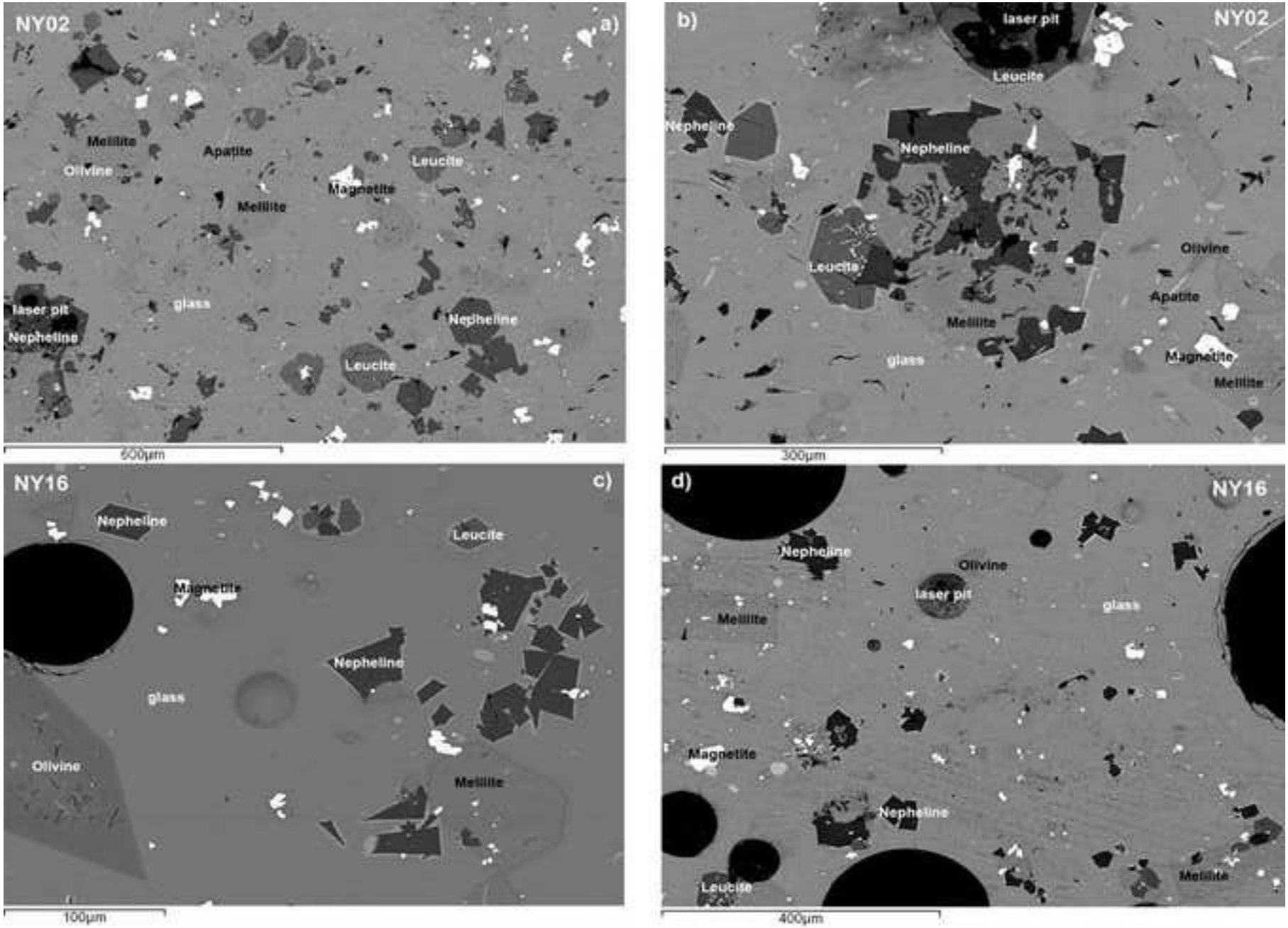

Figure 3

Click here to download high resolution image

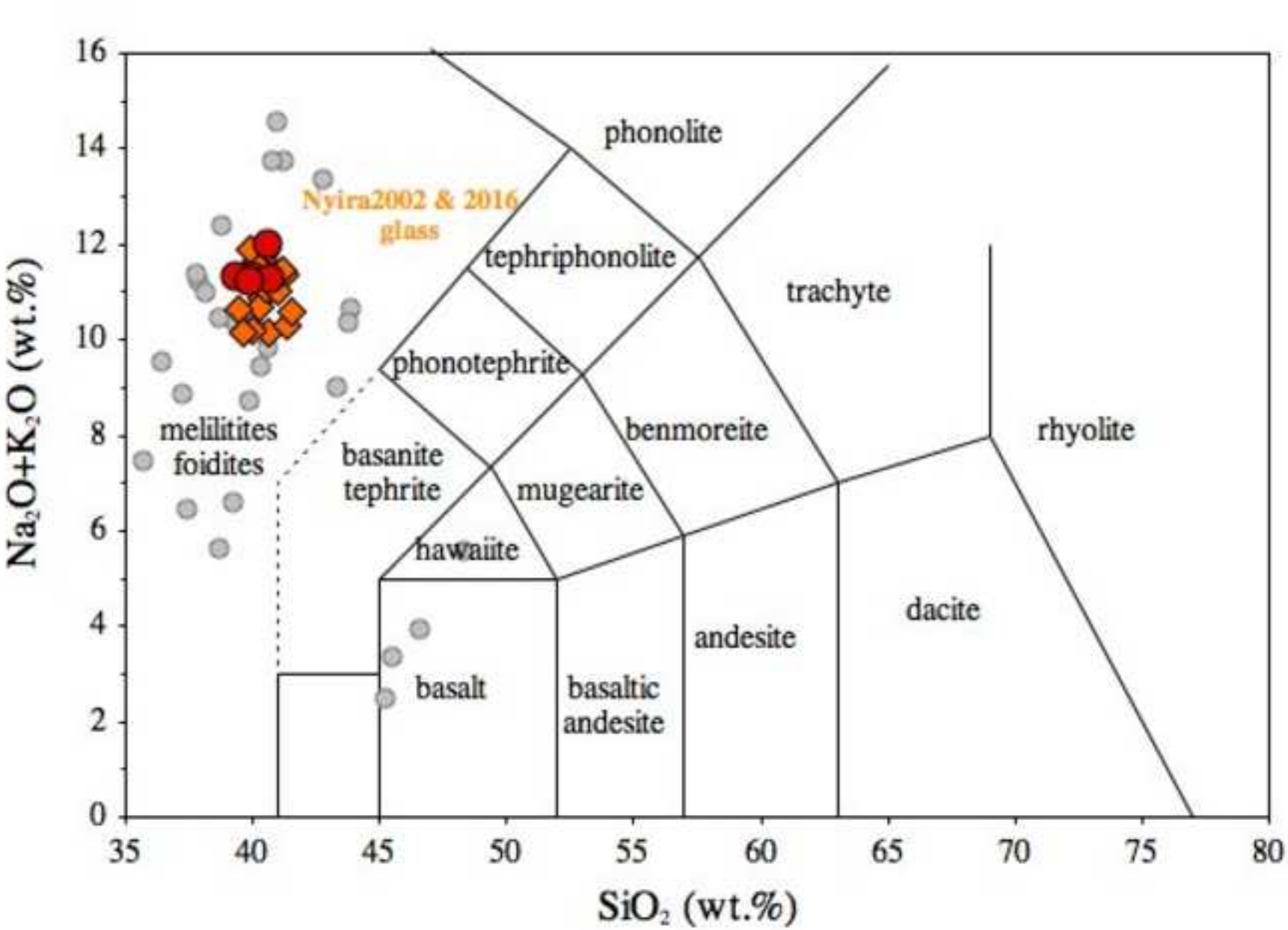

Figure 4

Click here to download high resolution image

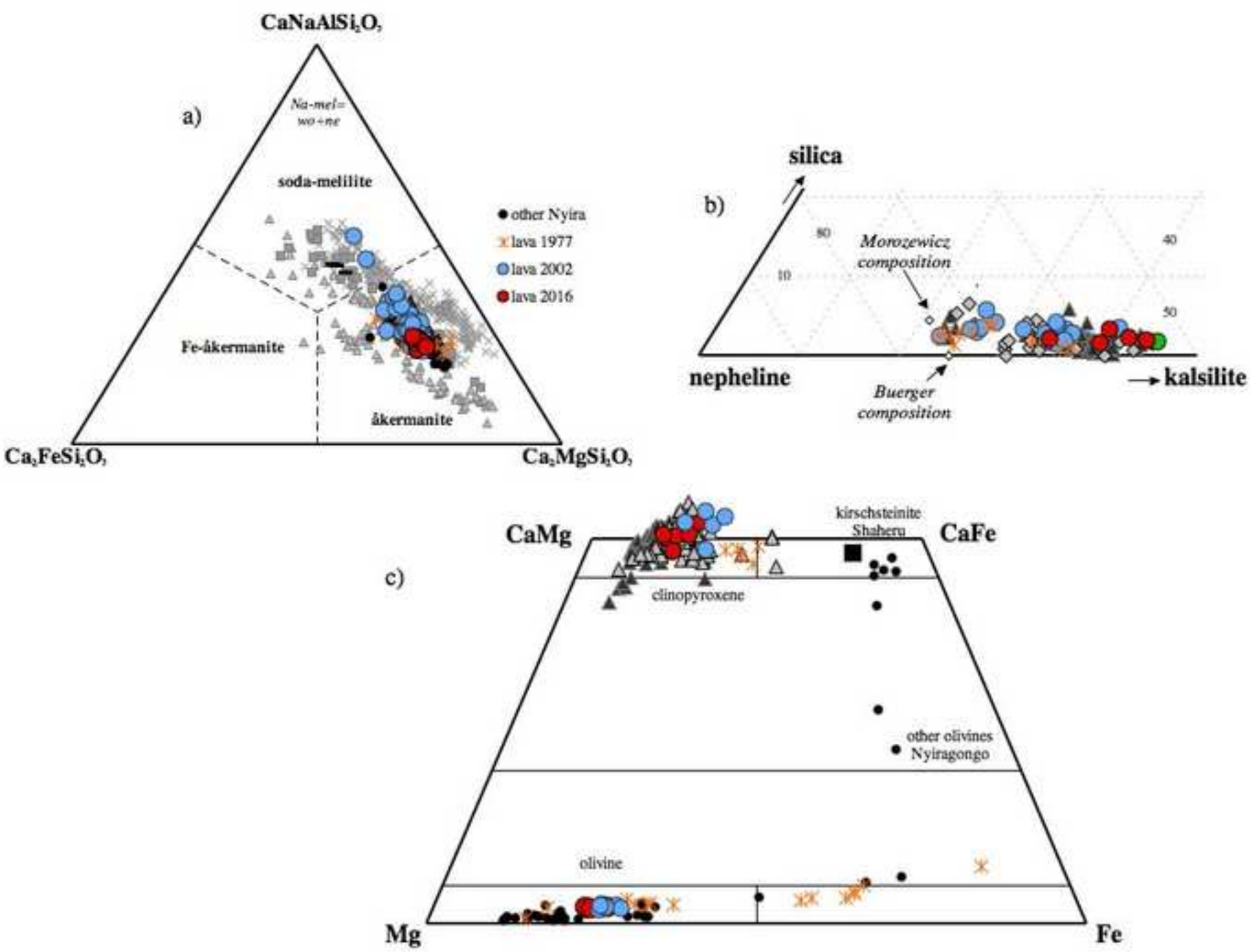

Figure 5

Click here to download high resolution image

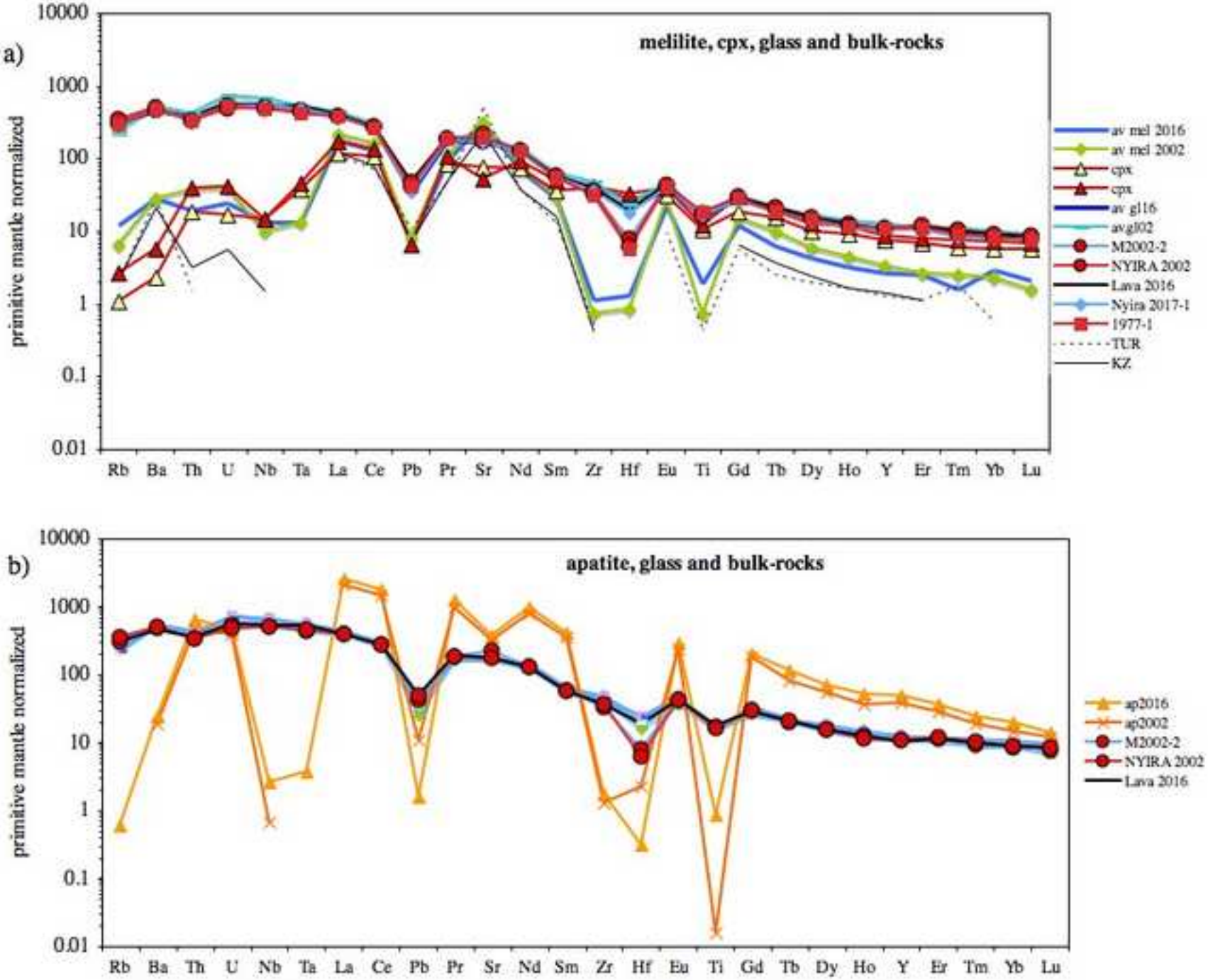

Figure 6

Click here to download high resolution image

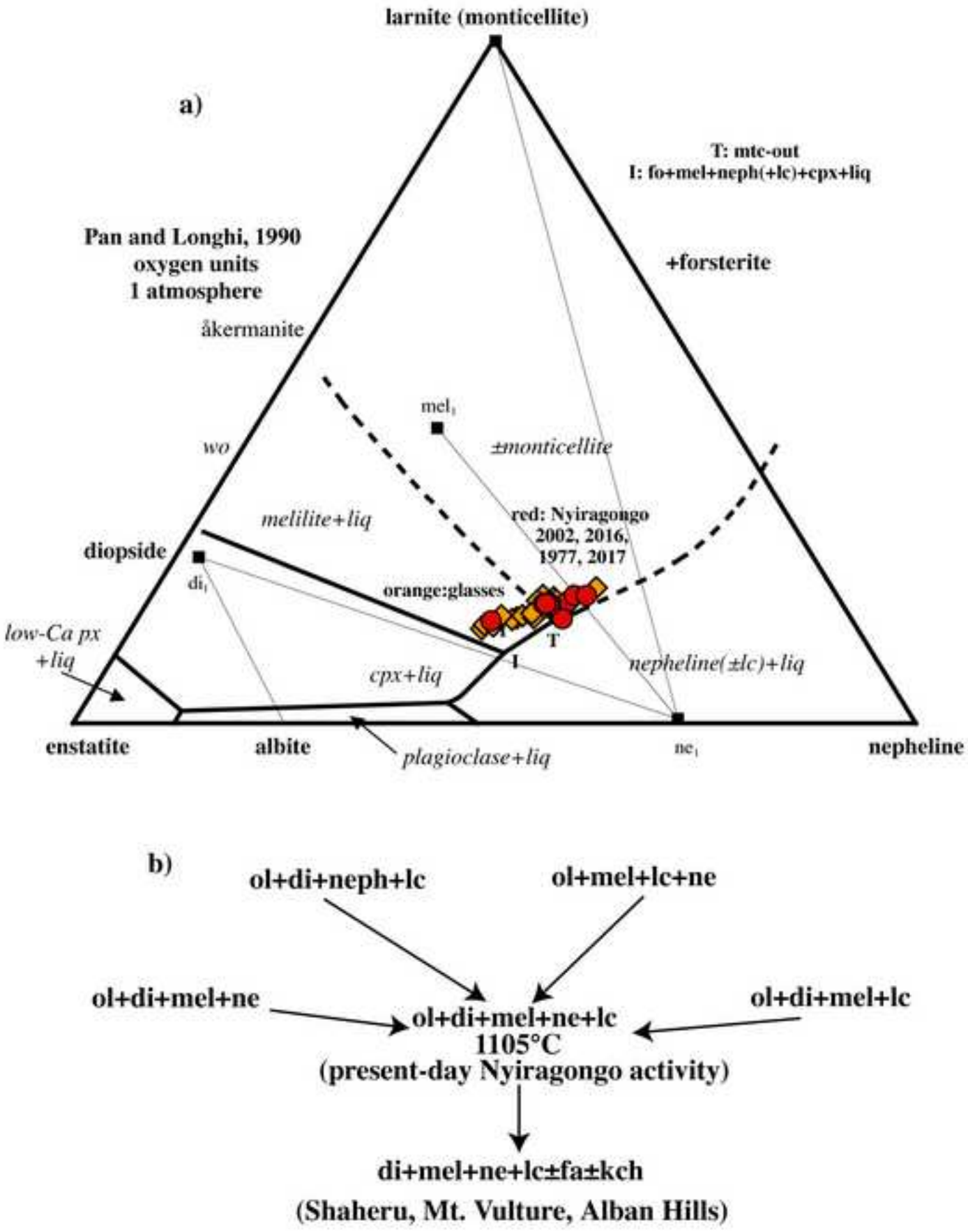

Figure 7

Click here to download high resolution image

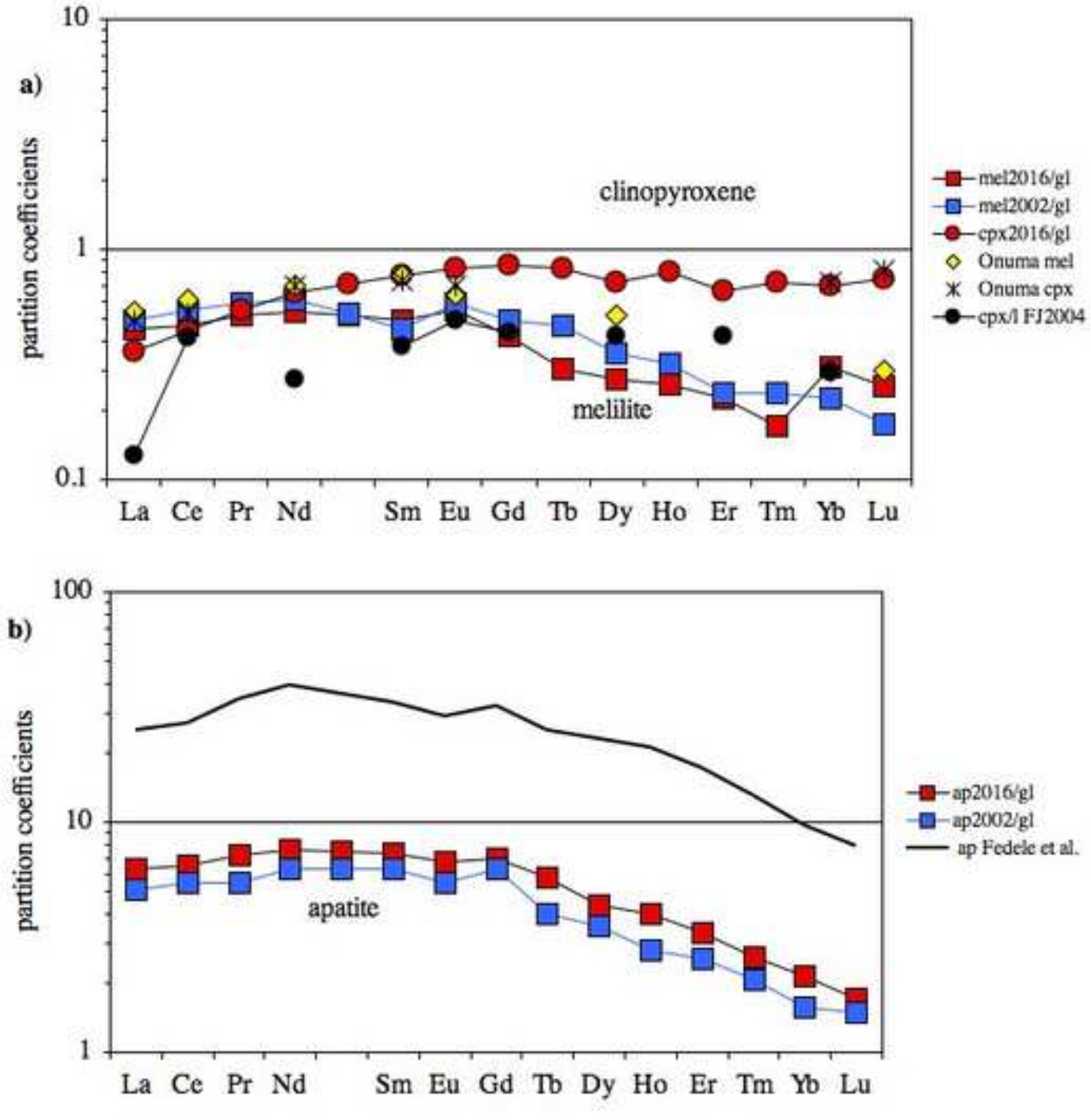

Table 1

Click here to download Table: Table1Nyira.xls

Table 1

	Lava 2002	Lava 2002-2	Lava 2016	Lava 2017-1	Lava 1977-1
SiO_2	40.17	40.77	39.12	41.00	40.10
TiO_2	2.74	2.54	2.81	2.70	2.88
Al_2O_3	14.72	16.13	14.87	14.72	14.90
Fe_2O_{3t}	13.22	12.92	13.41	13.38	13.50
MnO	0.29	0.30	0.29	0.29	0.29
MgO	4.19	3.39	4.02	3.99	4.16
CaO	12.21	11.00	12.01	11.85	11.90
Na_2O	5.80	5.76	5.62	5.71	5.64
K_2O	5.55	6.29	5.64	5.61	5.63
P_2O_5	1.47	1.27	1.59	1.45	1.48
LOI	-1.63	-0.59	0.39	-1.04	-1.01
Total	98.74	99.78	99.78	99.66	99.47
Be	4	4	4	4	4
Sc	5	3	4	5	5
V	285	241	287	277	290
Cr					
Co	40	36	45	42	42
Ni			50	30	
Cu	180	160	180	190	200
Zn	130	140	120	120	130
Ga	20	21	20	20	20
Ge	1	1	1	1	1
Rb	140	162	138	137	141
Sr	3474	2751	2693	2702	3133
Y	37	37	34	36	37
Zr	273	306	313	303	268
Nb	227	236	239	243	223
Mo	6	6	7	7	7
Sn	2	2	27	2	3
Sb	0.5	0.5			
Cs	1.5	1.6	1.5	1.4	1.5
Ba	2389	2593	2278	2350	2422
La	197.0	195.0	201.0	194.0	194.0
Ce	365.0	364.0	373.0	359.0	357.0
Pr	37.7	38.2	38.8	36.5	37.3
Nd	125.0	128.0	129.0	123.0	125.0
Sm	18.3	18.9	18.9	17.4	18.2
Eu	5.1	5.3	5.3	4.9	5.2
Gd	12.6	12.9	12.5	10.9	12.4
Tb	1.6	1.7	1.7	1.5	1.5
Dy	8.1	8.4	8.4	7.7	7.8
Ho	1.5	1.4	1.5	1.3	1.4
Er	3.9	4.2	4.0	3.6	3.8
Tm	0.5	0.6	0.5	0.5	0.5
Yb	2.9	3.1	3.1	2.7	2.9
Lu	0.4	0.5	0.5	0.4	0.4
Hf	1.8	1.4	4.3	4.1	1.3
Ta	13.0	13.7	16.3	14.4	12.8
W	3	2	2	2	7
Tl				0.4	
Pb	6	7	7	5	6
Th	21	20.7	22.3	21.4	20.8
U	9	8.4	9.9	9.2	9.1
Cl%			0.13		
F%			0.17		
Total S%			0.20		
La/Yb_n	45.8	42.4	43.7	48.4	45.1
Th/U	2.3	2.5	2.3	2.3	2.3
Zr/Hf	151.4	218.6	72.8	73.9	206.4
Nb/Ta	17.5	17.2	14.7	16.9	17.4
Nb/U	25.2	28.1	24.1	26.4	24.5
La/Nb	0.9	0.8	0.8	0.8	0.9
Ba/Nb	10.5	11.0	9.5	9.7	10.9
Zr/Nb	1.2	1.3	1.3	1.2	1.2
Eu/Eu*	1.03	1.04	1.04	1.07	1.04
SREE	780	782	798	763	767
PI	1.06	1.01	1.03	1.05	1.03
Mg#	39	34	37	37	38

Table 2

Click here to download Table: Table2Nyira.xls

Table 2

	Nyiragongo 2016 glass an. 1	Nyiragongo 2016 glass an. 2	Nyiragongo 2016 glass an. 3	Nyiragongo 2016 glass an. 4	Nyiragongo 2016 glass an. 5	Nyiragongo 2016 glass an. 6	Nyiragongo 2016 glass an. 7	Nyiragongo 2016 glass an. 8	Nyiragongo 2016 glass an. 9	Nyiragongo 2016 glass an. 10	Nyiragongo 2016 glass an. 11	Nyiragongo 2016 glass an. 12	Nyiragongo 2002 glass an. 1	Nyiragongo 2002 glass an. 2	Nyiragongo 2002 glass an. 3	Nyiragongo 2002 glass an. 4	Nyiragongo 2002 glass an. 5	Nyiragongo 2002 glass an. 6	Nyiragongo 2002 glass an. 7
Li	12.9	13.3	12.4	14.0	13.6	13.7	14.0	13.0	13.4	16.1	10.0	13.4	16.4	16.9	16.8	12.3	18.6	13.7	16.8
B	61.9	55.2	55.2	54.8	50.0	21.9	27.8	24.0	26.9	23.9	10.2	30.4	18.3	16.1	12.4	34.9	27.4	18.1	31.1
Sc	5.8	6.4	6.0	5.7	5.9	5.8	5.4	5.7	5.7	5.8	5.9	5.2	6.5	6.1	6.0	6.5	6.1	5.7	6.1
V	239.8	251.7	242.8	252.5	236.1	268.7	258.6	236.7	248.7	237.2	221.5	222.4	231.0	213.2	223.2	212.7	236.3	207.4	204.8
Cr	5.3	3.2	3.6	1.9	5.3	7.5	5.2	2.9	3.2	5.3			3.7	<1.28	1.4	5.6	2.2	1.6	3.6
Co	40.5	47.2	39.9	41.6	39.4	42.3	42.5	39.8	41.1	41.2	41.7	36.4	37.7	35.2	36.9	35.5	38.7	36.5	34.0
Ni	14.6	14.7	16.3	15.5	13.6	22.3	19.9	15.2	15.3	16.3	13.5	16.7	9.6	8.8	7.9	10.0	7.2	10.3	6.6
Zn	209.8	225.0	211.3	232.0	162.4	155.8	150.6	147.6	148.9	155.6	207.5	158.4	222.4	180.1	171.9	191.0	161.0	146.5	152.6
Rb	147.6	153.6	143.6	151.8	143.9	139.3	139.6	140.0	144.6	146.0	136.8	135.8	112.4	104.5	118.1	110.1	115.8	97.6	104.8
Sr	2721.1	2890.2	2731.7	2758.2	2609.9	2628.4	2696.9	2605.0	2831.5	2652.7	2599.8	2484.4	2920.7	2723.3	2807.6	2776.4	2928.7	2636.1	2633.9
Y	38.1	39.9	37.2	42.4	36.5	36.9	36.8	37.2	40.1	37.8	36.3	34.3	43.1	42.7	42.3	42.5	43.9	40.3	41.0
Zr	346.1	369.1	344.5	360.7	325.3	325.1	333.3	330.4	335.5	333.3	316.9	326.1	414.0	385.3	404.0	396.4	414.0	367.6	377.3
Nb	262.6	280.5	266.1	268.5	247.4	250.2	251.4	245.4	258.0	255.0	242.9	243.6	322.4	297.4	308.9	298.7	318.7	294.7	281.1
Cs	1.7	1.5	1.4	1.7	1.5	1.6	1.5	1.5	1.6	1.6	1.9	1.3	1.0	0.8	0.9	0.8	1.0	0.9	0.8
Ba	2451.0	2607.5	2459.6	2518.0	2299.2	2360.5	2394.3	2337.2	2403.3	2363.8	2287.8	2309.0	2890.9	2664.7	2791.2	2667.3	2828.6	2580.2	2516.2
La	208.4	219.3	210.5	211.4	199.1	197.1	203.0	196.8	226.6	199.8	194.4	192.3	233.0	226.0	219.7	225.4	229.9	222.9	223.2
Ce	364.0	386.0	362.2	367.9	342.3	345.5	357.0	350.4	409.3	355.2	382.0	336.8	402.8	394.1	386.3	400.3	394.9	400.6	390.4
Pr	36.5	39.1	35.8	36.4	35.0	34.6	36.0	34.9	40.1	35.0	34.0	31.9	39.0	40.0	37.5	40.9	39.4	37.3	39.7
Nd	125.9	137.9	131.5	130.0	122.2	121.9	128.3	125.6	146.6	121.5	121.9	113.8	137.4	141.3	135.8	135.9	145.3	134.9	136.2
Sm	17.3	17.9	18.5	19.3	18.2	17.1	17.7	17.9	21.5	18.8	16.5	18.1	21.2	21.4	19.9	21.7	21.1	19.2	21.8
Eu	5.3	5.9	5.2	5.4	4.8	4.9	5.5	4.9	5.9	4.8	5.0	4.3	6.0	6.0	6.2	6.1	6.2	4.9	5.9
Gd	11.9	14.3	12.2	13.5	11.5	11.0	12.5	11.8	13.4	13.0	11.9	11.0	15.8	14.9	14.3	14.6	13.3	10.7	11.8
Tb	1.7	1.6	1.8	1.6	1.6	1.6	1.6	1.6	1.8	1.5	1.5	1.7	1.6	1.7	2.0	1.7	1.8	1.6	1.6
Dy	8.1	9.4	9.6	9.5	8.0	7.4	7.9	7.6	9.6	8.4	9.6	8.0	9.7	8.7	7.9	9.9	10.1	8.6	10.0
Ho	1.6	1.7	1.6	1.6	1.6	1.6	1.5	1.4	1.7	1.4	1.3	1.4	1.5	1.8	1.6	1.5	1.9	1.6	1.7
Er	3.9	4.1	3.8	3.8	4.2	4.3	3.9	3.3	3.9	3.8	3.6	3.6	3.3	3.7	4.2	3.7	4.1	4.0	3.6
Tm	0.5	0.5	0.5	0.5	0.5	0.4	0.4	0.5	0.6	0.4	0.6	0.5	0.6	0.6	0.7	0.5	0.6	0.6	0.6
Yb	3.3	2.9	3.4	3.3	3.3	3.2	2.9	3.1	3.7	3.4	3.7	3.1	3.2	3.6	2.8	3.4	3.6	3.9	3.7
Lu	0.5	0.4	0.4	0.4	0.4	0.4	0.5	0.5	0.5	0.4	0.5	0.5	0.5	0.5	0.4	0.6	0.5		0.5
Hf	5.3	4.6	4.7	4.2	4.5	4.1	4.5	4.7	4.9	4.6	3.9	3.4	5.2	4.7	5.9	5.4	5.4	5.5	5.4
Ta	13.5	14.4	12.9	14.2	12.7	12.9	13.3	12.9	13.9	13.0	12.5	13.0	16.7	16.1	16.9	15.2	17.5	16.0	15.8
Pb	4.7	6.0	5.5	6.0	4.5	5.0	5.0	4.7	5.2	5.2	4.0	3.5	6.5	5.8	6.9	6.0	6.0	6.7	6.1
Th	22.8	24.1	23.4	23.6	23.1	24.3	23.4	23.8	25.2	23.5	23.6	24.5	28.5	27.9	26.9	26.1	28.7	24.3	25.9
U	9.3	10.2	9.9	10.0	9.9	10.0	9.7	9.6	10.6	10.1	7.8	8.9	13.3	12.5	13.0	12.8	12.3	12.4	11.6

	Nyiragongo 2016 mel xtl 1	Nyiragongo 2016 mel xtl 2	Nyiragongo 2016 mel xtl 3	Nyiragongo 2016 mel xtl 4	Nyiragongo 2016 mel xtl 5	Nyiragongo 2016 mel xtl 6	Nyiragongo 2016 mel xtl 7	Nyiragongo 2016 mel xtl 8	Nyiragongo 2016 mel xtl 9	Nyiragongo 2002 mel xtl 1	Nyiragongo 2002 mel xtl 2	Nyiragongo 2002 mel xtl 3	Nyiragongo 2002 mel xtl 4	Nyiragongo 2002 mel xtl 5	Nyiragongo 2002 mel xtl 6	Nyiragongo 2002 mel xtl 7	Nyiragongo 2002 mel xtl 8	Nyiragongo 2002 mel xtl 9	Nyiragongo 2002 mel xtl 10	Nyiragongo 2002 mel xtl 11	Nyiragongo 2002 mel xtl 12
Li	2.2	4.9	1.7	0.7	1.5	0.6	1.9	4.2	1.3	1.2				1.5	3.4	0.9	2.4	1.1	0.5	5.9	1.1
B	25.8	31.2	37.0	42.2	<6.29	21.4	25.6	6.9		15.2				18.4	21.3	7.4	19.8	26.3	29.6	15.7	26.7
Sc	1.9		3.4	2.8	1.4	2.5	1.5	1.9		1.3				0.9	2.2	1.2	1.4	1.5	2.3	1.8	0.8
V	11.5	31.7	70.3	30.9	153.1	32.5	49.5	33.7	9.8	10.5	24.8	20.3	22.6	7.9	15.0	27.0	40.0	10.8	16.8	12.4	11.4
Cr			9.5	3.6	5.5	<3.10	<3.23	<3.02	7.0	3.8						5.5			5.4	5.8	
Co	41.9	47.8	50.1	42.4	56.7	43.7	45.4	42.5	46.5	37.5	43.2	40.5	41.8	39.6	41.8	41.8	44.6	42.0	35.0	37.3	38.4
Ni	13.1	15.0	15.0	12.4	35.3	19.7	17.3	12.7	10.7	9.5	8.0	17.6	12.8	4.3	8.4	6.3	12.2	8.9	10.3	5.2	6.8
Zn	389.4	396.5	342.5	313.0	314.1	299.2	272.9	283.8	321.7	322.8	188.2	218.1	203.2	228.5	310.2	352.6	341.9	355.2	270.4	255.1	209.8
Rb	6.0	1.6		17.9	1.1	1.1	5.2	12.2	0.2	1.0	0.6	3.4	2.0	3.1	3.9	0.9	15.0	2.6	0.7	0.2	1.6
Sr	5094.5	5094.0	5215.3	5007.4	4939.0	5054.8	4782.9	5019.5	4916.3	4704.6	4804.2	4773.2	4788.7	4692.6	5181.7	5088.1	5196.0	5035.2	4928.2	5003.7	4675.0
Y	8.1	8.6	13.1	11.1	8.3	6.9	7.7	10.9	7.0	8.2	20.9	16.2	18.5	6.2	8.1	9.6	8.9	10.5	15.9	8.7	7.0
Zr	8.9	4.2		24.7	6.4	2.4	4.0	27.1	0.1	1.6	4.8	3.0	3.9	3.3	11.5	1.3	31.7	6.3	3.0	1.5	3.5
Nb	8.3	3.1		9.0	3.4	1.0	2.4	21.8	0.2	0.7	2.5	1.6	2.1	1.3	9.0	1.3	26.0	5.3	0.8	0.4	3.1
Cs								0.1								0.1	0.3		0.2		
Ba	148.2	118.1		194.1	113.6	103.3	112.8	278.8	96.5	100.1	138.1	119.7	128.9	113.1	183.3	109.2	342.1	140.5	110.5	100.8	115.9
La	86.6	93.0	113.2	99.4	90.4	79.5	85.4	106.8	77.3	88.0	180.6	160.2	170.4	66.7	77.5	89.7	86.6	94.7	146.7	90.8	83.8
Ce	160.9	170.0	199.9	176.6	176.7	146.7	158.2	192.1	147.8	178.8	373.7	267.0	320.4	124.3	158.1	169.4	174.1	187.6	287.5	179.7	158.4
Pr	17.3	17.3	20.8	19.3	20.1	17.0	16.7	20.9	16.0	18.5	40.0	28.3	34.1	13.1	15.9	19.0	18.8	19.0	30.9	19.0	16.8
Nd	63.1	66.0	76.3	73.9	69.5	64.2	62.3	81.2	56.1	67.2	141.2	105.3	123.3	54.8	60.0	66.4	67.3	71.4	116.0	68.4	62.7
Sm	9.5	7.7	8.4	7.9	11.5	11.0	8.5	9.6	7.0	7.0	11.1	14.6	12.8	7.8	6.3	7.2	9.3	13.8	9.6	5.6	8.3
Eu	3.1	3.2	3.6	3.2	2.8	1.9	2.9	2.8	1.8	2.8	4.4	6.4	5.4	2.1	2.6	1.9	3.1	1.9	5.0	3.4	2.5
Gd	4.7	4.9	5.6	5.8	6.6	4.7	4.6	5.7	3.9	4.8	8.0	18.4	13.2	2.6	3.9	4.9	4.9	5.6	6.1	4.4	4.1
Tb	0.5	0.5	0.6	0.6	0.4	0.4	0.5	0.5	0.5	0.5	1.1	1.3	1.2	0.3	0.5	0.6	0.7	0.6	1.6	0.7	0.5
Dy	2.1	2.0	4.2	3.4	1.7	1.7	1.5	2.6	2.0	2.2	7.7	3.9	5.8	1.6	1.9	3.3	2.9	2.4	3.0	2.5	2.1
Ho	0.4	0.4	0.6	0.6	0.3	0.3	0.3	0.5	0.3	0.2	1.4	0.6	1.0	0.3	0.5	0.4	0.4	0.1	0.6	0.5	0.3
Er	0.8	0.7	1.1	1.1			0.8		0.7	0.5	1.7	1.4	1.6		0.4	0.7	0.9	0.5	0.8	1.0	0.6
Tm	0.1	0.1					0.1		0.1		0.3	0.2	0.2	0.1			0.2	0.1	0.1	0.0	0.1
Yb			1.4	1.2	0.8		0.7			0.5					1.0				0.8		
Lu	0.1	0.1													0.1			0.1	0.1	0.1	0.0
Hf		0.3		0.4	0.2			0.3		0.1				0.3	0.2			0.2			
Ta	0.4	0.2		0.6	0.3	0.1	0.2	1.0			0.3		0.3	0.1	0.4		1.6	0.4	0.1		0.1
Pb	1.6	1.2	1.5	1.5	0.3	0.5	0.4	1.1	1.2	0.8	2.0	2.0	2.0	1.4	1.6	0.6	1.1	0.4	0.2	1.2	0.9
Th	0.8	1.2		1.9	1.2	0.6	1.1	3.0	0.2	1.6	4.7	4.5	4.6	0.3	1.7	1.3	2.4	0.9	4.5	1.1	1.3
U	0.3	0.3		0.2	0.7	0.3	0.3	0.8		0.1	1.7	1.0	1.3		0.5	0.2	1.2	0.3	0.7	0.2	0.2

Table 3

Click here to download Table: Table3Nyira.xls

Table 3

	av. of 12 an. glass 2016 ppm	av. of 7 an. glass 2002 ppm	av. of 9 an. mel/gl	av. of 12 an. mel/gl	av. of 2 an. cpx/gl	av. of 8 an. ol/gl	av. of 11 an. lct/gl	av. of 10 an. neph/gl	2002 lava ap/gl	2016 lava ap/gl	av .of 7 an. mgt/gl	literature mel/liq Onuma81	mel/matrix Arzamastsev	cpx/l AmbAzz18	cpx/l FJ04	cpx/l Onuma81	lc/l FJ04	ap/l PK06
Li	13.3	15.9	0.16	0.13	0.03	0.66	0.09	0.09			0.10							
B	36.8	22.6	0.74	0.89	0.27	0.91	1.61	1.21	0.45	0.00								
Sc	5.8	6.2	0.38	0.24	4.03	0.67					1.48			3			0.072	
Ti			0.12	0.05	0.71	0.05			0.05	0.001								
V	243.1	218.4	0.19	0.08	0.86	0.07			0.79	0.72	13.67				0.43			
Cr	4.3	3.0	1.48	1.71	1.49	7.13					81.13			9.63	48.9			
Co	41.1	36.4	1.13	1.11	0.93	5.14					8.47			0.572	1.89			
Ni	16.1	8.6	1.04	1.07	2.09	21.60					41.82			1.66	11.8			
Zn	180.4	175.1	1.81	1.55	0.23	1.19	0.05	0.08	0.11	0.12	4.00		2.45	0.172				
Rb	143.5	109.0	0.04	0.03	0.01		12.51	1.04	0.00	0.00			0.03	0.029	0.022		5.46	
Sr	2684.1	2775.2	1.87	1.77	0.38		0.02	0.27	2.22	1.79			3.67	0.211	0.303		0.0011	3.79
Y	37.8	42.2	0.24	0.27	0.71				4.35	3.13			0.31	0.27	0.387			5.69
Zr	337.2	394.1	0.03	0.02	1.02						0.24			0.249	0.022			0.02
Nb	256.0	303.1	0.02	0.01	0.03						0.20			0.009	0.007			0.0011
Cs	1.6	0.9	0.05	0.20			31.43	0.28						0.006			9.79	0.0002
Ba	2399.3	2705.6	0.06	0.05	0.01		0.97	0.10	0.05	0.04			1.86	0.004			0.046	0.16
La	204.9	225.7	0.45	0.49	0.36				6.37	4.64		0.54	0.51	0.096	0.128	0.49		13.3
Ce	363.2	395.6	0.47	0.54	0.44				6.53	5.06		0.61	0.47	0.12	0.416	0.53		13.6
Pr	35.8	39.1	0.51	0.58	0.55				7.27	5.09			0.54	0.192				14.6
Nd	127.2	138.1	0.53	0.61	0.65				7.75	5.83		0.7	0.55	0.266	0.274	0.7		
Sm	18.2	20.9	0.49	0.45	0.77				7.46	5.49		0.77	0.46	0.333	0.377	0.73		16.4
Eu	5.2	5.9	0.54	0.59	0.83				6.91	4.85		0.64	0.46	0.364	0.494	0.7		
Gd	12.3	13.6	0.42	0.49	0.85				7.06	5.74			0.42	0.311	0.436			
Tb	1.6	1.7	0.30	0.46	0.83				5.75	3.85			0.34	0.293				
Dy	8.6	9.3	0.27	0.35	0.73				4.32	3.24		0.52	0.3	0.317	0.424			
Ho	1.5	1.7	0.26	0.32	0.80				4.11	2.65			0.27	0.283				
Er	3.8	3.8	0.23	0.24	0.66				3.34	2.61			0.23	0.28	0.424			
Tm	0.5	0.6	0.17	0.24	0.72				2.55	1.75			0.25	0.417				
Yb	3.3	3.5	0.31	0.23	0.69				2.11	1.47		0.3	0.18	0.281	0.292	0.72		
Lu	0.4	0.5	0.25	0.18	0.74				1.66	1.33		0.3	0.19			0.81		2.05
Hf	4.5	5.4	0.07	0.04	1.58				0.02	0.10	0.38			0.454				0.016
Ta	13.3	16.3	0.03	0.02	0.10				0.01	0.00	0.35			0.031				0.0017
Pb	4.9	6.3	0.20	0.19	0.19		0.06		0.05	0.24			0.18					0.62
Th	23.8	26.9	0.05	0.09	0.08				1.72	1.08				0.045				0.4
U	9.6	12.6	0.04	0.05	0.05				0.82	0.54				0.03				0.35

supplementary tables

Click here to download Background dataset for online publication only: supptablesminNyirakd.xls

supplementary figure 1

Click here to download Background dataset for online publication only: SuppFig1nyira.jpg

supplementary figure 2

Click here to download Background dataset for online publication only: SupplFig2nyira.jpg

supplementary figure 3

Click here to download Background dataset for online publication only: supplemfig3Nyira.jpg

supplementary figure 4

Click here to download Background dataset for online publication only: supplemfig4Nyira.jpg